



HAL
open science

Numerical and experimental studies for the conception of a robust hydrothermal liquefaction reactor

Moeen El Bast

► **To cite this version:**

Moeen El Bast. Numerical and experimental studies for the conception of a robust hydrothermal liquefaction reactor. Chemical and Process Engineering. Ecole nationale supérieure Mines-Télécom Atlantique, 2022. English. NNT : 2022IMTA0321 . tel-04224307

HAL Id: tel-04224307

<https://theses.hal.science/tel-04224307v1>

Submitted on 2 Oct 2023

HAL is a multi-disciplinary open access archive for the deposit and dissemination of scientific research documents, whether they are published or not. The documents may come from teaching and research institutions in France or abroad, or from public or private research centers.

L'archive ouverte pluridisciplinaire **HAL**, est destinée au dépôt et à la diffusion de documents scientifiques de niveau recherche, publiés ou non, émanant des établissements d'enseignement et de recherche français ou étrangers, des laboratoires publics ou privés.

THESE DE DOCTORAT DE

L'ÉCOLE NATIONALE SUPERIEURE MINES-TELECOM ATLANTIQUE
BRETAGNE PAYS DE LA LOIRE - IMT ATLANTIQUE

ECOLE DOCTORALE N° 602
Sciences pour l'Ingénieur
Spécialité : Énergétique, Thermique, Combustion

Par

Moeen EL BAST

Etudes Numériques et Expérimentales pour la Conception d'un Réacteur de Liquéfaction Hydrothermale

Thèse présentée et soutenue à Nantes, IMT Atlantique, le 15 / 12 / 2022
Unité de recherche : GEPEA UMR-CNRS 6144
Thèse N° : 2022IMTA0321

Rapporteurs avant soutenance :

Talib DBOUK Université de Rouen-Normandie
Mahmoud KHALED The International University of Beirut

Composition du Jury :

Présidente :	Agnès MONTILLET	Nantes Université
Examineurs :	Frederic MARIAS	Université de Pau et des Pays de l'Adour
	Talib DBOUK	Université de Rouen-Normandie
	Mahmoud KHALED	The International University of Beirut
	Nadine ALLAM	Lebanese International University, Beirut
	Youssef ABOUMSALLEM	CESI Ecole D'ingénieurs
Dir. de thèse :	Sary AWAD	IMT Atlantique, Nantes
Co-dir. de thèse :	Khaled LOUBAR	IMT Atlantique, Nantes

Numerical and Experimental Studies for
the Conception of a Robust Hydrothermal
Liquefaction Reactor

Remerciements

This thesis, which was full of discoveries, took up a great challenge. However, it was not able to achieve this milestone without the help and the encouragement of few people who I am grateful to.

I would like to thank the project's team; the directors, Sary AWAD and Khaled LOUBAR, and the supervisors, Youssef ABOU MSALLEM and Nadine ALLAM for their great efforts and follow up during this time. I would like to extend my deep thanks to Prof. Mahmoud KHALED, and Prof. Talib DBOUK, who agreed to be the reviewers of this thesis. Moreover, I would like to thank Prof. Agnès MONTILLET and Prof. Frederic MARIAS for examining this work. In addition, I am grateful to both engineering schools which provided the optimum conditions for achieving this goal; the DSEE department of IMT Atlantique, Nantes, and the Mechanical Engineering Department of the Lebanese International University, Beirut.

In addition, I would like to thank my parents for their care, sacrifice, and all means of help to achieve this success.

Finally, this work is dedicated for my lovely wife, Rayana AL KATTAN, who supported, encouraged and stood beside me in all the ups and downs during these years.

Résumé

La biomasse est une matière biologique, incorporant toute la matière vivante sur terre. En raison de sa forte teneur en carbone, la biomasse peut être brûlée directement pour produire de la chaleur ou convertie en biocarburants à travers divers procédés. Plusieurs techniques sont utilisées pour la production de biocarburants ; cependant, la liquéfaction hydrothermale (HTL) est établie comme une technique de conversion prometteuse, produisant des carburants liquides de haute qualité. La liquéfaction hydrothermale de la biomasse est définie comme la conversion des ressources carbonées en substances huileuses dans de l'eau liquide chaude sous pression, ou d'autres solvants liquides. Les conditions typiques d'HTL varient entre 220 et 370 °C et 4 à 22 MPa.

Dans cette thèse, la conception d'un système continu de liquéfaction hydrothermale de la biomasse est proposée. Pour atteindre cet objectif, un plan a été suivi, commençant par une enquête sur l'état de l'art actuel des systèmes de liquéfaction hydrothermale continus, suivie de la proposition et la validation des modèles thermochimiques représentant les phénomènes se déroulant au sein d'un réacteur batch, à travers d'une campagne expérimentale et à l'aide du logiciel de modélisation multiphysique COMSOL. Ensuite, les modèles validés ont servi à la conception d'un nouveau système continu.

L'originalité de ce travail est illustrée par le développement d'un système continu à l'échelle du laboratoire qui peut être mis à niveau à l'échelle industrielle et commerciale, produisant des quantités notables de carburants.

Un grand nombre de travaux déjà rapportés sur les systèmes continus sont étudiés et analysés. Le composant principal du système continu est le réacteur lui-même, dans lequel la réaction a lieu. Les réacteurs continus peuvent être classés en trois catégories principales ; réacteurs tubulaires continus (CTR) ou réacteurs pistons (PFR), réacteur continu à cuve agitée (CSTR), ou systèmes hybrides associant un CSTR et un CTR en série. En raison de la haute pression de réaction de liquéfaction hydrothermale, un système d'alimentation est nécessaire pour alimenter le réacteur. Pour cette raison, deux techniques différentes sont

utilisées, soit en pompant les intrants par des gaz sous pression, comme l'azote comprimé, soit en utilisant des pompes à haute pression. Le chauffage de la biomasse à la température de réaction peut se faire selon différents modes; le chauffage par résistance électrique, le chauffage solaire, le chauffage par les fumées et le chauffage par lits fluidisés. De plus, un système de séparation est nécessaire pour séparer les carburants liquides produits des solvants, qui peuvent être recyclés, et des particules solides qui peuvent se trouver dans les produits.

En plus des composants du système, l'étude bibliographique a couvert les effets des paramètres de réaction sur le processus de liquéfaction, les rendements des produits et la conception systématique. On remarque que la réaction de liquéfaction requiert une température optimale pour laquelle les rendements en biohuile seront maximisés. Cette température optimale dépend du choix de la biomasse. L'augmentation de la température de réaction au-delà de la valeur optimale diminue les rendements, du fait de la présence de réactions secondaires et tertiaires. De plus, on remarque que la variation de la pression du milieu n'a pas d'effet direct sur les rendements en produits du procédé de liquéfaction hydrothermale. Cependant, la pression élevée maintient un milieu monophasique, évitant l'absorption de chaleur latente par les solvants, augmentant l'efficacité thermique du procédé. La composition de la charge (composition élémentaire, et composition lignocellulosique) a un grand impact sur les rendements en produits et la température optimale de conversion. De plus, les temps de séjour des réactions de liquéfaction sont étudiés, et on constate qu'il existe un temps optimal pour chaque charge, auquel les rendements sont maximisés et au-delà duquel les réactions secondaires et tertiaires les détériorent. Enfin, on remarque qu'une partie des chercheurs ont utilisé des solvants et des catalyseurs pour améliorer le rendement et la qualité des produits recherchés.

De plus, une section de l'étude bibliographique est dédiée au passage du traitement par batchs au traitement continu, où les effets de la conception du réacteur, la température, la pression, la vitesse de chauffe et les temps de séjour sur la réaction sont interprétés et comparés entre les systèmes de traitement batch et continu.

La dernière partie de l'étude bibliographique traite de l'état actuel de la modélisation et de la simulation CFD des processus de liquéfaction hydrothermale. Les équations gouvernantes avec leurs conditions aux limites pertinentes sont interprétées, y compris les équations de continuité, de conservation de la quantité de mouvement, de conservation de l'énergie et des transferts de masse et de chaleur. Cette section présente également les différents modèles cinétiques adaptés aux équations de transfert de masse, en se concentrant sur la cinétique d'Arrhenius, reliant la vitesse de réaction à la température de la réaction.

A l'issue de l'étude bibliographique, un modèle de réacteur discontinu est construit et calibré à l'aide de COMSOL Multiphysics, sur la base des résultats d'une campagne expérimentale menée sur un réacteur batch. Bien que l'objectif final du projet soit de concevoir un système continu, le système batch reste une nécessité, grâce à sa capacité à tester les conditions de la réaction et à calibrer ses paramètres (température, pression, charge de lisier, temps de séjour, etc.).

Les expériences menées sont détaillées, notamment leurs conditions opératoires, et les méthodes de caractérisation des produits. De plus, l'approche adoptée pour construire le modèle de simulation est discutée, en ce qui concerne les équations gouvernantes, les propriétés des matériaux, les hypothèses et approximations, etc. Le modèle de simulation est validé selon une méthodologie en trois étapes. D'abord, en chauffant un réacteur vide et en comparant les courbes de température et de pression simulées et expérimentales, puis, en chauffant plusieurs types de solvants (eau, méthanol et éthanol), et la dernière étape est la validation de la cinétique chimique du traitement hydrothermal de principales macromolécules modèles telles que les lipides, les glucides, les protéines et la lignine. Dans ce travail, l'étape de modélisation cinétique s'est limitée à la transestérification des lipides en présence du méthanol. Cette réaction a été choisie parce que son mécanisme réactionnel bien connu et établi dans la littérature et parce que ses produits restent à l'état liquide. Ainsi, après le processus de validation étape par étape, cette réaction est la plus simple à modéliser et à utiliser avant de modéliser des réactions plus complexes.

Des expérimentations ont été menées au Laboratoire GEPEA du département DSEE d'IMT Atlantique à Nantes. Le réacteur hydrothermal utilisé est un réacteur batch de 998 mL de volume de forme

cylindrique ayant une hauteur de 35,95 cm, 3 cm de rayon intérieur et 8,5 cm de rayon extérieur et fabriqué en acier inoxydable. La puissance de chauffe est fournie au réacteur par des résistances électriques intégrées dans ses parois, capables de délivrer jusqu'à 20 kW de puissance de chauffe. La température est limitée à un maximum de 450 degrés Celsius, et le réacteur supporte une pression maximale de 190 bars, au-delà de laquelle une soupape de sécurité s'ouvre et le purge. Le réacteur est équipé d'un transducteur de pression pour mesurer la pression instantanée absolue à l'intérieur de la zone de réaction. De plus, quatre thermocouples sont installés à quatre positions différentes dans le réacteur. Le réacteur est relié à un système d'alimentation en gaz. Avant de commencer toute expérience, le réacteur est purgé avec de l'azote gazeux s'écoulant à un débit de 0,1 L/sec ($\pm 0,005$) pendant 10 minutes pour éliminer l'oxygène et assurer un milieu inerte. En plus de la purge, le système d'alimentation en gaz permet de pressuriser le réacteur avec de l'azote. Un système d'acquisition de données est connecté au réacteur, pour enregistrer la pression (bars), les températures (degré Celsius) et la puissance d'entrée (Watts) au cours de l'expérience. Le pas de temps de ce système d'acquisition est fixé à une seconde, jugée comme étant le meilleur compromis entre la précision et les ressources nécessaires au traitement des données.

Dans l'expérience de chauffage du réacteur vide (chauffage à l'azote), le réacteur est purgé avec de l'azote gazeux, puis le réacteur est fermé à la pression atmosphérique, scellé et mis en marche. L'azote s'échauffe dans le milieu fermé, ainsi, selon les lois de la thermodynamique, il va subir une montée en pression.

Pour le chauffage des solvants, l'eau, le méthanol et l'éthanol sont testés. Deux expériences concernant le chauffage de l'eau ont été menées. Dans la première expérience, 300 mL d'eau sont introduits dans le réacteur à température ambiante, le réacteur est purgé à l'azote, fermé et scellé, et les réchauffeurs sont allumés. Dans la seconde expérience, le même volume d'eau est utilisé, le réacteur est fermé et scellé, et purgé puis pressurisé à l'azote jusqu'à 42,7 bars pour éviter toute évaporation de l'eau tout au long de l'expérience où la température finale peut atteindre les 300 °C. Le méthanol et l'éthanol sont achetés chez Thermo Fisher Scientific, France, ayant des densités respectives de 792 kg/m³ et 789 kg/m³, et des masses

molaires de 32,04 g/mol et 46,07 g/mol respectivement. Dans chaque expérience, 300 mL du solvant sont introduits dans le réacteur, puis, le réacteur est purgé, fermé et scellé, et pressurisé avec de l'azote à 47 bars, assurant une phase liquide tout en le chauffant de la température ambiante jusqu'au point critique.

En ce qui concerne la transestérification du méthanol supercritique, l'huile de colza a été achetée dans un magasin local. Sa masse volumique est de 915 kg/m³ et sa masse molaire est de 882 g/mol. Pour obtenir un rapport de 42:1 de méthanol à l'huile, 100 grammes d'huile de colza, correspondant à 0,11338 moles ont été ajoutés à 152,4 grammes de méthanol, correspondant à 4,7625 moles, avec un volume total de 300 ml. Le mélange a été agité à l'aide d'un agitateur magnétique à 600 tr/min pendant 10 minutes et introduit dans le réacteur. Le réacteur a été fermé, scellé et purgé puis pressurisé avec de l'azote, pour atteindre 47 bars, une pression de départ suffisante pour assurer un méthanol liquide monophasique tout au long de l'expérience. Une expérience de référence a été réalisée, laissant le réacteur fonctionner pendant plus de six heures pour assurer la conversion complète de l'huile de colza en biodiesel. Après avoir terminé l'expérience, le réacteur est laissé refroidir, puis les produits sont collectés dans un évaporateur rotatif pour éliminer tout le méthanol du mélange. Les produits restants sont placés dans une ampoule à décanter pendant environ une heure, temps suffisant pour séparer complètement les produits. On a remarqué que deux couches apparaissaient clairement dans l'ampoule à décantation après séparation, la supérieure étant du biodiesel et l'inférieure étant du glycérol. Après cela, trois expériences différentes ont été réalisées, visant à stabiliser la température interne du réacteur au-dessus de 270 degrés Celsius. Le temps de séjour dans la première expérience était d'une heure, dans la seconde de deux heures et dans la troisième de trois heures. La phase légère des produits de chaque expérience est censée être un mélange de biodiesel et d'huile de colza n'ayant pas réagi. La quantification du biodiesel produit et de l'huile n'ayant pas réagi dans chaque expérience a été effectuée à l'aide de la formule de Gambill pour la viscosité d'un mélange liquide-liquide.

Un modèle de simulation est construit à l'aide de COMSOL Multiphysics, pour simuler les phénomènes thermophysiques et chimiques se produisant à l'intérieur du réacteur discontinu. Les dimensions du réacteur tirées du manuel du concepteur sont implémentées dans COMSOL à l'aide de

coordonnées axisymétriques 2D. À chaque seconde du temps de l'expérience, le système d'acquisition du réacteur enregistre la puissance d'entrée (Watts) qui est extraite et importée dans COMSOL en tant que fonction d'interpolation pour la source d'alimentation. Ainsi, la puissance expérimentale est appliquée avec précision au modèle de simulation. Une interface de domaine isotherme a été adoptée dans la zone de réaction en raison du faible gradient de température attendu au sein du mélange. Dans cette interface, des propriétés homogènes (température, pression, densité, viscosité, etc.) sont définies. La pressurisation de la phase gazeuse est simulée à l'aide de l'équation de Van der Waals, décrivant le comportement des gaz réels. Pour la pression de vapeur des solvants, on remarque qu'elle est en parfaite adéquation avec la courbe de saturation PT.

Les résultats expérimentaux sont comparés aux résultats obtenus à partir du modèle de simulation. L'expérience de chauffage du réacteur vide permet de calibrer les phénomènes de diffusion de la chaleur et de pressurisation de l'azote. L'erreur de température maximale dans ce cas est restée inférieure à 4 % et l'erreur relative maximale de pressurisation a atteint 8,88 %.

L'expérience de chauffage de l'eau à partir de la pression atmosphérique aide à calibrer le phénomène d'évaporation en ajoutant la composante de chaleur latente qui fait converger l'erreur entre les résultats expérimentaux et de simulation à moins de 0,5 % à l'équilibre.

Les expériences de chauffage au méthanol et à l'éthanol aident à calibrer le comportement supercritique des solvants, où l'erreur de température est restée inférieure à 1% à l'équilibre.

Pour la transestérification au méthanol supercritique de l'huile de colza, l'erreur entre les données de température expérimentales et de simulation est négligeable. Le taux de conversion des lipides à la fin de chaque expérience est comparée aux résultats du modèle de simulation. Des erreurs de 2,47 %, 5,88 % et 1,85 % ont été constatés respectivement pour les expériences de 1 heure, 2 heures et 3 heures.

Les résultats du modèle de réacteur batch validé sont utilisés pour concevoir un système continu pour la transestérification au méthanol supercritique de l'huile de colza. La première étape consiste à

concevoir un réacteur tubulaire continu, qui est considéré comme la forme la plus simple d'un réacteur continu. Le réacteur est composé d'acier inoxydable 316L, résistant à la corrosion et capable de supporter les conditions de température et de pression élevées du procédé. Une couche d'isolation est utilisée pour recouvrir le corps du réacteur, pour des raisons de sécurité, et afin de réduire les déperditions thermiques du système, augmentant ainsi son efficacité globale. Le réacteur a une forme cylindrique de rayon intérieur de 1 cm, comme un compromis entre les petits diamètres assurant un chauffage rapide, et les grands diamètres évitant les problèmes de colmatage dans le réacteur. Bien que dans la transestérification du méthanol supercritique, le colmatage ne soit pas attendu puisque les réactifs et les produits sont en phases liquides, le réacteur a néanmoins un rôle futur à jouer pour divers procédés de liquéfaction hydrothermale traitant de différents types de matières premières. Après avoir fixé le rayon intérieur, l'épaisseur de la paroi du réacteur a été choisie de tel sorte à supporter les pressions élevées que peut atteindre le système. Pour cette raison, une analyse des contraintes 3D dans des récipients sous pression épais est utilisée, avec un facteur de sécurité de 1,5, ce qui mène à un rayon extérieur de 1,3 cm. La longueur du réacteur est calculer de tel sorte à assurer un taux de conversion des lipides de 99 %. En raison des gradients de température élevés à l'intérieur du réacteur, COMSOL Multiphysics a utilisé pour déterminer cette longueur, pour différentes températures et différents débits de fonctionnement.

Après avoir conçu un réacteur tubulaire autonome, un réacteur continu parfaitement agité est proposé et conçu. En raison de la caractéristique d'uniformité et du milieu homogène à l'intérieur du réacteur agité, des calculs manuels sont applicables. Les temps de séjour et le volume interne du réacteur sont calculés pour différentes températures de fonctionnement et différents débits de suspension à l'aide des équations d'état stationnaire. Une étude de démarrage du réacteur agité est menée, où il est constaté qu'il est toujours préférable de remplir le réacteur avec le mélange réactif avant son démarrage plutôt que de le remplir avec le solvant.

Cependant, les systèmes autonomes ont des dimensions extrêmes, une grande longueur pour le réacteur tubulaire et un grand volume pour le réacteur agité, même pour les systèmes à l'échelle du

laboratoire. Pour cette raison, une combinaison de ces 2 types de réacteurs en série, peut être envisagée comme compromis, où le réacteur agité assure une conversion primaire en chauffant les réactifs pendant un temps défini, après quoi la réaction se poursuit dans le réacteur tubulaire jusqu'à la fin de la réaction. Cette combinaison diminue significativement la taille et la consommation d'énergie de l'ensemble de l'unité de réaction. Deux grandes approches seront étudiées ; le premier utilise le réacteur agité pour une conversion à 80 % et complète le reste dans le réacteur tubulaire, alors que le second utilise le réacteur agité pour une conversion à 90 % et complète le reste dans le PFR. Après avoir examiné les différentes configurations possibles, un réacteur agité de 1,02 L de volume et un réacteur tubulaire de 2,44 m de longueur seront utilisés pour assurer un débit maximal de 10 L/h à une température de 350 degrés Celsius. Le dimensionnement et la pale du réacteur agité sont conçus selon les règles de l'état de l'art lui permettant de fonctionner dans des conditions idéales.

Une pompe est sélectionnée pour alimenter la suspension dans les réacteurs, ce qui est optimal pour le processus de transestérification du méthanol supercritique. Cependant, une liste d'autres pompes est proposée, qui sont applicables pour une large utilisation de différentes propriétés de la charge d'alimentation, puisque l'objectif principal de ce système est de fonctionner efficacement pour divers procédés de liquéfaction hydrothermale.

De plus, un système de séparation est conçu, intégré à un système de récupération de chaleur. L'avantage de ce système est de récupérer 92,8 % du méthanol nécessaire au processus de transestérification supercritique et de diminuer de 37,7 % l'apport d'énergie nécessaire au chauffage du méthanol.

Ainsi, un système continu à l'échelle du laboratoire pour la transestérification au méthanol supercritique de l'huile de colza est étudié et conçu. Ce système peut être mis à niveau pour traiter différentes matières premières et peut être adapté aux applications commerciales et industrielles.

Cependant, plusieurs points peuvent encore être abordés et résolus pour améliorer la conception, notamment :

- Étude des performances du système pour d'autres macromolécules : glucides, protéines, cellulose, hémicellulose, lignine, etc.
- Étudier la solubilité du dioxyde de carbone (en tant que principal produit gazeux des réactions HTL) dans l'eau au sein du réacteur à différentes températures et pressions
- Réalisation d'un bilan énergétique total, améliorant l'efficacité thermique totale
- Mise à l'échelle du système, remplacement du chauffage électrique par d'autres modes de chauffage (gaz de combustion et énergie solaire)
- Optimisation des systèmes de récupération de chaleur
- Optimisation de la topologie du réacteur pour maximiser le transfert de chaleur et réduire les pertes de chaleur

Abstract

In this thesis, a design of a continuous biomass hydrothermal liquefaction system is proposed. After a study of the different existing hydrothermal liquefaction processes and the different mechanisms involved, models simulating the different underpinning thermochemical phenomena have been proposed. These phenomena were studied at the scale of a 1L batch reactor and modeled using COMSOL Multiphysics software. To do so, an experimental campaign is carried out, starting from the heating of the empty reactor and ending with a complete elementary chemical reaction; supercritical transesterification of rapeseed oil. The experimental curves of temperature at different places in the reactor and of pressure helped to calibrate different models of heat diffusion, pressurization, evaporation and transport of species. Finally, the chemical kinetics model of the supercritical transesterification of lipids was experimentally validated using the conversion rate as a comparison parameter. The maximum relative error on the different modeled parameters is less than 6%. The validated batch reactor model helps in the design of a continuous system. A process combining a continuous stirred tank reactor (CSTR) and a plug flow reactor (PFR) has been proposed. After scanning the different temperature and flow rate ranges, a 1 L CSTR and a 2.44 m x 1 cm diameter PFR were chosen to handle a flow rate of 10 L/h of reactive mixture. After the dimensioning of the various organs, a complete and integrated system was proposed.

Contents

Remerciements	3
Résumé	5
Abstract	15
List of Figures	21
List of Tables	25
Nomenclature	27
Symbols	27
Abbreviations	29
Introduction	31
Chapter 1. Literature Review – State of the Art	37
1. Introduction	37
2. Continuous Systems, Components and Operation	42
2.1. Reactor	42
2.2. Feeding Systems	52
2.3. Heating Mode	58
2.4. Separators	63
3. Effects of Reaction Parameters on the Liquefaction Process, Products Yields and Systematic Design	66
4. Transition from Batch to Continuous Processing	72
4.1. Reactor Design	72
4.2. Temperature	72
4.3. Pressure	73
4.4. Heating Rate and Residence Time	73
5. CFD Modelling and Simulation of the HTL Process	75
5.1. Governing Equations and Boundary Conditions	75
5.2. Kinetic Models	84
5.3. Material Properties	85
5.4. Software Adaptation	88
6. Conclusion	89
Chapter 2. Batch Reactor Model, Materials and Methods	93
1. Introduction	93
2. Experimental Setup	95

2.1.	Empty Reactor Heating (Nitrogen Heating)	98
2.2.	Solvents Heating	98
2.3.	Supercritical Methanol Transesterification of Rapeseed Oil	98
3.	Reactor Modelling and Implementation into COMSOL.....	100
3.1.	Reactor's Geometry	100
3.2.	Isothermal Domain Interface	101
3.3.	Power Zone Assumption.....	101
3.4.	Pressurizing the Reactor's Medium	103
3.5.	Governing Equations.....	109
3.6.	Material Properties	111
4.	Validation of Other Chemical Reactions	112
4.1.	Decomposition of Sodium Bicarbonate	112
4.2.	Kinetics of Sodium Bicarbonate Decomposition.....	113
4.3.	Thermogravimetric Analysis of Decomposition of Sodium Bicarbonate	114
4.4.	Decomposing Sodium Bicarbonate in the Batch Reactor	114
5.	Conclusion	115
Chapter 3. Batch Reactor Model, Results and Discussions		117
1.	Introduction.....	117
2.	Empty Reactor Heating.....	117
2.1.	Heat Diffusion.....	117
2.2.	Pressurization.....	119
3.	Liquid Solvents Heating.....	120
3.1.	Water Heating	121
3.2.	Methanol and Ethanol Heating	125
4.	Supercritical Methanol Transesterification.....	128
5.	Decomposition of Sodium Bicarbonate	131
5.1.	TGA Analysis of Sodium Bicarbonate Decomposition.....	132
5.2.	Decomposition of Sodium Bicarbonate in the Batch Reactor.....	133
6.	Results Validity.....	138
7.	Conclusion	139
Chapter 4. Design of a Continuous System for the Supercritical Methanol Transesterification of Rapeseed Oil 141		
1.	Introduction.....	141

2.	Plug Flow Reactor, PFR.....	141
2.1.	Materials Selection.....	142
2.2.	Geometry.....	143
2.3.	Fluid Flow inside the Reactor	148
2.4.	Reactor's Length Estimation.....	150
3.	Continuous Stirred Tank Reactor, CSTR.....	160
3.1.	Steady State Governing Equation	160
3.2.	Reactor Sizing.....	161
3.3.	Reactor Start-up	162
4.	Hybrid System	164
4.1.	Sizing Methodology	165
4.2.	CSTR Dimensions.....	167
4.3.	CSTR Agitation.....	170
4.4.	Pumping System	171
4.5.	Separation System.....	172
4.6.	Final System Representation.....	174
5.	Conclusion	175
	Conclusions and Perspectives	177
	Bibliography	181

List of Figures

Figure 1: Methodology used for achieving the main goal of the project	34
Figure 2: Phase diagram of water showing the regions of thermochemical processes	39
Figure 3: A plug flow reactor section	43
Figure 4: Tube Reactor of Prapaiwatcharapan et al, redrawn from [19].....	43
Figure 5: Continuous plug flow reactor of Makishima et al, redrawn from [23].....	44
Figure 6: Wadryzka coiled tubular reactor, redrawn from [24]	45
Figure 7: Jazrawi's reactor, redrawn from [25]	46
Figure 8: Parabolic trough reactor and absorber acting as a plug flow reactor, redrawn from [26]	47
Figure 9: Cassava Rhizome Continuous Carbonization Reactor, redrawn from [27].....	47
Figure 10: Continuous stirred tank reactor	49
Figure 11: CSTR continuous reactor for the production of bio-oil, redrawn from [34]	50
Figure 12: Combined CSTR-Plug flow reactor, redrawn from [36]	51
Figure 13: Two-stage pumping system.....	53
Figure 14: Feed delivery system using pressurized nitrogen gas.....	54
Figure 15: Golden Catalyst bed of Christinen's experiment [42]	55
Figure 16: Xiao's Solar hydrothermal liquefaction system cooler, redrawn from [26].....	61
Figure 17: Jazrawi's reactor, heat exchangers arrangement, redrawn from [25].....	62
Figure 18: The first three separators of Haverly's system, redrawn from [29]	64
Figure 19: Second two separators of Haverly's system, redrawn from [29]	65
Figure 20: Last separators of Haverly's system, redrawn from [29]	66
Figure 21: Reaction network for the HTL of microalgae [2].....	84
Figure 22: Step-by-step methodology utilized to build and validate the numerical model	95
Figure 23: Batch reactor used for the hydrothermal liquefaction in the GEPEA Laboratory of DSEE department in IMT Atlantique	96
Figure 24: Reactor's axial cross-section.....	97
Figure 25: Individual heating to power zone assumption	102
Figure 26: Real heaters model vs power zone assumption model mesh.....	103
Figure 26: F(T) versus temperature for the seven different obtained correlations.....	107
Figure 28: Averaged Correlation F versus the other correlations	108
Figure 29: Linearized kinetics reported by Kusdiana et al as pseudo first order	111
Figure 30: Experimental versus simulation temperature profiles for the nitrogen heating experiment....	118

Figure 31: Experimental pressure and simulation pressures using ideal and real gas laws plotted versus the inner temperature of the reactor	119
Figure 32: Experimental vs simulation inner temperature for the water heating experiment, starting from atmospheric pressure and neglecting the evaporation phenomenon	121
Figure 33: Experimental vs simulation internal pressure for the water heating experiment, starting from atmospheric pressure and neglecting the evaporation phenomenon	122
Figure 34: Experimental vs simulation inner temperature for the water heating experiment, starting from atmospheric pressure and taking the evaporation phenomenon into account	123
Figure 35: Experimental vs simulation internal pressure for the water heating experiment, starting from atmospheric pressure and taking the evaporation phenomenon into account	123
Figure 36: Experimental and simulated inner temperature in the water heating starting from nitrogen-pressurized medium	124
Figure 37: Experimental and simulated internal pressures in the water heating starting from nitrogen-pressurized medium	125
Figure 38: Experimental and simulated inner temperature in the methanol heating starting from nitrogen-pressurized medium	126
Figure 39: Experimental and simulated internal pressures in the methanol heating starting from nitrogen-pressurized medium	126
Figure 40: Experimental and simulated inner temperature in the ethanol heating starting from nitrogen-pressurized medium	127
Figure 41: Experimental and simulated internal pressures in the ethanol heating starting from nitrogen-pressurized medium	127
Figure 42: Experimental and simulated inner temperature of the reactor in the one-hour transesterification experiment.....	129
Figure 43: Experimental and simulated inner temperature of the reactor in the two-hour transesterification experiment.....	129
Figure 44: Experimental and simulated inner temperature of the reactor in the three-hour transesterification experiment.....	130
Figure 45: Numerical conversion curve, with the final products' experimental conversion points	131
Figure 46: TGA analysis of sodium bicarbonate decomposition.....	132
Figure 47: Comparison of the conversion of decomposition of sodium bicarbonate using Hartman's model and TGA results	133
Figure 48: Inner temperature of the reactor and the instantaneous number of moles of produced carbon dioxide in the 473K sodium decomposition experiment.....	134

Figure 49: Inner temperature of the reactor and the instantaneous number of moles of produced carbon dioxide in the 423K sodium decomposition experiment.....	134
Figure 50: Inner temperature of the reactor and the instantaneous number of moles of produced carbon dioxide in the 373K sodium decomposition experiment.....	135
Figure 51: Temperature and pressure curves for the sodium decomposition experiment after cooling down and stabilizing	136
Figure 52: Variation of number of moles occupying the gaseous volume in the reactor throughout the experimental time and cooling time.....	137
Figure 53: The three stress components presented in a thick-walled vessel under pressure.....	145
Figure 54: Basic operation mechanism of a plug flow reactor	150
Figure 55: Temperature profiles across the 3D model of the reactor	153
Figure 56: Centerline axial temperature along the reactor's length.....	154
Figure 57: Reaction conversion inside the reactor's inner zone	155
Figure 58: Centerline axial conversion along the reactor's length	156
Figure 59: Starting up the CSTR with zero initial concentration.....	163
Figure 60: Starting up the CSTR with the reactant's slurry inside it	164
Figure 61: Standard Dimensions of a CSTR.....	168
Figure 62: Von Mises stress distribution across the CSTR's wall when subjected to 25 MPa internal pressure	170
Figure 63: Schematic representation of the continuous system	175

List of Tables

Table 1: Recent surveys covering the hydrothermal liquefaction of biomass	40
Table 2: Temperature ranges and optimum temperature values for different continuous HTL processes .	67
Table 3: Arrhenius kinetics for the HTL of microalgae [4]	84
Table 4: Microalgal properties reported by Brown et al.[17]	86
Table 5: Coefficients of the 3 rd degree polynomials describing the seven different experiments	106
Table 6: Calibrated coefficients of the 3 rd degree polynomials describing the seven different experiments	107
Table 7: Thermal conductivity of stainless steel 316L	111
Table 8: Thermal conductivity of the insulation material	112
Table 9: Viscosity of the supercritical transesterification products, and the conversion of each experiment	130
Table 10: Mechanical and thermal properties of AISI 316L stainless-steel	142
Table 11: Thermal properties of glass wool insulation.....	143
Table 12: Stress components and Von Mises stress in the cylindrical tube with an internal pressure of 19 MPa.....	146
Table 13: Average flow velocities calculated from the selected flow rates inside the reactor	149
Table 14: Reynolds number at the inlet conditions for the selected flow rates	150
Table 15: Required length to achieve 99% conversion at different temperatures	157
Table 16: Predicted and exact length of the reactor at Q = 5 L/hr and 10 L/hr	159
Table 17: Residence time required to achieve 99% at the different operating temperatures.....	161
Table 18: Minimum CSTR volume (L) required for 99% conversion at different reaction conditions....	162
Table 19: CSTR volume (L) and PFR length (m) for achieving a final 99% for all the different volumetric flow rates and operating temperatures	166
Table 20: CSTR volume (L) and PFR length (m) for achieving a final 99% for all the different volumetric flow rates and operating temperatures	167

Nomenclature

Symbols

α : thermal expansion coefficient	(1/K)
a: intermolecular forces correction	(Pa.m ⁶ /mol ²)
A: surface area	(m ²)
A _i : pre-exponential term of species i	(1/s)
b: particles volume correction	(m ³ /mol)
C _i : concentration of species i	(mol/m ³)
C _p : heat capacity at constant pressure	(kJ/kg.k)
ΔH_{rx} : heat of reaction	(kJ/mol)
D: diameter	(m)
D _i : diffusion coefficient of species i	(m ² /s)
c: material strain	(mm/mm)
ϵ : porosity	(g/cm ³)
E: Young's modulus	(Pa)
E _a : activation energy	(J/mol)
F _A : molar flow rate	(mol/s)
g: gravitational acceleration	(m/s ²)
G: mass flux	(kg/m ² s)
h: convective heat transfer coefficient	(W/m ² K)
h _i : specific enthalpy	(kJ/kg)
k: thermal conductivity	(W/m.K)
k _i : reaction rate constant of species i	
L: length	(m)

L_i : latent heat of vaporization	(kJ/kg)
μ : dynamic viscosity	(Pa.s)
\dot{m} : mass flow rate	(kg/s)
ν : kinematic viscosity	(mm ² /s)
n : number of moles	(mol)
N : revolution speed	(rpm)
N_{FR} : Froud's number	
Nu : Nusselt's number	
P : pressure	(Pa)
Pr : Prandtl number	
ρ : density	(kg/m ³)
q'' : convective heat flux	(W/m ²)
Q : volumetric flow rate	(m ³ /s)
r : radius	(m)
r_A : rate of reaction	(mol/s)
R : universal gas constant	(J/mol.K)
Re : Reynolds number	
σ : material stress	(Pa)
τ : characteristic time	(s)
t : time	(s)
T : temperature	(K)
u : velocity	(m/s)
U : overall heat transfer coefficient	(W/m ² K)
V : volume	(m ³)
w_i : weight fraction of species i	

X: reaction conversion

y_i : mass fraction of species i

Abbreviations

AP: aqueous phase

BC: biocrude

CTR: continuous tubular reactor

CTW: cooling tower water

CSTR: continuous stirred tank reactor

F.S: safety factor

HHV: higher heating value

HP: high pressure

HPH: high pressure homogenization

HTL: hydrothermal liquefaction

HX: heat exchanger

LCA: life cycle assessment

PEF: pulsed electric field

PFR: plug flow reactor

PRV: pressure relief valve

SEP: separator

SEQHTL: sequential hydrothermal liquefaction

TOC: total organic compounds

VM: Von Mises

Introduction

Biomass is a biological matter that incorporates all living matter on earth. Normal human activity produces daily huge quantities of mixed biomass, such as cooking wastes, sewage sludge, sawdust, manure, etc. [1]. The annual global production of land based biomass is in the range of 50 billion tons [2]. Based on its origin, biomass can be classified into agricultural residues, forest residues, animal manure & human excreta, municipal solid wastes, industrial wastes, aquatic plants and algae, etc. [3]. Biomass consists mainly of cellulose, hemicellulose, lignin, small extractives, fats, proteins, sugars, water, ash, beside additional mixtures [4]. Typical biomass contains carbon (C), hydrogen (H), oxygen (O), sulfur (S) and Nitrogen (N).

Since biomass is rich in carbon, which is the core element of any fuel, it can be burned directly for heat production, or converted to renewable fuels via various processes [5]. The continuous increase in the global energy demand, and the essential needs of renewable energy sources guided researchers to process biomass into bioenergy. Biomass processing techniques include biochemical and thermochemical conversions. Biochemical conversions of biomass utilize enzymes, microorganisms and bacteria to decompose biomass into gaseous or liquid fuels [6], whereas, thermochemical conversions are based on heating the biomass, sometimes in a pressurized - oxygen deprived medium to produce biofuels, which is established as a fast process, producing higher quality fuels compared to the biochemical conversion products [7].

Thermochemical conversion techniques of biomass include combustion, pyrolysis, and hydrothermal processes [7]. Hydrothermal processes can be classified into carbonization, fractionation, liquefaction and gasification. Among these processes, the products of hydrothermal liquefaction are known for their higher energy content compared to the products of other processes [8]. The hydrothermal liquefaction process is defined as the conversion of carbonaceous resources into oily substances in hot pressurized liquid water or other liquid solvents. During this process, constitutive biomass molecules

decompose into thousands of organic compounds, following complex reaction mechanisms [9]. It is considered as an established process for producing liquid fuels, at a temperature ranging between 250 and 370 °C, and a pressurized medium, ranging from 4 up to 25 MPa. In addition to the main product of hydrothermal liquefaction, biocrude oil, other components are produced in solid, aqueous, and gaseous phases. Hydrothermal liquefaction of biomass has been investigated in a lot of previous works, including its process mechanism [9], [10], operating parameters [11]–[16], and process optimization through the effect of operating parameters on its products. The majority of works on the hydrothermal liquefaction process are reported on a lab-scale. However, to produce significant amounts of biofuels, this process needs to be commercialized and scaled up to an industrial scale.

Due to its elevated temperature and pressure values, hydrothermal liquefaction of biomass requires heavy duty reactors. Reactors are classified into two broad types; batch reactors and continuous reactors. Batch reactors are the simplest types of reactor vessels used for chemical or industrial processes. A typical batch reactor is a closed tank where chemical reactions occur. On the other side, continuous reactors, commonly referred as flow reactors, carry material as a flowing stream, where the reactants are continuously fed, and the products are continuously extracted. The choice of a reactor type depends on the reason behind it; studying the process and investigating for its optimization through calibrating the parameters is preferred to be done in a Lab-scale batch reactor, whereas, commercializing the process and scaling it up to produce large amounts of biofuels requires a continuous reactor.

The main goal of this thesis is to design a continuous reactor for the hydrothermal liquefaction of biomass. This is achieved through a set of pre-fixed milestones. A survey on the hydrothermal liquefaction of biomass will be conducted. The majority of studied works are oriented towards the continuous systems. The process operating parameters will be presented, including the temperature, pressure, residence time, and biomass composition, in addition to the use of solvents and catalysts for enhancing the products yields. Previous continuous systems will be presented and discussed, including the types and geometries of the reactors, pumping systems, heating modes, heat recovery systems and separation systems. In addition, the

approaches for transitioning from batch to continuous processing will be discussed. Moreover, a part of this survey will aim for the CFD simulations and modelling of the hydrothermal liquefaction, including the governing equations and boundary conditions describing the phenomena occurring in this process, material properties, kinetic models and software adaptation. The next step is the validation of a batch reactor model, since batch reactors are simpler in calibration. This step, when validated, will help in modelling the continuous reactor based on the results achieved. For this reason, an experimental campaign will be conducted on a 1L batch reactor. The aim of these experiments is to collect sufficient data, including temperature profiles, pressurization curves and chemical reactions conversions for building and calibrating a simulation model, which, when calibrated, will be used for modelling the hydrothermal liquefaction process, and proposing a new design for a continuous system, ready for scaling up. A simulation model will be built using COMSOL Multiphysics, and calibrated using the results of the experiments conducted. Step-by-step methodology for building and validating the model will be followed, by comparing the experimental and numerical results, starting from the simplest phenomena (heat diffusion experiments), ending with a full chemical reaction process occurring inside the reactor. The validation is based on the results of supercritical methanol transesterification of rapeseed oil to produce biodiesel. Finally, based on the experimental results and numerical results achieved, and the validation of the thermophysical and chemical phenomena using COMSOL Multiphysics, a new design for a continuous reactor for the hydrothermal liquefaction of biomass will be proposed, studied, and simulated. A standalone plug flow reactor is proposed first, after which a standalone continuous stirred tank reactor is proposed. Then, a hybrid design consisting of a continuous stirred tank reactor – plug flow reactor (CSTR – PFR) connected in series is proved to be more efficient. The system is capable of processing slurries up to 350 Celsius degrees at pressures up to 250 bars, with a flow rate of 10 L/hr.

Figure 1 shows the thesis methodology followed to achieve its final objective.

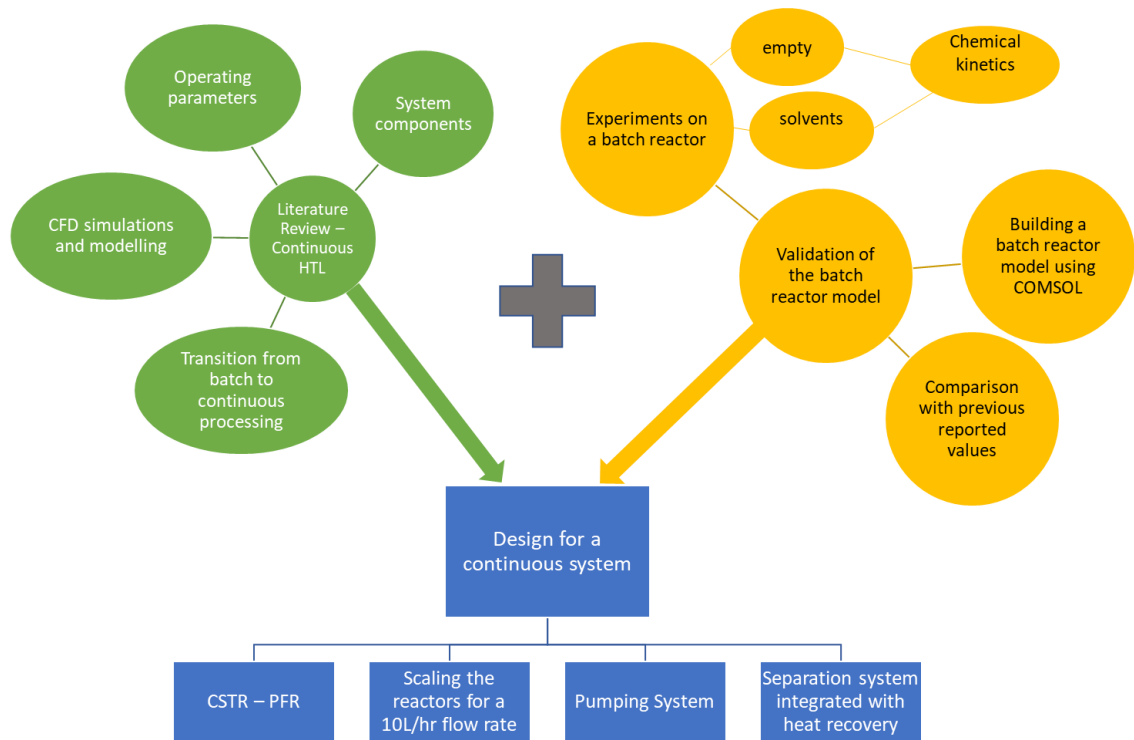


Figure 1: Methodology followed for achieving the main goal of the project

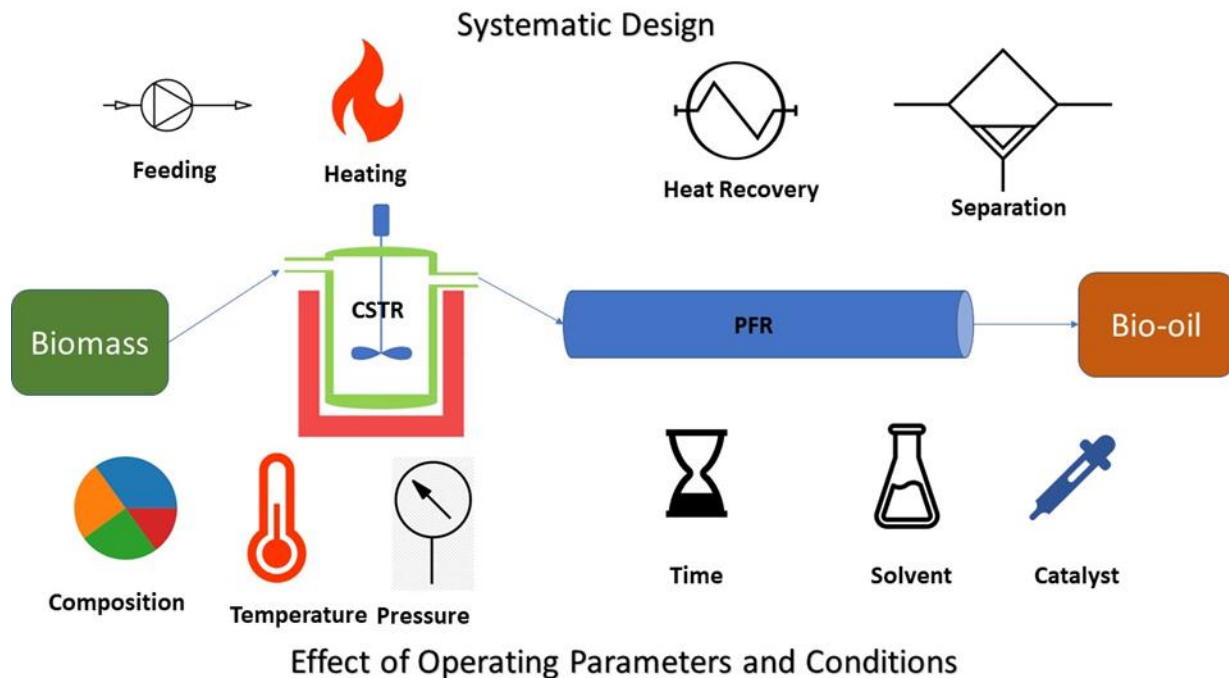
This thesis is divided into four main chapters:

- Chapter 1, Literature Review – State of the Art: is a literature review presenting the HTL process parameters, systematic designs, CFD simulations and modelling of the continuous hydrothermal liquefaction of biomass.
- Chapter 2, Materials and Methods: is a description of the setup used for conducting the experiments, characterizing the products and building the simulation model using COMSOL Multiphysics.
- Chapter 3, Results and Discussions: is a comparison between the experimental and simulation results achieved for the modelling of the batch reactor, and validating the results.

- Chapter 4, Design of a Continuous System for the Supercritical Methanol Transesterification of Rapeseed Oil: is a detailed step-by-step design of a continuous system, tuned for optimizing the supercritical methanol transesterification process, and capable of processing other hydrothermal liquefaction reactions.

Chapter 1. Literature Review – State of the Art

Graphical Abstract



1. Introduction

Biomass is an organic matter, involving both flora and fauna. It includes many resources such as wood and its wastes, animals and agricultural wastes, aquatic plants, and energy crops. Normal human activity produces daily huge quantities of mixed biomass, such as cooking wastes, sewage sludge, sawdust, manure... Typical biomass contains mainly carbon (C), hydrogen (H), oxygen (O), sulfur (S) and nitrogen (N).

Fossil fuels that humans extract had undergone a long process; thousands of years of geochemical process converting raw biomass to crude oil and gas. To facilitate this process, researchers have focused on

the conversion pathways of biomass to crude oil. Biomass conversion technologies are broadly classified into two main categories: thermochemical conversion, and biochemical conversion [17]. Biochemical conversion of biomass utilizes enzymes, microorganisms and bacteria to decompose biomass into gaseous or liquid fuels [18]. In general, the unprocessed biocrude derived from biochemical conversion has low energy output, high moisture content, and creates problems in the reciprocating engines due to its physical properties. The main goal of thermochemical conversion is to upgrade biomass to crude oil by heating, and in some cases under pressurized and oxygen-deprived medium. Researchers focused on thermochemical conversions, which are much faster and applied at higher degrees of temperature compared to the biochemical process, producing higher quality fuels. Thermochemical conversions could involve catalysts and include combustion, pyrolysis, and hydrothermal processes [7]. Hydrothermal processes can be classified into carbonization, fractionation, liquefaction and gasification.

Hydrothermal biomass carbonization is an effective, environment friendly technique that produces high energy density solid fuels (with high carbon density). It converts different biomass feedstock into high carbon content, smokeless solid fuels at a pressure ranging from 2 to 10 MPa and temperature ranging between 180 and 250 Celsius degrees [19]. Hydrothermal fractionation is a process where biomass can be transformed into energy carriers and other chemicals, in which certain types of biomass are fractioned back into their initial block compositions, producing hydrocarbons and other chemical products at subcritical or supercritical water conditions [20]. Hydrothermal liquefaction is a chemical process used to convert wet biomass into crude oil, known as biocrude, under high temperature condition (280-370 Celsius degrees) in a pressurized medium (10-25 MPa) [21]. Along with the main product, which is biocrude oil, other components are produced in solid, aqueous and gaseous phases. The products of this process have high energy contents and unique feature of enhanced heat recovery compared to other processes [21]. Hydrothermal biomass gasification aims to benefit from the special properties of near and supercritical water as solvent and its presence as reaction partner to achieve a special gas composition, in addition to

high gas yields [22]. Figure 2 shows the different operating parameters of water in each specific region where a thermochemical conversion takes place.

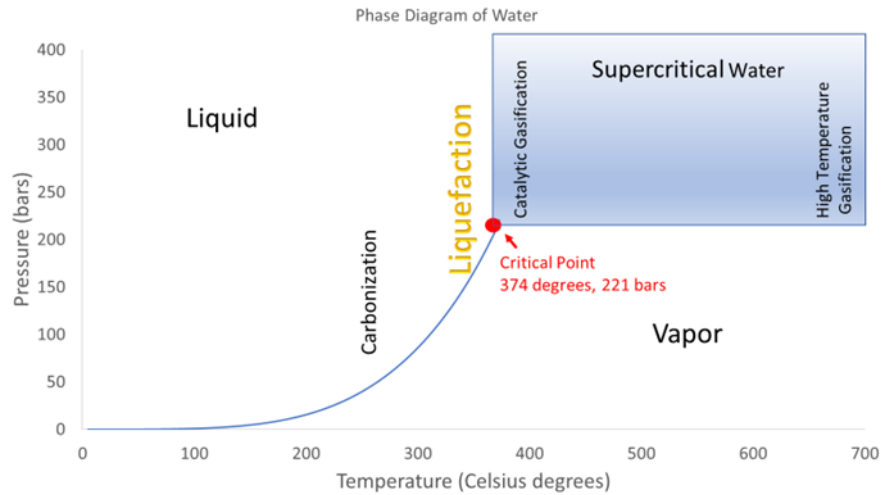


Figure 2: Phase diagram of water showing the regions of thermochemical processes

Hydrothermal processes can be grouped based on reactor type i.e., batch or continuous. In a batch reactor, the biomass is stored in a closed tank, where it is subjected to the required pressure and temperature, and left long enough so the liquefaction reaction occurs completely [23]. While in a continuous reactor, the biomass slurry is pumped continuously to a pressurized heat exchanger, where the reactants are heated and the products are separated and collected. Batch reactor systems are efficient to use in small scales, where the investigation of the reaction conditions to obtain optimum product yields is required but they have some drawbacks, such as transient thermal conditions, difficulties in decoupling pressure and temperature, since the pressure is obtained by increasing the temperature of the batch tank, and different contact pattern [23]. When it comes to the process design and non-dimensional analysis for commercial systems, the continuous systems studies give more reasonable basis.

Recently, several works have been interested in understanding the full aspects of hydrothermal liquefaction, focusing on upgrading the process to commercial scales. Table 1 shows the recent surveys covering this topic.

Table 1: Recent surveys covering the hydrothermal liquefaction of biomass

Title	Topics covered	Year	Ref
A review on hydrothermal liquefaction of biomass	<ul style="list-style-type: none"> • Elemental composition of biomass • Biomass feedstock • Evolution of HTL over decades • HTL process mechanism • Energy efficiency of HTL process 	2018	[21]
Catalytic hydrothermal liquefaction of algae and upgrading of biocrude: a critical review	<ul style="list-style-type: none"> • Catalytic hydrothermal liquefaction of algae • Catalytic upgrading of biocrude • Reaction mechanism in algae HTL and its biocrude upgrading • Perspective and challenges 	2018	[24]
A review on hydrothermal processing of microalgal biomass to biocrude, knowledge gaps and recent advantages	<ul style="list-style-type: none"> • Biomass to biofuel conversion techniques • Effect of hydrothermal liquefaction process conditions • Knowledge gaps and directions for future research 	2019	[25]
A review on hydrothermal co-liquefaction of biomass	<ul style="list-style-type: none"> • Fundamentals of HTL • Hydrothermal co-liquefaction • HTL of biomass model compounds • Modelling of HTL of biomass • Challenges and recommendations 	2019	[26]
Recent development of hydrothermal liquefaction for algal biorefinery	<ul style="list-style-type: none"> • Reaction pathways in algal HTL process • Direct HTL of algae for biocrude production • A novel modified HTL process – sequential HTL (SEQHTL) • High value co-products from algae • Technoeconomic analysis and life cycle assessment 	2020	[27]
Hydrothermal liquefaction of biomass to fuels and value-added chemicals: Product applications and challenges to develop large – scale operations	<ul style="list-style-type: none"> • Advantages and weaknesses of using water as reaction media • Characteristics of HTL products • Potential applications of HTL products • Continuous HTL and key challenges for its industrialization • Future perspectives 	2020	[28]
Review on sustainable production of biochar through hydrothermal liquefaction:	<ul style="list-style-type: none"> • HTL biochar • Mechanism • Biochar yield • Physical properties of HTL biochar 	2020	[29]

Physiochemical properties and applications	<ul style="list-style-type: none"> • Chemical properties of HTL biochar • Applications of HTL biochar • Life cycle assessment (LCA) and energy analysis • Opportunities, challenges and perspectives 		
Hydrothermal liquefaction of lignocellulose for value added products: Mechanism, parameters and production application	<ul style="list-style-type: none"> • Liquefaction mechanism of lignocellulose • Process parameters of hydrothermal liquefaction • Hydrothermal liquefaction products and applications • Techno-economic and environmental analysis • Perspectives and prospects 	2021	[30]
Hydrothermal liquefaction of biomass for biocrude production: a review	<ul style="list-style-type: none"> • Elemental composition of biomass • Types of biomass • Evolution of HTL process over decades • HTL process mechanism and depolymerization reaction of biomass • Effect of operating parameters • Description and evaluation of products and process advancements • Energy efficiency of HTL • Kinetic analysis 	2022	[13]
Hydrothermal systems to obtain high value-added compounds from microalgae for bio-economy and bio-refineries	<ul style="list-style-type: none"> • Macroalgae as a sustainable source of valuable compounds • Current challenges for the cultivation and extraction of high-value compounds from macroalgae • Engineering principles of hydrothermal systems to obtain high value-added compounds • High-value added compounds from macroalgae obtained with hydrothermal treatments • Potential of hydrothermal systems to obtain valuable compounds from macroalgae • Perspectives 	2022	[31]

Referring to the above table, several aspects of hydrothermal liquefaction were studied in previous literature, but no review was directly oriented on continuous systems used for hydrothermal liquefaction of

biomass, regarding all the systematic design and the effect of operating parameters, in addition to the transition from batch to continuous processing, and the challenges facing the commercialization of such a process.

The next section describes the different types of continuous hydrothermal liquefaction systems, their main components, their mode of operation, and the effect of operating parameters and biomass composition on reaction product yields and system design. It also discusses previous research works concerning this technology, by comparing and analyzing them, trying then to achieve a common base for design and operating conditions choices leading to the conception of continuous reactors.

2. Continuous Systems, Components and Operation

Any continuous liquefaction system consists of a set of typical components: a feeding system, where the biomass slurry is introduced into the reactor at a high pressure capable of reaching the desired temperature of the reaction, a reactor, where the pressurized biomass is heated through an external heating source and the liquefaction reaction takes place, and a separator for collecting the products.

2.1. Reactor

The reactor may be considered as the heart of the continuous hydrothermal liquefaction systems, it is the part where the chemical reaction takes place. Continuous reactors can be classified into two main broad types; plug flow reactors (PFRs) and continuous stirred tanks reactors (CSTRs).

2.1.1. Plug Flow Reactor

The most common reactor type used for continuous hydrothermal processing is the plug flow reactor (PFR), known also as piston flow reactor, or continuous tubular reactor (CTR). It is used to study the chemical reactions accompanied with the heat transfer occurring due to these chemical reactions, whether they are endothermic or exothermic [32]. A typical plug flow reactor could be a tube packed with catalyst, called packed bed reactors or PBR's. Sometimes, the reactor's setup can be a shell and tube heat exchanger. Figure 3 shows a cylindrical section of a plug flow reactor.

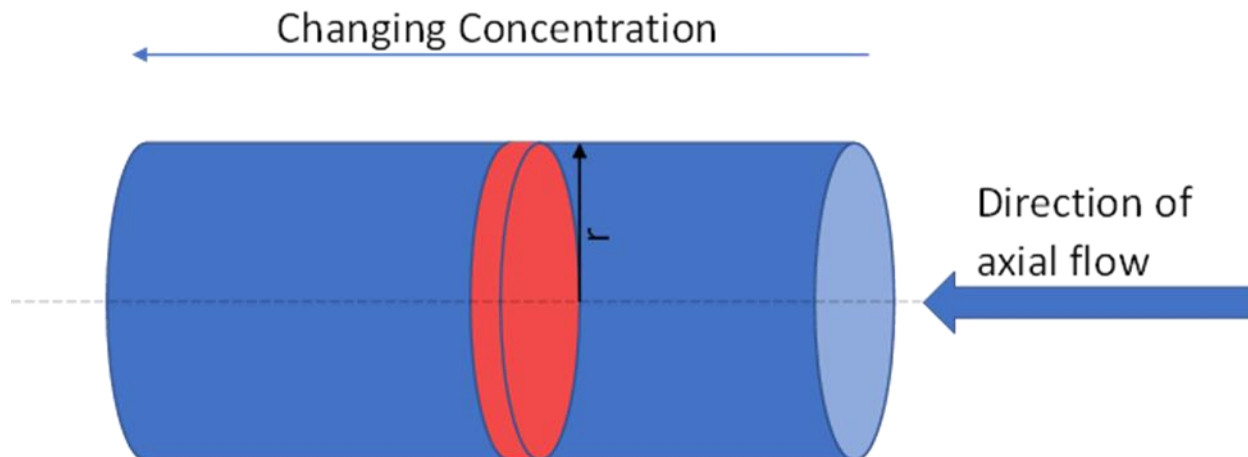


Figure 3: A plug flow reactor section

The simplest example of a plug flow reactor may be considered in Prapaiwatcharapan's et al [33] experiment for the hydrothermal liquefaction of microalgae to produce biocrude, as shown in Figure 3. The reactor has a 0.5" outer diameter, and 0.083" steel pipe thickness, placed in an electric heater, capable to increase the biomass slurry temperature to 360 Celsius degrees [33].

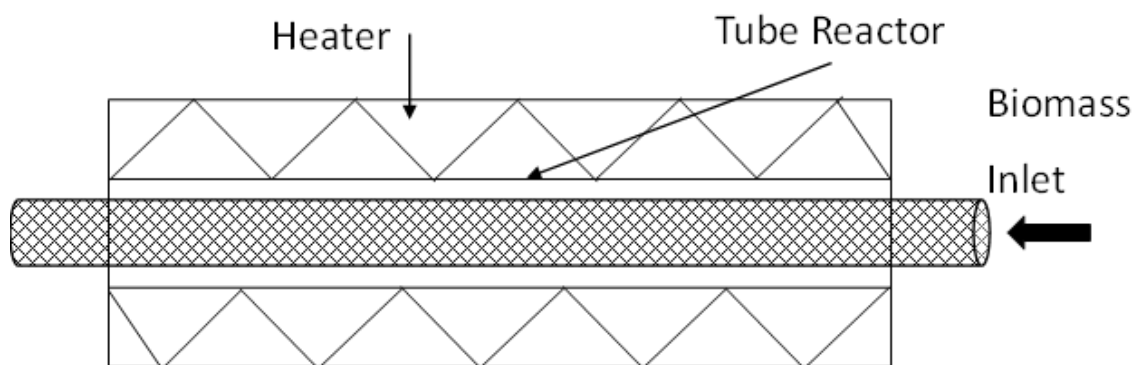


Figure 4: Tube Reactor of Prapaiwatcharapan et al, redrawn from [33]

Researchers used many simple lab-scale reactors of this form. For example, Vo. TK et al [34] used a 7.5 mL micro tube reactor for the liquefaction of microalgae, Xiu S et al [35] used a 1 L PFR in the liquefaction of swine manure. Bi Z et al [36] used also a simple 25 mL tubular PFR in the liquefaction of Sorghum.

Other reactors might be scaled up even though they are still at lab scale. As an example, the semi-pilot scale continuous reactor built by Makishima et al [37] is shown in Figure 5.

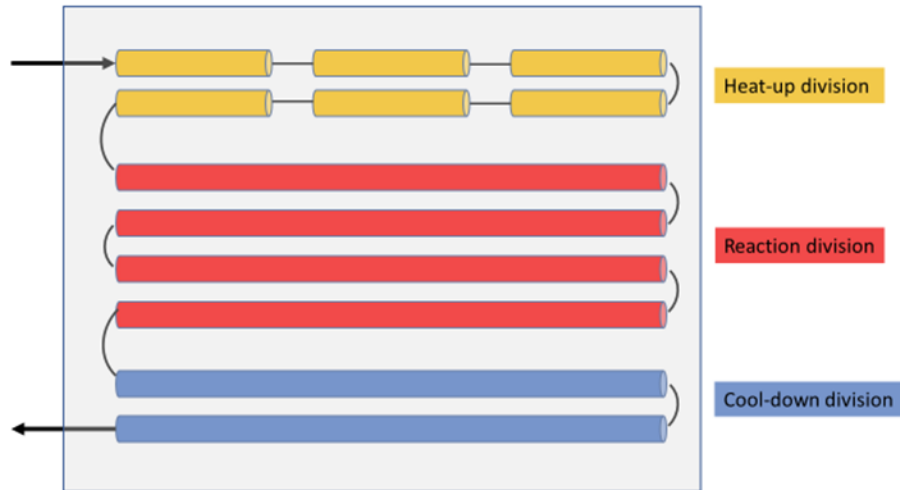


Figure 5: Continuous plug flow reactor of Makishima et al, redrawn from [37]

This reactor is a plug flow type; it is an assembly of different sections in a transportable box shape. It consists of three main divisions; a heating division, in which six identical Metalock heaters (electric resistances), 1.25 kW each, are placed to ensure the preheating on the biomass slurry, a reaction division in which four super sheathed heaters, 1 kW each, are placed to rise the temperature to about 230 Celsius degrees, and finally, a cool down division, where double chilled water pipes are used to bring back the products to ambient temperature [37].

Wadryzka et al [38] used a cylindrical reactor, plug flow type, for the hydrothermal liquefaction of microalgae; the reactor was made of stainless-steel, with a length of 5.5 m, 6 mm outer diameter and 3 mm inner diameter. The reactor was coiled in 22 rings for compacity reasons. A vertical tubular electric furnace was used for heating. Figure 6 shows a schematic representation of the reactor's setup.

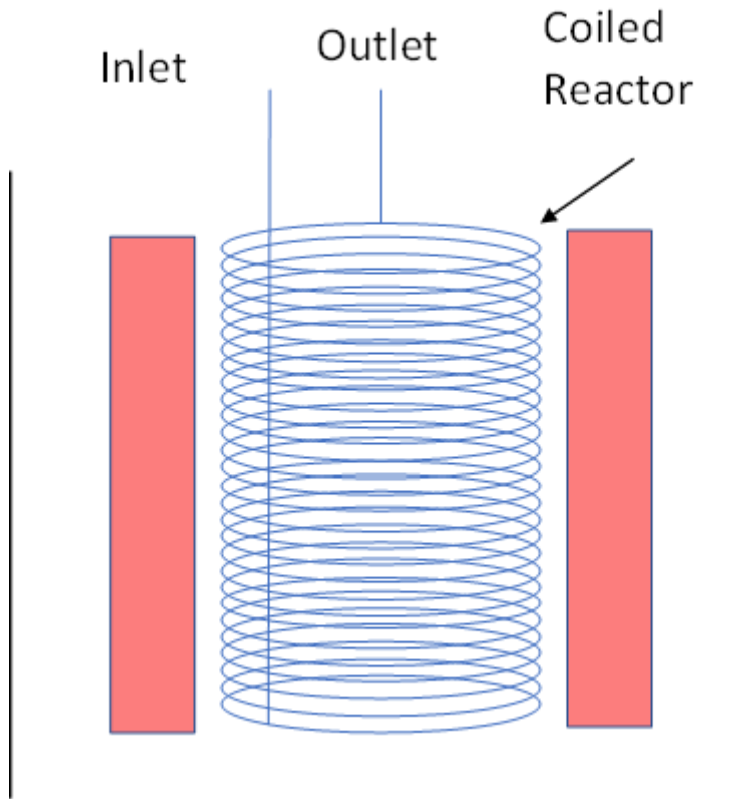


Figure 6: Wadryzka coiled tubular reactor, redrawn from [38]

Another coiled reactor was used by Jazrawi et al. [39] for the hydrothermal liquefaction of microalgae. The reactor consists of four stainless steel coils placed in a heated fluidized bed; each is 16 m in length, 9.5 mm outer diameter and 1.65 mm wall thickness. Four electric heaters, 6 kW each, are used

for heating. The reactor's setup allowed varying the residence time between 0 and 30 minutes. The reactor's configuration is shown in Figure 7.

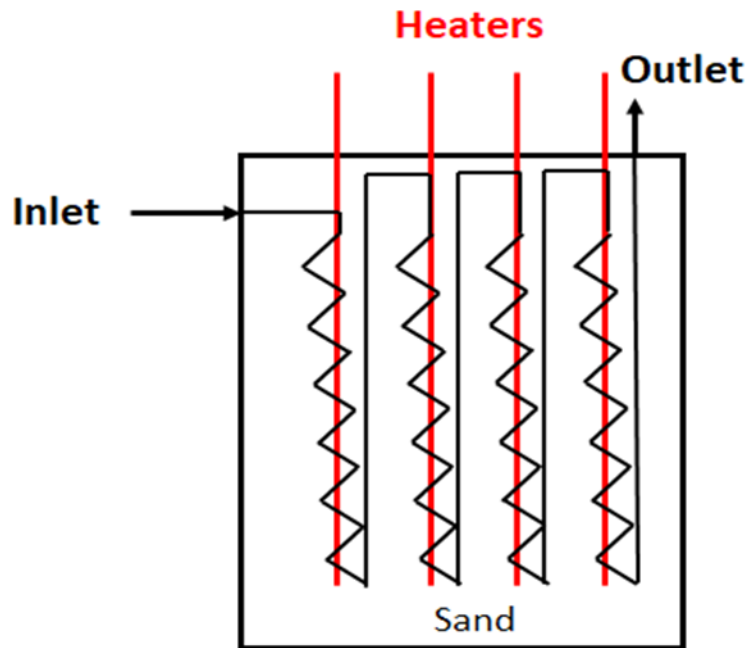


Figure 7: Jazrawi's reactor, redrawn from [39]

In addition to electric heaters, flue gases and solar energy can be used to heat up the hydrothermal reactors, which will be discussed in the Heating Modes section 2.3. For example, Chao Xiao et al [40] used a parabolic trough collector to collect solar energy and heat up their reactor for the liquefaction of microalgae, as shown in Figure 8 **Error! Reference source not found.** The absorber of this collector, which acts as a plug flow reactor, is a double tube, where the microalgae slurry passes through the internal tube, and a glass vacuum tube surrounds it.

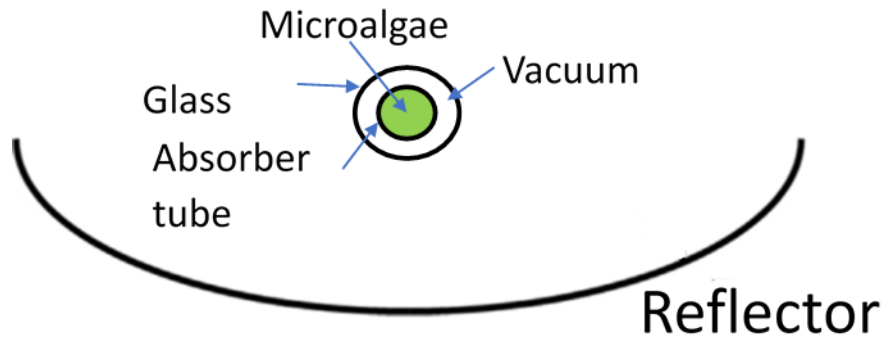


Figure 8: Parabolic trough reactor and absorber acting as a plug flow reactor, redrawn from [40]

In addition, Tippayawong et al [41] had built a continuous plug flow reactor for the carbonization of cassava rhizome, as shown in Figure 9. The reactor is made of 6 mm thick tube of stainless steel SS400, of 1.4 meters length and 1.05 cm internal diameter, heated by the flue gases coming from the furnace due to the combustion of diesel in a separate combustion chamber [41].

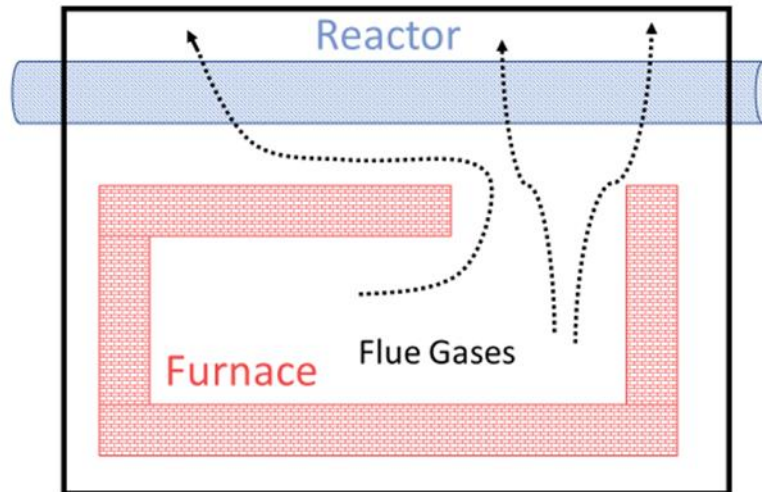


Figure 9: Cassava Rhizome Continuous Carbonization Reactor, redrawn from [41]

Another PFR reactor was used by Hammerschmidt [42] in the hydrothermal treatment of waste biomass. The reactor is up-flow type, half a meter long and 18 mm internal diameter, equipped with an integrated heater.

Haverly et al [43] used a stainless-steel vessel in their experiments of biomass liquefaction in a hydrocarbon solvent. The vessel is a 108.1 cm length and 8.9 cm internal diameter pipe, having a volume of 7.1 L. The reactor was made of 316 series stainless steel to reduce corrosion.

Wagner et al [44] used a continuous-type reactor in the liquefaction of microalgae. The reactor has a double tube, heated by a furnace. Feedstock entered through the inner tube from the top, the products then flowed back up the outer tube of the reactor and to exit again from the top.

The plug flow reactors have some dominating advantages. The maintenance of those reactors is easy due to the fact that they have no moving parts, they are mechanically simple, and have high conversion rate per reactor volume. They are practical for studying rapid reactions and ensure unvarying product quality. Also, they can be used for large capacity processes because of their efficient use of reactor volume, and low pressure drops. On the other hand, these reactors are considered difficult to control due to the composition and temperature variations [45]. This means, in these continuous reactors, reactions have no unique temperature range; they differ from each other according to the biomass used, and according to the required final composition of products.

The operating temperature of a liquefaction system has a direct influence on the material used to build the reactor. For example, high liquefaction temperatures (300 Celsius degrees and above) require stainless steel reactors, regardless of the reactor's type. Although some other metals may have higher conductivity, such as copper, but may have high thermal expansion ratios which are not favored in such applications [46]. When Keerati et al [33] reached 360 Celsius degrees in their hydrothermal liquefaction of microalgae, they used a 30 mL stainless steel tube as a reactor. Also, when Mariusz et al [38] reached 350 Celsius degrees in their hydrothermal liquefaction of microalgae, they used a coiled steel reactor. Whereas in the experiment of Chao et al [40], the required temperature did not reach 200 Celsius degrees, then the use of a copper was more efficient than steel, in order to enhance the heat transfer between the solar collector and the biomass slurry.

The operating pressure of the hydrothermal liquefaction system creates internal forces and stresses in the materials used to build the reactor. Usually, stainless steel is suitable for any range of operating pressure based on the reactor's design to hold these conditions. Many researchers, [33], [37], [42], [43],[44] used stainless steel reactors in their experiments with operating pressures ranging from 30 to 250 bars.

2.1.2. Continuous Stirred Tank Reactor

Continuous stirred tank reactors (CSTRs) are open systems through which the feedstock flows and can enter and exit the reactor. CSTRs usually operate in a steady state phase, where the conditions in the reactor are assumed constant with time. Reactants and products are continuously added and removed from the system.

The slurry's properties inside the reactor, such as the pressure, density, temperature, etc...are considered uniform, because of the perfect mixing the CSTRs undergo. In addition, the products conditions at the exit are the same as those inside the reactor.

CSTRs are used in chemical engineering to estimate the key unit operation variables in a chemical reaction such as residence time[25][39]. Figure 10 shows an example of a stirred tank reactor used by Kumara et al [47] for the production of biocrude through the liquefaction of microalgae.

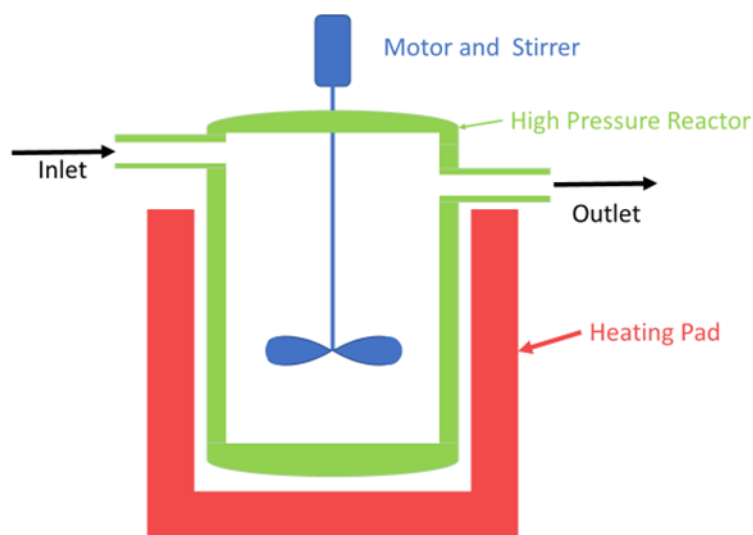


Figure 10: Continuous stirred tank reactor

Bingfeng Guo et al [48] worked on the production of biocrude from microalgae, and upgrading it using a nickel catalyst. The liquefaction reaction took place in a stirred tank reactor, as shown in Figure 11, at 350 Celsius degrees, and 24 MPa.

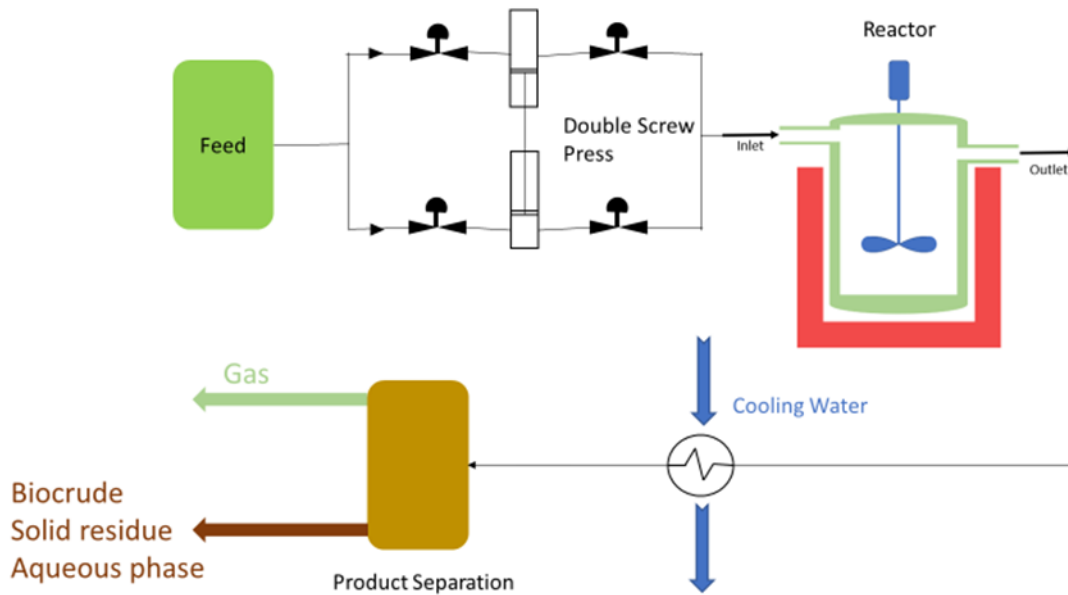


Figure 11: CSTR continuous reactor for the production of bio-oil, redrawn from [48]

While Osfemia et al [49] chose a CSTR to achieve an easier temperature control in the reactor to produce biocrude from swine manure through hydrothermal liquefaction.

The CSTRs are considered as simple reactors, cheap to construct, and their interior is easily accessed. On the other hand, they have large heat capacities and the conversion of reactants per unit volume in a CSTR is too small compared to PFRs; it can also develop dead zones, where no mixing occurs. Furthermore, if the outlet is improperly placed, reactants can bypass [45].

The material used in building the CSTRs is mainly stainless steel, which is used in Kumar's [47], Guo's [48], and Osfemia's [49] reactors. This is due to its relatively high heat transfer coefficient, capability to hold high temperatures, and its resistance to internal forces caused by the reaction's pressure.

2.1.3. Combined CSTR – PFR Reactors

In 2013, Elliott et al [50] built a catalytic continuous hydrothermal liquefaction system, in which they used a stirred tank and a plug flow reactor combined together, as shown in Figure 12. Here, the CSTR is considered as a perfect preheater for the biomass slurry.

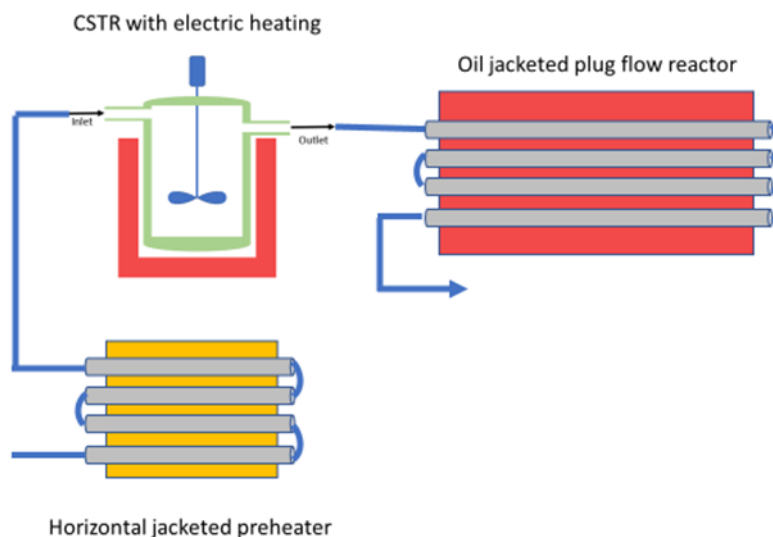


Figure 12: Combined CSTR-Plug flow reactor, redrawn from [50]

The strength of the combination between CSTR and PFR in Elliot’s reactor was its ability to avoid plugging in the PFR by reaching 200 Celsius degrees in the PFR [50]. Also, scaling up the hybrid system costs less than a CSTR (alone) based design [51].

Elliot’s reactor was an inspiration for other researchers and scientists to do experiments on hydrothermal liquefaction using combined CSTR-PFR reactors due to their previously mentioned advantages.

For example, in 2016, Albrecht et al [52] used the model of Elliot et al for studying the effectiveness of biocrude production from microalgae through catalytic hydrothermal liquefaction process in continuous-flow reactors. A continuous stirred tank reactor of 415 mL volume was followed by a continuous plug flow reactor of 270 mL volume to build the hydrothermal system acquired.

In another work, Collett et al [53] also used the model of Elliot et al for obtaining renewable diesel through hydrothermal liquefaction of lignin and yeast. The model consisted of a continuous stirred tank reactor of 1000 mL volume followed by continuous plug flow reactor of 300 mL volume.

The choice of a reactor configuration for a continuous hydrothermal liquefaction system depends on several criteria. In the case of abundant cheap heat source (Flue gas for example) and/or the need of simple and robust system (for small scales or rural areas for example), the CSTR might be a good choice. In another case, if the energy cost is taken into consideration, and the space issue is important, the choice of a plug flow reactor would be a better choice. The mixed CSTR-PFR reactor would be ideal in cases where the biomass slurry needs heating and mixing before undergoing hydrothermal liquefaction, especially if the viscosity of the reactants decreases with the increase in temperature, which will help in avoiding plugging inside the plug flow reactor [54].

2.2. Feeding Systems

A continuous hydrothermal liquefaction system needs a continuous flow of biomass slurry, and in catalytic liquefaction, it needs a continuous catalyst flow. This could be achieved through high pressure feeding systems.

2.2.1. Biomass Feed

Feeding through high pressure pumps

The feeding of reactors can be achieved using high-pressure pumps to ensure the required head needed for hydrothermal reactions to take place. Pumps may vary from one system to another; either by type, maximum pressure head or required flow rate. Xiao et al [40] used a plunger pump to drive their solar system for the liquefaction of microalgae, with an outlet pressure of 28 bars and a volumetric flow rate up to 90 L/hr.

Some high-pressure pumps need an inlet head above atmospheric pressure to operate, thus, in some high-pressure systems; two-stage pumping is required. Jazrawi et al. [39] used two pumps in their

continuous system for the continuous hydrothermal liquefaction of microalgae (Figure 13). The first pump is the “low-pressure” pump (screw type) providing the required inlet pressure, about 2 to 6 bar, for the high-pressure stage. The second pump is a triplex piston pump; it delivers viscous fluids and slurries at flow rates up to 90L/h and pressures up to 600 bars.

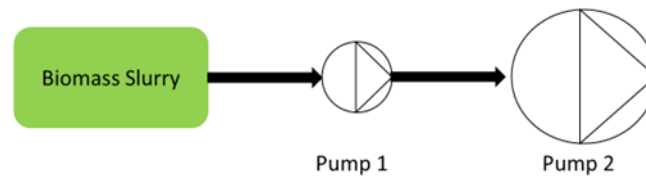


Figure 13: Two-stage pumping system

Feeding through pressurized gas

In the lab scale prototypes, the available pumps are not designed for biomass pumping, thus, they may face some problems concerning the continuous flow, the fluid friction and cavitation issues. For this reason, another biomass feeding method using pressurized gas, such as nitrogen, is used. The disadvantage of this method is that there is no precise control for the mass flow rate, as it can be achieved easily through pumps, thus regulating valves and tanks must be used (Figure 14) [44].

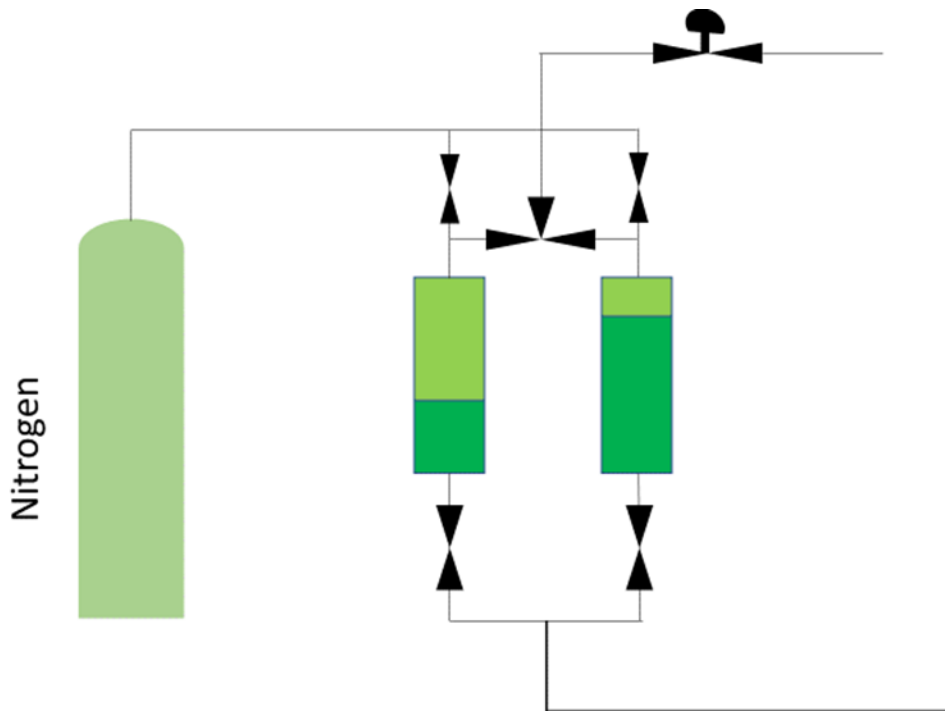


Figure 14: Feed delivery system using pressurized nitrogen gas

Using pressurized nitrogen gas, Mariusz et al [38] achieved a pressure of 150 bars in the liquefaction of microalgae and Wagner et al [44] reached a pressure of 165 bars. Whereas, Saqib et al [55] used high pressure pump to reach 250 bars in the liquefaction of distilled grains.

In small scale systems, no matter what is the chosen feeding system, both will operate normally, but when it comes to commercial systems with large scales, using large quantities of pressurized nitrogen would induce high costs, thus the use of high-pressure pumps is preferred.

2.2.2. Catalysts Feed

Christenen et al [56] studied the influence of ZrO_2 , as a catalyst, on the hydrothermal liquefaction of dried distiller grains to produce biocrude in a CSTR. They found that it is a poor catalyst, having minor changes on the biocrude yields, but they adopted an efficient technology for feeding the reactor with the desired catalyst. A 24-carat golden catalyst (Figure 15) was constructed and inserted into the reactor, to provide an inert chemical medium and protect the reactor from corrosion in addition to providing the

catalyst. The catalyst bed was able to rotate freely inside the CSTR. The catalyst remains in the bed and can be easily recovered after the end of reaction.

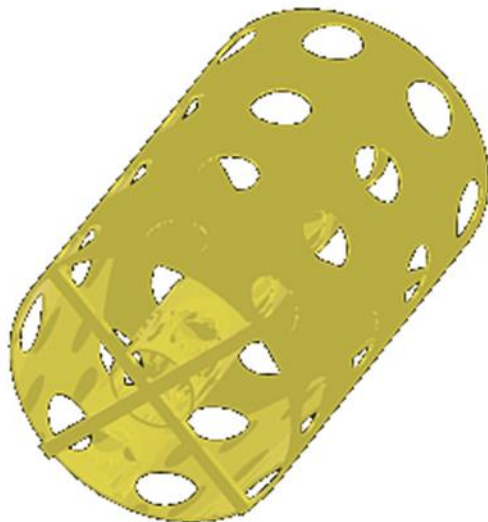


Figure 15: Golden Catalyst bed of Christinen's experiment [56]

Another experiment led by Jazrawi et al [39], a continuous tubular reactor was used for the liquefaction of microalgae. The potassium catalyst was placed in a stationary catalyst bed inside the reactor and the biomass flowed across the bed. This method is usable when the catalyst is heterogeneous.

In the case of homogeneous catalysts, the catalyst is mixed with the feed in the phase of pretreatment, and then the mixture (biomass-catalyst) enters the reactor. Hammerschmidt et al. [42] studied the influence of heterogeneous and homogeneous catalysts on hydrothermal liquefaction; the heterogeneous catalyst was remained as pellets in the catalyst bed, while the homogeneous catalyst was removed from the products through scavenging.

Different methods are applied for the separation of homogeneous catalysts from the products mixture in continuous flow. Most of these methods use the liquid/liquid biphasic systems. Another method for catalyst separation is scavenging, using solid-supported scavenging resins packed into columns. Recently, researchers are using the method of organic solvent Nano-filtration to separate the homogeneous catalyst in the final product flow [57].

2.2.3. Biomass Pre-treatment

In continuous hydrothermal liquefaction systems, in order to facilitate the pumping, it is necessary to prepare the feedstock slurry before introducing it to the pump; this is done through pretreatment process [58].

Biomass is a complex material, which contains various components. One major biomass, the microalgae, needs some pretreatment in order to increase hydrothermal liquefaction feasibility and efficiency. The target products of microalgal cells are usually found inside the cell's membrane, surrounded by a resistant cell wall, thus, the extraction of these products only by solvents is difficult. That is why pretreatment is necessary for microalgal biomass before applying solvent extraction [51], [59]. Pretreatment uses mechanical and non-mechanical methods. Usually, biomass pretreatment for hydrothermal liquefaction focuses on mechanical ones as discussed below.

Mechanical pretreatment methods of biomass include high-pressure homogenization, bead milling treatment, ultrasonication, microwave, and pulsed electric field.

High-pressure homogenization (HPH) pretreats microalgal cells with an elastic cell wall structure (Nannochloropsis for example). In high-pressure homogenization unit, the microalgal cells are pushed using high pressure through a very narrow nozzle, after which they collide to an impact ring, and sent out to a lower-pressure reservoir [60].

Bead milling was approved for crushing microalgal cell walls and extracting the intramolecular matter. This method is carried out through applying instant crushing or shear stresses to the microalgal cells through high speed solid beads, such as glass, ceramics, etc. [60].

Ultrasonication is another technique used for the extraction of sugars, lipids and proteins from microalgae. It operates generally under two main working principles; (1) the acoustic stream and the radiation force, and (2) the effects of cavitation [61]. Ultrasonication through radiation force and acoustic stream utilizes low ultrasonic powers to destroy directly cell walls [62]. In the second case, ultrasounds applied to the liquid microalgae causes the formation of microbubbles, which grow continuously and form

cavitation, after which these bubbles generate impact shock waves to destroy the walls of surrounding cells [63].

Another method used for cell wall disruption is the Microwave technology. Microalgal cells are subjected to microwave radiations which excite the movement of water molecules in the aqueous biomass-water solution. This excitation generates heats, and water reaches its boiling point in a short time, increasing the internal pressure of the microalgal cells. Thus, the cell wall is broken due to heat and pressure resulted from microwave radiations [64].

The last technique for microalgal cells' wall disruption is the pulsed electric field (PEF), which was demonstrated as a cheap method for this issue [65]. PEF treatment utilizes the electroporation effects, in which cells are subjected to high-intensity electric feeds for a short time, leading the cell membrane to become permeable, allowing the extraction on internal molecules (carbs, lipids and proteins) from the cell[60]. Carullo et al [66] investigated the effect of the PEF treatment to extract the intra-molecules from *C. vulgaris*. The results showed that the cell size decreased by about 6%, because of the disruption of the cell wall.

Lignocellulosic biomass is also a feedstock that needs pretreatment to enable its conversion in continuous HTL systems. Pretreatment process aims to extract hemicellulose and lignin from the cells, decrease the crystallinity of cellulose, and enlarge the permeability of the lignocellulosic matter. Lignocellulosic pretreatment must ensure the ability of the biomass to form sugars by hydrolysis, it should not lead to the loss or degradation of carbohydrates, neither to production of byproducts prohibiting or affecting the liquefaction process, besides it should be cost effective [67]. Several pretreatment methods can be applied to lignocellulosic biomass, which may be identical or similar to the ones of microalgae, including: pulsed electric field pretreatment, biological pretreatment, chemical pretreatment, physical pretreatment and physiochemical pretreatments [67]. However, it was found that the solid content of lignocellulosic biomass could not be increased above 15%. Iulia et al [58] had achieved a higher solid mass content (20%) using two different pretreatment methods. The first one is to use HTL recycle biocrude as a carrier fluid, and the other is mixing the slurry with alkalis, focusing on the particle size and its effect in

creating the pumpable biomass fluid. They also found that the slurries' viscosity is decreased from the range of 100 – 1000 Pa s to approximately 1 Pa s after the application of thermal treatment [58].

2.3. Heating Mode

The hydrothermal liquefaction reactions need high temperature, 280 to 370 Celsius degrees, to take place, which means that an external heating source needs to be implemented in the system to ensure the required temperature.

2.3.1. Electrical Resistance Heating

Makishima et al [37] used electrical resistance heating in their lab scaled reactor to obtain a temperature of around 230 Celsius degrees. Jazrawi et al [39] used 4×6 kW electric heaters for heating the fluidized bed of his reactor. Elliot et al [50], Albrecht et al [59] and Collett et al [68] also used electric resistance heating in the preheating step in the CSTR for the continuous combined hydrothermal liquefaction systems to achieve a temperature of around 300 Celsius degrees. In Hadhoum et al. work [69], [70], a batch reactor of 998 ml was used, it was heated using electric resistance power up to 20 kW, providing a temperature up to 450 Celsius degrees. Electric resistance is a great heating mode when it comes to laboratory scaled systems for control and precision issues, but when it comes to industrial large-scale applications electricity is not cost-effective.

Electric resistance heating is considered perfectly efficient (100%) due to the fact that all the consumed electric power is transformed to heat. Still, the greatest portion of electricity is produced from petroleum or coal generators. In these generators, only around 30% of the fuel's internal energy is transformed into electricity, in addition to the transmission losses. This fact increases the electric heating cost over that of heat generated by combustion appliances using conventional or biofuels [71].

Concerning the heating rate, a controlled heating rate or constant medium temperature can be best achieved using electrical resistance, because the solar heating and heating through flue gases are somehow

hard to be accurately controlled. Saqib et al [55] used electric resistance for heating up their reactor when it comes to varying the heat rate in a lab scale reactor.

2.3.2. Solar Heating

Another mode of supplying heat energy to the liquefaction reactor is the solar heating. Solar energy can be transmitted to the reactor through collecting and concentrating it in one region, using a parabolic trough collector for example[40], or a concaved solar mirror[72].

Xiao et al [40] used the parabolic trough collector in their liquefaction system to reach a biomass reacting temperature of around 200 Celsius degrees.

Solar heating is a good choice for hydrothermal liquefaction when it comes to large-scale applications, although it has a high building initial cost, but it will eliminate the running costs for heating the high flow rates of biomass slurry. For a successful efficient continuous hydrothermal liquefaction system, the solar heating mode may be the best choice.

Despite its advantages, solar heating mode cannot be used as a stand-alone solution due to its intermittent character.

2.3.3. Heating by Flue Gases

It is used when high temperature values are required for a liquefaction reaction, since the flue gases are able to carry much energy and reach high temperatures (more than 1000 Kelvins) [41]. In 2016, Tzanetiz et al [73] used a separate combustion chamber for preheating and heating the biomass for the production of renewable jet fuel, in which they attained high temperatures of 450 Celsius degrees.

Flue gases are not used in lab scale systems, but they are widely used in all industrial domains seeking high temperatures and high energy inputs.

For industrial systems, flue gases may be an excellent choice; flue gases are considered excellent energy carriers and can achieve relatively high temperatures. Furthermore, flue gases of power plants (engines or turbines) can be used as cheap sources of energy to feed HTL reactors.

2.3.4. Heating by Fluidized Beds

Fluid bed is a technology for drying, cooling or heating solid matter. In fluidized beds, gas (commonly air) passes through a porous plate, then it runs through a bed (layer) of solids to be heated. In this heat exchanging method, the gas plays two roles:

- Passing through the solid bed at an enough speed to carry the particle's weight, creating a fluidized medium, thus permitting the solid particles to flow.
- Cooling, heating and drying the solid particles, due to the direct contact between the solid and the gas phases [74].

Tippayawong et al [41] used flue gases in their continuous reactor, where they reached a biomass slurry temperature above 300 Celsius degrees where flue gases of more than 700 Celsius degrees were heating the reactor.

The required temperature and the heating rate affect the choice of the heating mode required for the hydrothermal liquefaction system. High temperatures may be achieved either by electric resistance heating or by flue gases. On small experimental scales, electric resistance may be a better choice due to its quick response, but on large commercial scales, flue gases dominate, due to their cost-effectiveness.

2.3.5. Heat Exchangers and Heat Recovery Systems

Other than the hydrothermal reactors (plug flow or stirred tanks), heat exchangers (HX) are used in the continuous hydrothermal systems for preheating, regeneration and cooling. The most common type of heat exchangers used is the concentric tubes (counter-current flow and concurrent flow, based on the operation). Xiao et al [40] used a double pipe steel cooler, 12-meter-long, 2 mm wall thickness, with 36

mm and 16 mm outlet diameters for cooling the products coming out from the reactor to ambient temperature, the cooler is shown in Figure 16.

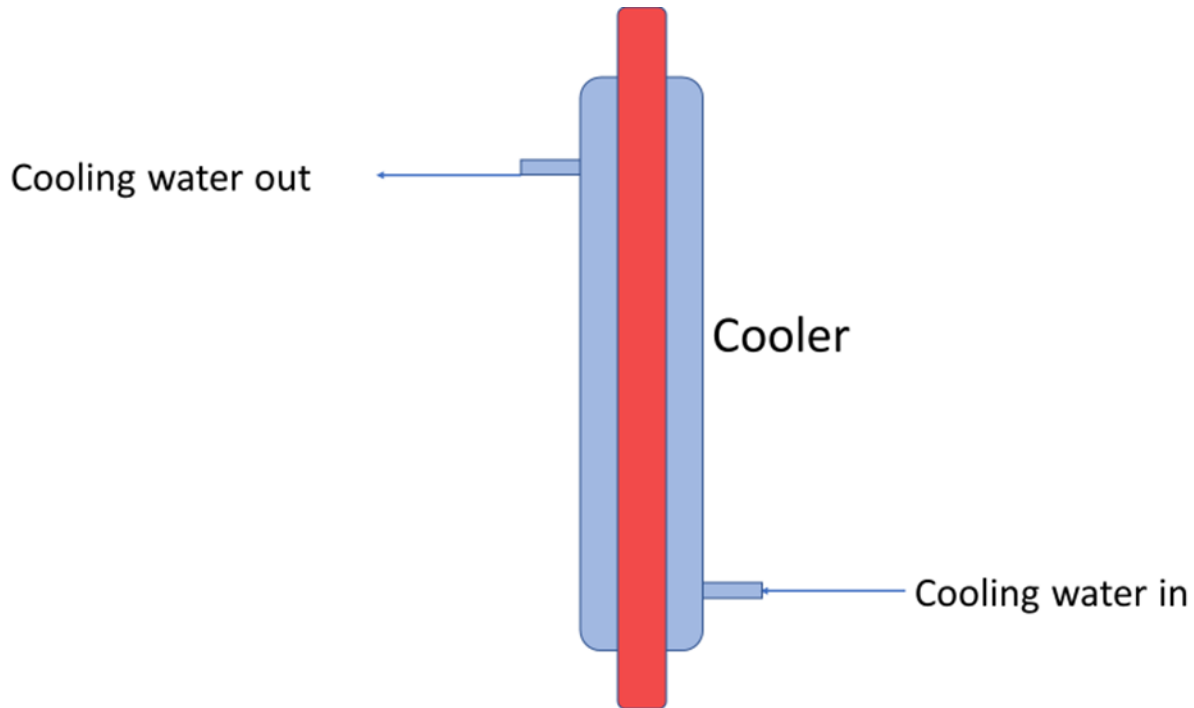


Figure 16: Xiao's Solar hydrothermal liquefaction system cooler, redrawn from [40]

Heat recovery systems are those that benefit from excess heat in the system and use it in preheating the biomass to be reacted. This operation is beneficial in economic and energetic terms, it decreases the heat input needed for the reaction, and increases the overall efficiency of the system.

Jazrawi et al [39] used a more advanced heating/cooling technology for their reactor, including regeneration through more than one heat exchanger as shown in Figure 17. The products of liquefaction exit the reactor to a first heat exchanger where they are cooled through a closed distilled water loop, then they pass through the two preheaters where they are cooled to the initial biomass temperature.

2.4. Separators

Products obtained from hydrothermal liquefaction are usually a mixture which needs specific separation methods to extract the desired sub products. For instance, in the hydrothermal liquefaction of microalgae, mixture obtained in the products comprises bio crude (mostly hydrocarbons), aqueous phase (wastewater) and residues. Normally, during the separation protocols for product recovery, organic solvent is added to the product mixture, which dissolves and allows phase separation for fractional yields[77]–[79].

The products of hydrothermal processes can exit in three states: solid, liquid and gaseous streams. First of all, the separation of gas streams apart of the mixture is done by holding the products in a receiver, where light gases flow to its top, and can be removed easily. The separation of solid residues or products (solid carbon) may be done through filtration and screening. Washing the remaining products with acetone may be helpful to obtain bio char apart from the products, and the liquid products are separated from each other through separating funnels[80].

Although there are no much studies dealing with continuous biomass liquefaction products separating systems. Haverly et al [43] used a number of separators in their hydrothermal liquefaction system to produce biocrude. This experiment may be enough to understand different mechanisms of separating hydrothermal liquefaction products (Figure 18, Figure 19 and Figure 20).

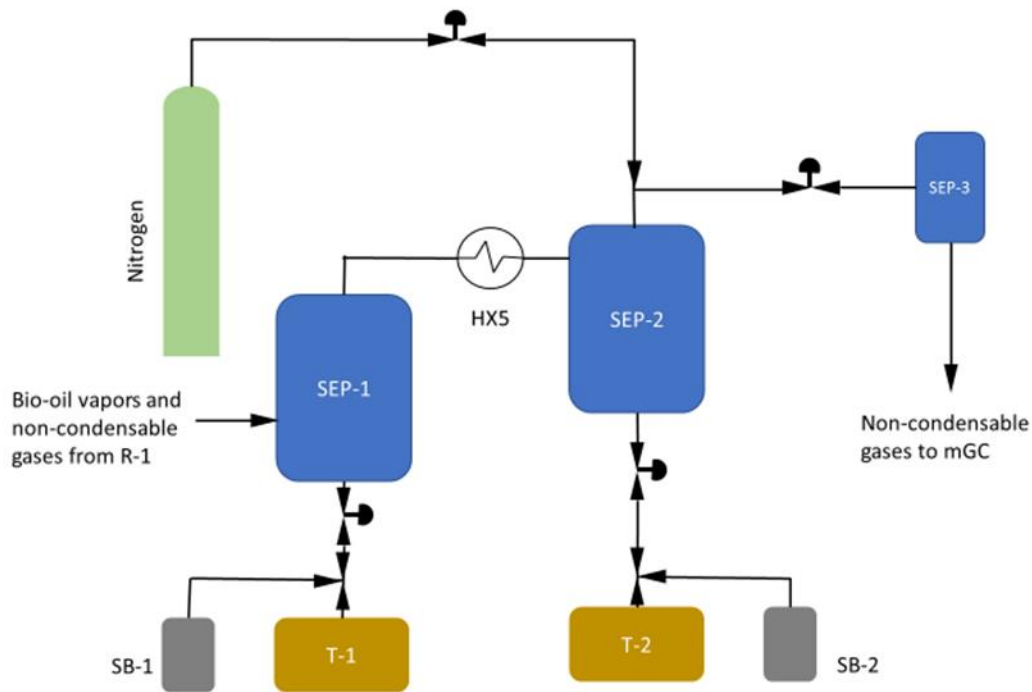


Figure 18: The first three separators of Haverly's system, redrawn from [43]

Figure 18 shows the first separation step of Haverly's system. Separators 1 and 2 (SEP-1 and SEP-2) are identical. Separator 1 contains two different heating areas. The bottom part ensures the temperature of liquid stabilized at 260 Celsius degrees, whereas the upper part maintains 302 Celsius degrees' vapor temperature. The zones' temperatures are selected to maintain a vapor phase for light oxygenates and water, and condense phenolic monomers and hydrocarbons generated from liquefaction of biomass. Vapor exiting separator 1 passes through a double tube heat exchanger, cooled with propylene-glycol, used to decrease its temperature to 27 Celsius degrees approximately. Separator 2 is not insulated; it operates at room temperature, in which remaining condensable products are gathered. Non condensable products (gases) in separator 2 pass to separator 3 to undergo analysis and monitoring, after trapping any remained liquid through the knockout vessel.

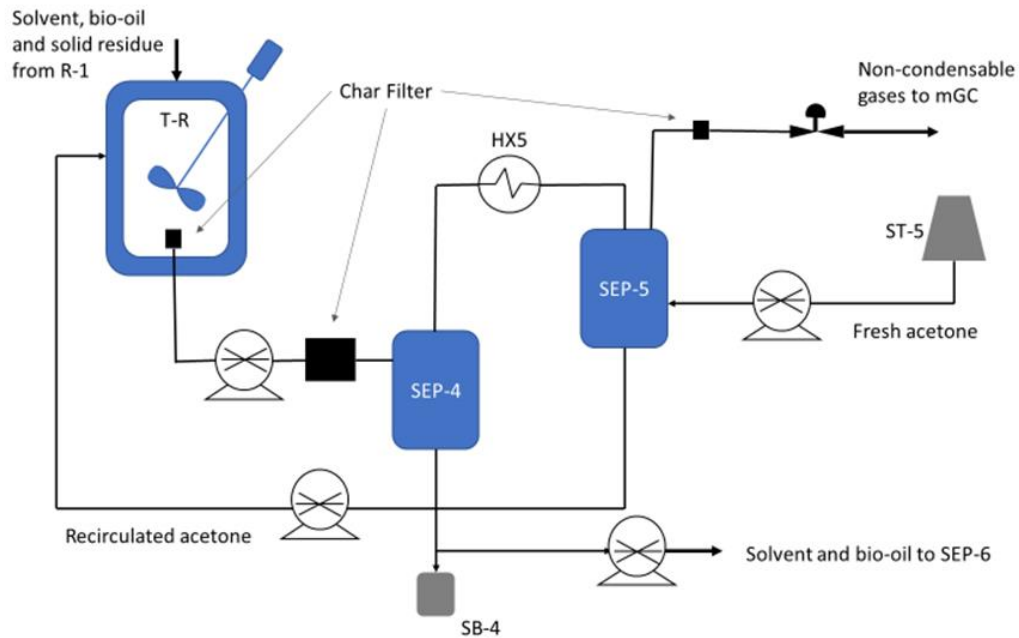


Figure 19: Second two separators of Haverly's system, redrawn from [43]

The second separation step of Haverly's system is presented in Figure 19. Liquid at about 120 Celsius degree enters separator 4, which is set at 93 Celsius degrees and a pressure of 1.1 bars. These conditions are set to allow the acetone to evaporate from the liquid phase and to be transferred to separator 5. Due to the presence of compounds with low volatility, acetone only is predicted to evaporate. The vaporized acetone passes through heat exchanger 5 (HX5), where it condenses and cools to 5 Celsius degrees. Separator 5 is similar to separator 4, but held at ambient pressure; in this separator acetone is collected. Fresh acetone is pumped from the storage tank ST-5 to separator 5, after which it is introduced to the solids' removal vessel T-R.

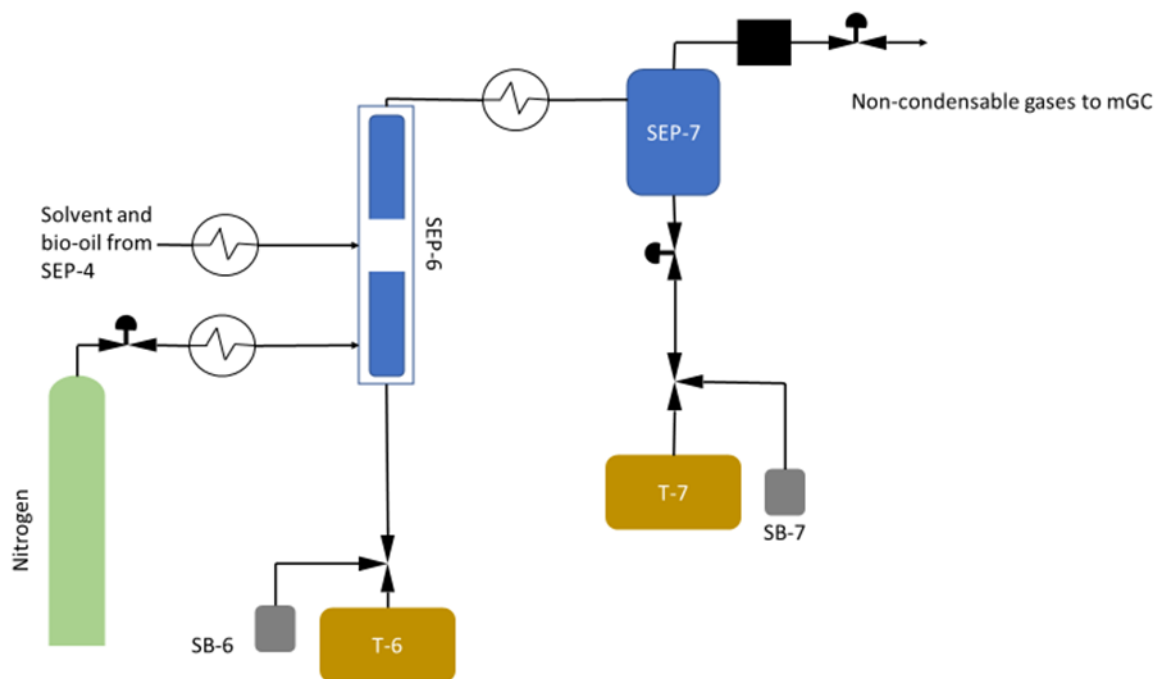


Figure 20: Last separators of Haverly's system, redrawn from [43]

The last separation step of Haverly's system is shown in Figure 20. After the removal of acetone and solids from the liquid phase, biocrude is conducted from separator 4 to the "biocrude fractionation system" shown in Figure 19. This fractionation system separates a portion of the biocrude, containing molecules with boiling points in the range of the hydrocarbon solvent one, and utilizes it as a recycled solvent. Separator 6 functions as a distillation column with 4.7 cm as inner diameter. Finally, the gaseous stream passes through heat exchanger 7, and condenses at 5 Celsius degrees, then it is collected in the separator 7 (similar to SEP-5 and at ambient temperature).

3. Effects of Reaction Parameters on the Liquefaction Process, Products Yields and Systematic Design

Hydrothermal liquefaction reaction occurs and behaves according to many parameters; the variation of these parameters may affect the products, the reaction process and the design of the reactor. These parameters can be, but are not limited to, operating pressure, temperature, residence time, biomass flow rate, solvents and catalysts used, and mass concentration.

Temperature

Previous experimental and theoretical studies proved that temperature is one of the most critical parameters that affect directly the hydrothermal processes of biomass. As the reaction temperature increases, the products' yields also increase till a certain optimal limit. Then, increasing the reaction temperature beyond the optimum value leads to a decrease in the products concentrations due to several side chemical reactions taking place within the reactor. The optimum temperature differs from one biomass to another; it also differs for the same biomass if the required final products are different.

Table 2 summarizes optimum HTL temperatures obtained earlier by different researchers using different feedstock and aiming different products.

Table 2: Temperature ranges and optimum temperature values for different continuous HTL processes

Biomass	Reactor Type	Target Product	Temperature Range (°C)	Optimum Temperature (°C)	Ref.
Jack pine powder	14mL microreactor	Biocrude	200-350	350	[81]
Palm	8.8mL CSTR	Biocrude	330-390	375	[82]
Algae	bench top PFR	Biocrude	180-330	300	[83]
Algae	100 mL bench top microreactor	Biocrude	180-300	300	[84]
Algal Cultures	100 mL cylindrical reactor	Biocrude	260-320	320	[85]
Microalgae	6m length, 32mm diameter PFR	Carbohydrates/Proteins	133.9-168.2	160	[40]
Microalgae	7.5 mL microtube reactor	Biocrude	250-400	400	[34]
Swine Manure	1L PFR	Biocrude	260-340	340	[35]
Crude glycerol and aspen wood	10 mL micro reactors	Biocrude/char	380-420	No temperature effect	[86]
Sorghum	25 mL tubular	Biocrude	300-350	300	[36]
Grassland Perennials	75 mL cylindrical reactor	Biocrude	300-450	374	[87]
Lignocellulose	Autoclave	Biocrude	280 – 360	320, 360	[88]
Lignin	50 mL batch	Biocrude	250 – 310	270	[89]
Alkali lignin	Autoclave	Biocrude	260 – 300	280	[90]
Cellulose	50 mL Batch	Biocrude	280 – 340	320	[91]
α -cellulose	Batch	Biocrude	240 – 340	300	[92]
Xylan-hemicellulose	10 mL Batch	Monosaccharide	110 – 250	210	[93]

Pressure

Pressure is the second parameter affecting the conversion of biomass in hydrothermal liquefaction. Pressure holds the single-phase media for both subcritical (liquid phase) and supercritical (gaseous phase) liquefactions [94]. By maintaining a single-phase medium, large enthalpy inputs are avoided, because two-phase reactions require larger heat supplies to maintain the system's temperature. For instance, using the water-steam charts, the enthalpy input needed to heat the liquid water from 100 Celsius degrees to 200 Celsius degrees superheated steam at 1 bar is 2457.84 kJ/kg of water, whereas the enthalpy input needed to heat compressed liquid water at 25 bars from 100 to 200 Celsius degrees is 431.5 kJ/kg of water.

Biomass Composition

Several works reported different results regarding the bio-oil yield resulting from processing different types of biomass [95]–[97] [70], [98] [82]. These results were analyzed, and it was found that the highest yield (38.53%) is obtained for the lowest hydrogen content (4%) and lowest carbon content (45%), in this case, the remaining elements are at their maximum percentage (around 50%), where oxygen is dominating, and nitrogen is at a lower amount, it may also include phosphorous and other complementary elements. Whereas, at relatively higher values of carbon (45 – 50%) and high hydrogen content (6 – 8%), the yield decreases and reaches its minimum value (8.6%) when the carbon content attains its maximum (50.7%). The results are due to the fact that lower carbon content with higher hydrogen content implies the presence of single bonds, which are stronger than double and triple bonds [99], thus, the energy needed to break down the structure of the biomass is decreased, raising the yield of the products.

In order to know if the ultimate composition of biomass can help to predict the optimum temperature of the HTL process (that gives the maximum biocrude yield), data are taken and analyzed from different studies [11], [28], [60], [61], [75], [77], [88]–[90], [93], [100]–[110]. Results show that highest optimum temperature (> 450°C) is obtained at the highest carbon content (> 55 %) and low hydrogen content (< 5%). For high carbon content, the optimum temperature decreases as the mass percentage of

hydrogen increases (increasing the percentage of other elements). The lowest optimum temperature (220 °C) is obtained for the lowest carbon content (26 %) and lower hydrogen content (< 4%), where other elements attain their maximum percentage.

In addition to the ultimate composition of biomass, the effect of the lignocellulosic composition (cellulose, hemicellulose and lignin) of the biomass on the optimum temperature is also studied. Using collected data [12], [35], [36], [49], [70], [85], [97], [98], [111]–[114]. The results show that the highest optimum temperature (> 350 °C) is obtained for the highest lignin content (> 40 %) and approximately equally cellulose and hemicellulose contents (28 to 32 %). The slightly lower temperature (300 – 330 °C) is obtained for a very low lignin content (2 to 20 %) and high hemicellulose content (> 50 %), in this case, as the hemicellulose content decreases, the optimum temperature decreases. Normally, cellulose and hemicellulose decompose at a range of 250 – 350 Celsius degrees, and lignin decomposes on a broad temperature range (150 – 900 Celsius degrees) [115]. Since the lignin is the primary carbon donor of the biofuel in hydrothermal liquefaction [116], carbon must be supplied with higher quantities in order to rise the yield of the liquid products which lead to the increase the optimum temperature. The effect of biomass composition on the optimum temperature and the yield product analyzed above offers the possibility to predict the yield and the range of the optimum temperature in the hydrothermal liquefaction function of the biomass used; this is a crucial point in the design of reactor.

Residence time and flow rate

Usually in supercritical conditions, conversions take place in a fast maneuver, thus low residence times are expected, where as in subcritical water conditions, residence times are relatively higher [94]. In addition, Karagoz et al. [117] noticed that increasing the residence time either at low temperature (150 Celsius degrees) or at high temperature (280 Celsius degrees) reactions favored an increase in the biocrude yield from saw dust conversion but the decomposition products in the biocrude were not the same for short and high retention times for both low and high temperatures. Qu et al [118] reported that for heavy biocrude conversions, the products yields decrease for longer residence times, meaning that the yields increase as

residence time increases, till it reaches an optimum limit. Beyond this time, side reactions (secondary and tertiary) initiate, decreasing the biocrude yield, and even changing the composition of the obtained oil.

The biomass slurry flow rate has an inverse relation with the residence time. As the flow rate decreases at a constant temperature, the products yield increase till a certain time limit, beyond this limit, side reactions take place diminishing the biocrude yield.

Solvents

Water is the cheapest solvent that can be used in the hydrothermal treatment of biomass, but its use as a solvent for hydrothermal liquefaction has some inadequacies face some operating conditions (high critical point of water), moreover, the produced biocrude has low yield, and low heating values of biocrude [119], thus, organic solvents are used in the hydrothermal processing of biomass [120]. The most commonly used organic solvents are methanol, phenol, butanol, acetone, propylene glycerol and ethanol [121]. Organic solvents are known for increasing the products yields of the hydrothermal liquefaction reactions when mixed with the slurry at their optimum ratio [65] [112] [122] [123] [124] [125] [126].

Solvents may also interfere with the chemical properties of the obtained products. Wang et al [127] showed that when ethanol or water is used as solvent, the fractions of oxygenated compounds reduce by 37.8 wt% and 6.1 wt%, respectively. The low content of oxygenated compounds shown in the biocrude derived with water as solvent might be due to the fact that some oxygenated compounds have been dissolved in water as the carbon content in the aqueous phase is very high. This means that these produced biofuels have higher heating values and better qualities than ones produced in water solvent only [127].

Catalysts

Many studies were conducted to assess the effects of catalysts on the biomass processing and to prove that the catalysts used affect products variety and type [112].

Liquefaction processes convert biomass into solid, liquid or gaseous fuels, however, the biocrude produced from the thermal degradation of lignocellulosic biomass is of low quality due to its high acidity and oxygen content, and low HHV. That is why catalytic liquefaction has been proved to be one among the

most efficient processes for transforming lignocellulosic biomass into higher quality fuels and chemicals [128].

In general, 40 to 50% of the biomass content is oxygen, which is better to remove in order to increase the quality of the produced biocrude. Decarboxylation and dehydration are two methods used to extract oxygen from the biomass in the form of carbon dioxide and water, respectively. Using catalysts, which enhance deoxygenating reactions, leads to lower oxygenated products, thus, enhances the yields of hydrocarbons [94].

Mass concentration

Usually, biomass is mixed with water to ensure a low density – viscosity feedstock stream. The ratio of biomass to water affects the products yields and percentages, as the ratio increases, the yields increase till a certain limit where the biomass/water ratio is considered to achieve its optimal value, beyond this limit, the yields slightly decrease. Kumara et al. [47] examined the effects of varying the mass concentration of microalgae on the biocrude yield obtained from hydrothermal liquefaction. As the ratio of biomass/water decreases from 1:6 to 1:10 (16.67% to 10%), biocrude yield raised from 11.5% at 1:6 to 17% at 1:9, then decreases to reach 15% at 1:10.

Particle Size

Different authors studied the effects of the biomass particles size on the properties of final product. Zang et al. [87] examined the influence of particle size on the yield of liquid oil produced through liquefaction of grassland perennials; the biomass was either cut into 25.4 mm length, or ground with 0.5 and 2 mm screens. They found that the yield of liquid at 350 Celsius degrees, did not improve by the size reduction, however, under water supercritical conditions, the particles' size reduction decreased residue yield from 14% to 7–9% of the total biomass. Francisco Tinaut et al [129] , by studying the effect of biomass particle size on the gas yield obtained from hydrothermal gasification have proved that the maximum efficiency was obtained at smallest particle size. Basu et al [130] showed that for the liquefaction of oak woody biomass into bio-coal, as the biomass particle length increases, the products yield increase, while as the biomass particle diameter increases, the products yield decrease.

It could be observed that in general particle size reduction enhances gaseous products yield on the expense of solid and liquid ones.

4. Transition from Batch to Continuous Processing

As stated before, producing biofuels using hydrothermal liquefaction technique is optimized through the use of continuous mechanisms, in which continuous flow reactors are used instead of batch ones. In most cases, while designing a continuous hydrothermal liquefaction reactor, the process is calibrated based on previous experiments conducted on batch reactors. However, parameters involved in hydrothermal liquefaction of biomass may differ from batch to continuous processes. In this section, the modifications on these parameters will be studied; some will remain unchangeable when transition is done, and others will vary depending on certain conditions listed and analyzed.

4.1. Reactor Design

Yun Yu and Hongwei Wu [131] studied the primary liquid products of cellulose hydrolysis in hot compressed water at various reaction temperatures. In their work, they discussed the major types of reactors, their differences, and specific fields of utilization. Biomass in batch reactors is usually subjected to long residence times, leading to extensive degradation of the products (cellulose in their case), producing low sugar yields, and high char and oil yields. In semi-continuous and continuous reactors, the contact time between the reacting solids and the solvents is much shorter, resulting usually in less degradation. That is why higher temperatures are favored in continuous reactors, to ensure higher conversion yields, compensating for shorter residence times. Higher temperatures may lead to the evaporation of the compressed solvent; thus, higher pressures are also required to ensure one liquid phase slurry, reducing the energy consumption wasted on evaporating the solvent.

4.2. Temperature

The reaction temperature of the hydrothermal liquefaction process determines the depolymerization of the biomass to biocrude. In addition, the optimum temperature depends on the composition of the

biomass used and the desired products [94], which means that the temperature used for converting a biomass to a desired biofuel in a batch and continuous reactor is the same.

However, in batch processing, the surface area to volume ratio is much less than in continuous processing, meaning that if the heat input (Q) is the same for both, increasing the area will decrease the temperature difference (ΔT) between the reactants and the heating fluid [132]. Therefore, the temperature difference between the heating fluid (or the heating medium) in a continuous reactor is lower than that in a batch one. Thus, to maintain a constant temperature for biomass inside a continuous reactor, the temperature needed is less than that required to do the same function in a batch reactor [132].

This issue can be clarified using the following equation:

$$Q = U \times A \times \Delta T$$

Where U stands for the overall heat transfer coefficient, and A represents the surface area.

4.3. Pressure

In batch reactors, pressurization of the medium is defined following the isochoric process; the pressure varies based on the reactor's temperature, solvent type, solvent quantity, and the volume of the reactor. Whereas, in continuous reactors, the biomass/solvent slurry is pressurized through high-pressure and low-flow rate pumps. In addition, the pressure is selected based on the required temperature, ensuring that the heated slurry remains in liquid form. This means that, after achieving the optimum conditions in batch experiment, the pump used in the corresponding continuous reactor should be able to pressurize the slurry to the pressure obtained previously in the batch reactor.

4.4. Heating Rate and Residence Time

The concept of batch processing is to heat the whole volume of reactants to a constant temperature, this temperature is maintained for a given time, and then the target products are produced and cooled. In

such process, due to the high heat capacity of batch reactors, the heating rate could not reach high values [133]. The energy needed for batch process is higher than that in continuous reactors. The heating rate in batch reactors may be as low as 5-50°C/min, but can reach more than 300 Celsius degrees per minute in continuous reactors [134], saving a lot of energy consumption, and reducing the energy requirements of the process[54].

Concerning the residence time, batch hydrothermal processing studies aim to deduce the optimum residence time corresponding to the highest biocrude yield production; in batch experiments, the residence time may be higher than 1 hour: 105 minutes for the HTL of fermented cornstalks in the work of Li et al. [135] and 120 minutes for the HTL of swine carcasses in Zheng's work [136]. However, such long residence times are not applicable at all in continuous reactors; a residence time higher than one hour means a very low flow rate (approximately stalled) which increases the possibility of blockage and plugging [137]. On the other hand, experiments showed that very short residence times, in continuous reactors, produce similar yields to longer residence times in batch studies which reduces the energy requirements[54].

Previous experiments and studies on the hydrothermal liquefaction of biomass showed that high heating rates lead usually to shorten reaction times [138]. Higher heating rates are so useful when it comes to inevitable degradation and recombination of the initial product, thus, increasing the reaction rate, reducing by that the residence time required to achieve the desired yield [139]. For example, biocrude yields of up to 66% were obtained during the conversion of *Nannochloropsis* using a holding time of only one minute. This was achieved by placing batch reactors into a sand bath with a temperature significantly above the required set-point temperature, enabling very fast heating rates (230°C/min \pm 5) [140]. In another work dealing with the hydrothermal liquefaction of wood, tripling the heating rate of the biomass led to produce the same biocrude yield (35.8%) but during a shorter residence time : 15 min instead of 60 minutes [141]. Increasing the heating rate in hydrothermal liquefaction reactions resulted in decreasing the reactor volume [139], which is a good approach in designing continuous reactors.

Thus, the concept of building a continuous reactor, which includes diminishing the residence time in order for the reactor to function properly and to have an acceptable and logical size, is highly dependent on increasing the heating rate.

5. CFD Modelling and Simulation of the HTL Process

In this section, the governing equations and boundary conditions utilized by previous works on the modelling and simulation of hydrothermal liquefaction processing will be presented and discussed. After which we can select the suitable conditions and equations for building our desired model.

5.1. Governing Equations and Boundary Conditions

For the analysis of thermochemical conversion biomass, especially hydrothermal liquefaction, CFD analysis adopts four major governing equations:

- Conservation of mass (continuity)
- Conservation of momentum
- Conservation of energy
- Mass transport equations

5.1.1. Conservation of mass; continuity equation

In 2013, Zhang [142] studied the simulation of hydrothermal liquefaction of biomass in a continuous reactor, using ANSYS Fluent, the mass conservation equation took the following form:

$$\frac{\partial \rho}{\partial t} + \nabla \cdot \vec{u} = S_m \quad (1)$$

The upper form can be considered as the most general form of the continuity equation, where S_m represents the source term added to the continuous phase which comes from second phase scattering mass, or from a separate user defined source, ρ represents the density and t stands for time. The utilization of the continuity equation in various thermochemical conversion applications differs from a case to another depending on the conditions of each.

In 2013, Syed modelled the liquefaction of lignocellulosic biomass by sub/supercritical water in a tubular continuous flow micro-reactor [143], he used the governing equation of a mixture model, for the continuity equation, it took the following form:

$$\frac{\partial}{\partial t}(\rho_m) + \nabla \cdot (\rho_m u_m) = 0 \quad (2)$$

Where u_m stands for the averaged mixture velocity, and ρ_m is the averaged density.

In 2018, Ranganathan et al [144] modelled the hydrothermal liquefaction of microalgae in a continuous plug flow reactor, they assumed a two dimensional, unsteady, laminar single-phase incompressible flow, where the density is independent of time, thus the first term of the continuity equation was eliminated, and it took the following form:

$$\nabla \cdot \vec{u} = 0 \quad (3)$$

Where \vec{u} represents the velocity vector.

A velocity boundary condition was specified at the reactor's inlet, which is considered the initial velocity of the biomass – water mixture, u_0 , corresponding to a flow rate of 6 L/h with a biomass concentration of 15 wt%.

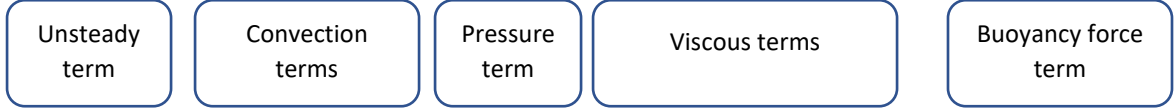
5.1.2. Conservation of momentum

Solving numerically the hydrothermal liquefaction system requires the adaption of conservation of momentum equations, expressed as follows:

$$\rho \left(\frac{\partial u}{\partial t} + u \frac{\partial u}{\partial x} + v \frac{\partial u}{\partial y} + w \frac{\partial u}{\partial z} \right) + \frac{\partial p}{\partial x} = \mu \left(\frac{\partial^2 u}{\partial x^2} + \frac{\partial^2 u}{\partial y^2} + \frac{\partial^2 u}{\partial z^2} \right) + g_x \rho \quad (4)$$

$$\rho \left(\frac{\partial v}{\partial t} + u \frac{\partial v}{\partial x} + v \frac{\partial v}{\partial y} + w \frac{\partial v}{\partial z} \right) + \frac{\partial p}{\partial y} = \mu \left(\frac{\partial^2 v}{\partial x^2} + \frac{\partial^2 v}{\partial y^2} + \frac{\partial^2 v}{\partial z^2} \right) + g_y \rho \quad (5)$$

$$\rho \left(\frac{\partial w}{\partial t} + u \frac{\partial w}{\partial x} + v \frac{\partial w}{\partial y} + w \frac{\partial w}{\partial z} \right) + \frac{\partial p}{\partial z} = \mu \left(\frac{\partial^2 w}{\partial x^2} + \frac{\partial^2 w}{\partial y^2} + \frac{\partial^2 w}{\partial z^2} \right) + g_z \rho \quad (6)$$



Where p represents the pressure, μ is the dynamic viscosity [Pa.s], and the components of gravitational acceleration in the x, y and z directions are denoted by g_x , g_y , and g_z respectively. These equations are called also Navier Stokes equations, which are used to describe the motion of fluid substances. Navier Stokes equations can be written also in vector form:

$$\rho \frac{\partial \vec{u}}{\partial t} + \rho(\vec{u} \cdot \nabla) \cdot \vec{u} = \nabla \cdot \left[-p \cdot \vec{I} + \mu(\nabla \vec{u} + (\nabla \vec{u})^T) - \frac{2}{3} \mu(\nabla \cdot \vec{u}) \vec{I} \right] + \vec{F} + \rho \vec{g} \quad (7)$$

In his work, Ranganathan [144] neglected the gravitational effect and any external forces, which yielded to the following form of the momentum conservation equation:

$$\rho \frac{\partial \vec{u}}{\partial t} + \rho(\vec{u} \cdot \nabla) \cdot \vec{u} = \nabla \cdot \left[-p \cdot \vec{I} + \mu(\nabla \vec{u} + (\nabla \vec{u})^T) \right] \quad (8)$$

A velocity boundary condition was specified at the reactor's inlet, which is considered the initial velocity of the biomass – water mixture, u_0 , corresponding to a flow rate of 6 L/h with a biomass concentration of 15 wt%. The outlet pressure was set to 1 atmosphere, the reactor walls were modelled with no-slip conditions, the diffusivities of all the species in the liquid were defined to be $1 \times 10^{-9} \text{ m}^2/\text{s}$ due to the data lack in the literature followed. This assumed diffusivity value was used in previous simulation works in case of lack of data.

The axial velocity of the slurry inside the reactor is calculated using the following equation:

$$u_z = 2u_0 \left[1 - \left(\frac{r}{R} \right)^2 \right] \quad (9)$$

Where u_z represents the axial velocity at a location r , and R is the radius of the reactor.

In his modelling for the direct liquefaction of lignocellulosic biomass, Syed [143] used the equation of momentum of mixture:

$$\begin{aligned} \frac{\partial}{\partial t}(\rho_m u_m) + \nabla \cdot (\rho_m u_m u_m) \\ = \nabla \cdot [-p \cdot \vec{I} + \mu_m (\nabla u_m + (\nabla u_m)^T)] + \rho_m g + F \\ + \left[\sum_{k=1}^n \alpha_k \rho_k u_{dr,k} u_{dr,k} \right] \end{aligned} \quad (10)$$

Where $u_{dr,k}$ is the drift velocity given by $u_k - u_m$, and μ_m is the mixture averaged viscosity. Boundary conditions were set on velocity constraints at inlets, and pressure constraints at the outlet to stabilize the solution, the velocity of the slurry was varied between 0.1 and 0.5 m/s, and the pressure was set at 20 MPa.

5.1.3. Conservation of energy

The energy equation obeys the energy principle, describing the conservation of energy in a control volume, where energy cannot be created nor destroyed, it is just changing form.

The energy equation is:

$$\rho C_p \left(\frac{\partial T}{\partial t} + u \frac{\partial T}{\partial x} + v \frac{\partial T}{\partial y} + w \frac{\partial T}{\partial z} \right) = \frac{\partial}{\partial x} \left(k \frac{\partial T}{\partial x} \right) + \frac{\partial}{\partial y} \left(k \frac{\partial T}{\partial y} \right) + \frac{\partial}{\partial z} \left(k \frac{\partial T}{\partial z} \right) + \dot{q} \quad (11)$$



Where c_p is the specific heat at constant pressure, and k represents the thermal conductivity of the material, and \dot{q} represents the amount of generated energy per unit volume, originating from a heat flux, chemical energy, etc... The energy equation can be written in the following vector form:

$$\rho C_p \left(\frac{\partial T}{\partial t} + \vec{u} \cdot \nabla T \right) = \nabla(k\nabla T) + \dot{q} \quad (12)$$

In his work, Ranganathan [144] considered the energy generation coming from the external heating fluid in the reactor, then the energy equation took the following form:

$$\rho C_p \left(\frac{\partial T}{\partial t} + \vec{u} \cdot \nabla T \right) + \nabla(-k\nabla T) = U_H S (T_{ext} - T) \quad (13)$$

Where U_H represents the overall heat transfer coefficient of the reactor, S represents the surface area of the reactor, and T_{ext} and T are respectively the temperatures of the external heating fluid and the subcritical state biomass slurry inside the reactor.

In addition to the 2D energy equation used, Ranganathan used a simpler one-dimensional heat transfer model. In such model, the fluid properties are assumed to be uniform along the reactor's length. In addition, the inner convective resistance and the conductive resistance are neglected. The solution of this 1D equation will give the axial temperature profile:

$$T_m = T_f - (T_f - T_0) e^{\left(\frac{-x}{m C_p r_{eff}} \right)} \quad (14)$$

Where the local fluid temperature is denoted by T_m , the external fluid temperature used for heating is denoted by T_f , the inlet fluid temperature is represented by T_0 , x represents the axial position, m denotes the total mass flow rate, C_p is the specific heat, and $r_{eff} = \frac{1}{2\pi r_0 h_b}$ is the effective resistance of the reactor per unit length. r_0 represents the outer radius of the reactor, and h_b is the heat transfer coefficient of the heating fluid. The temperature of the heating fluid was set to 573 K, while the initial temperature of the biomass slurry was set to 300 K, replicating the experimental setup.

In 2013, Zhang [142] studied the simulation of hydrothermal liquefaction of biomass in a continuous reactor, using ANSYS Fluent, the energy equation took the following form:

$$\frac{\partial}{\partial t}(\rho E) + \nabla \cdot [\vec{u}(\rho E + p)] = \nabla \cdot \left[k_{eff} \nabla T - \sum_j h_j \vec{J}_j + (\bar{\tau}_{eff} \cdot \vec{u}) \right] + \dot{q} \quad (15)$$

Where k_{eff} represents the effective conductivity.

The effective stress tensor is defined by:

$$\bar{\tau}_{eff} = \mu \left[(\nabla \cdot \vec{u} - \nabla \cdot \vec{u}^T) - \left(\frac{2}{3} \nabla \cdot \vec{u} \cdot I \right) \right] \quad (16)$$

The total energy E in the energy equation is defined as:

$$E = h - \frac{p}{\rho} + \frac{u^2}{2} \quad (17)$$

Where the sensible enthalpy h is defined for ideal gas as:

$$h = \sum_j h_j Y_j \quad (18)$$

And for an incompressible fluid as:

$$h = \sum_j h_j Y_j + \frac{p}{\rho} \quad (19)$$

Where Y_j is the mass fraction of species j , and h_j is defined as:

$$h_j = \int_{T_{ref}}^T c_{p,j} dT \quad (20)$$

For $T_{ref} = 273.15$ K. Specific boundary conditions were provided to the model to initiate it, including the wall heat flux, set at 20 582 W/m², and inlet temperature of 483°C.

In 2019, Alshammari [145] studied the conversion of a heavy oil in a continuous reactor using COMSOL Multiphysics, the energy equation took the following form:

$$\nabla \cdot (-k \nabla T + \rho u c_p T) = \Delta H_{rx} r_A \quad (21)$$

Where k represents the heat conduction coefficient, ΔH_{rx} represents the heat of the reaction, and r_A defines the rate of the reaction, the temperature of the reactor's wall was held constant at 595 °C

In 2018, Mekala [146] studied the supercritical transesterification of triolein using methanol, under COMSOL Multiphysics, to investigate the wall-to-fluid and particle-to-fluid transport effects. For the estimation of the radial thermal conductivity, a classical energy balance equation was applied:

$$G C_{p,f} \frac{\partial T}{\partial x} = k_r \frac{1}{r} \frac{\partial}{\partial r} \left(r \frac{\partial T}{\partial r} \right) + k_{ax} \left(\frac{\partial^2 T}{\partial x^2} \right) \quad (22)$$

Where G represents the mass flux, k_r and k_{ax} are the radial and axial thermal conductivity respectively. The boundary conditions set to solve the classic energy balance were used from a previous reported work for Marshall and Coberly [147], listed as follows:

$$T = T_0 \text{ at } z = 0 \quad (23)$$

$$\frac{\partial T}{\partial r} = 0 \text{ at } r = 0 \quad (24)$$

$$k_r \frac{\partial T}{\partial r} = h_w (T_w - T) \text{ at } r = R \quad (25)$$

Where h_w is the wall heat transfer coefficient, and T_w is the wall's temperature.

To estimate the particle-to-fluid heat transfer coefficients, the following steady state energy balance equation was used [147]:

$$u \frac{dT_f}{dx} + \frac{6h \cdot (1 - \varepsilon)}{d_p \cdot \varepsilon \cdot C_p \rho} (T_f - T_p) = \alpha_{ax} \frac{d^2 T_f}{dx^2} \quad (26)$$

Where T_f is the fluid temperature, the bed void fraction, or porosity, is denoted by ε , d_p and T_p are respectively the particle diameter and temperature, and α_{ax} is the axial thermal diffusion coefficient. The steady state equation in Mekala's work was solved previously by Danckwerts [148] applying the following initial conditions:

$$u(T_f - T_0) = \alpha_{ax} \frac{dT_f}{dx} \text{ at } x = 0 \text{ (inlet)} \quad (27)$$

$$\frac{dT_f}{dx} = 0 \text{ at } x = x_L \text{ (outlet)} \quad (28)$$

5.1.4. Mass transport equations

The mass transport equation describes the movement of species from one location (stream, phase...) to another. In hydrothermal liquefaction, this equation may be applicable in two different ways, depending on the solvent quantity used. Usually if the biomass quantity is less than 10% of the solvent quantity, the mixture is considered diluted, the solvent will be the major component in the reaction, and the transport of diluted species is adopted, otherwise, the equation transport of concentrated species is used.

The equation of concentrated species transport is given by

$$\frac{\partial}{\partial t}(\rho\omega_i) + \nabla \cdot J_i + \nabla \cdot (\rho\omega_i u) = R_i \quad (29)$$

And for the diluted species transport, the equation becomes:

$$\frac{\partial c_i}{\partial t} + \nabla \cdot \vec{J}_i + \vec{u} \cdot c_i = R_i \quad (30)$$

Where c_i denotes the concentration of species i (mol/m^3), \vec{J}_i is the mass flux relative to the mass averaged velocity ($m^{-2}s^{-1}$), R_i represents the reaction rate term, and ω_i is the mass fraction of species i .

The reaction rate term, or net production rate R_i , used in the mass transport equation is evaluated using Arrhenius kinetics for chemical reactions. The expression for reaction rate term R_i can take many forms depending on the order of the reaction taking place. Consider the following reaction:



The rate of this reaction is defined as:

$$R_i = k[A]^m[B]^n \quad (32)$$

Where k represents the reaction rate constant, calculated through Arrhenius kinetics, and will be discussed later in the kinetic models section, m and n represent the order of the reaction with respect to the reactants A and B respectively [149].

In his investigation, Ranganathan [144] used a mixture averaged diffusion model for the diffusion flux, given by the following equation:

$$J_i = - \left[\rho D_i^m \nabla \omega_i + \rho \omega_i D_i^m \frac{\nabla M_n}{M_n} \right] \quad (33)$$

Where D_i^m is the mixture averaged diffusion coefficient, and M_n is the average molar mass, expressed as:

$$D_i^m = \frac{1 - \omega_i}{\sum_{k \neq i}^N \frac{x_k}{D_{ik}}} \quad (34)$$

$$M_n = \left(\sum_i \frac{\omega_i}{M_i} \right)^{-1} \quad (35)$$

Where D_{ik} represents the diffusion coefficient (m^2/s), and M_i represents the molar mass of species i .

In Mekala's work [146] for the study of wall-to-fluid and particle-to-fluid effects on the transport phenomenon, the steady-state mass balance equation for the species transport is given by the following equation:

$$U \frac{\partial C}{\partial x} = D_{ax} \frac{\partial^2 C}{\partial x^2} - \frac{a}{\varepsilon_b} k_c (C - C_{ps}) \quad (36)$$

Where D_{ax} represents the dispersion or diffusion coefficient, ε_b defines the porosity, k_c represents the mass transfer coefficient, and C_{ps} is the concentration on particle surface. To solve the steady-state mass balance equation for the species transport, the following boundary conditions were taken into consideration:

$$U(C - C_{in}) = D_{ax} \frac{\partial C}{\partial x} \text{ at } x = 0 \text{ (inlet)} \quad (37)$$

$$\frac{dC}{dx} = 0 \text{ at } x = x_L \text{ (outlet)} \quad (38)$$

5.2. Kinetic Models

The decomposition of biomass is a complex network of reversible and irreversible sub-reactions, each acting on one or more of the biomass constituents to produce one or more step or final products. Thus, to model biomass decomposition and study its kinetics, some break down must be done. Several kinetic models were proposed and studied by researchers and scientists. These models differ by the type of biomass used, the step products and final products, and the order of the reactions taking place.

Ranganathan [144] referred to Valdez's [150] kinetic model for the liquefaction of microalgae, shown in Figure 21:

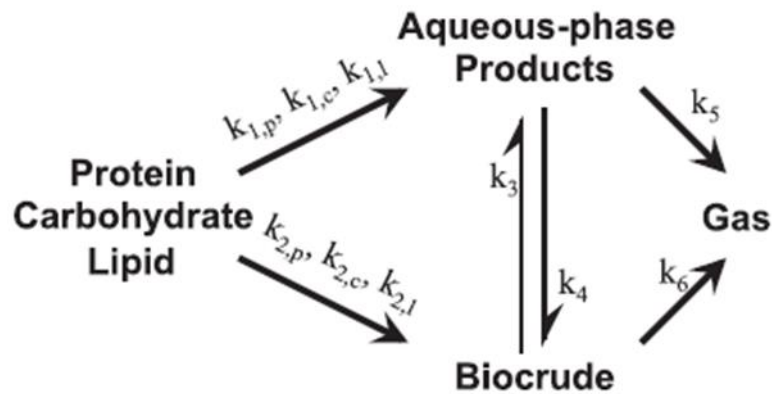


Figure 21: Reaction network for the HTL of microalgae [2]

Where each rate constant k of each single reaction in the above network follows Arrhenius kinetics is:

$$k = A e^{-\frac{E}{RT}} \quad (39)$$

Where A is the pre-exponential term, E is the activation energy, R represents the gas constant and T is the absolute temperature. For the whole network, the following data were reported by Sheehan [151] for the reaction kinetics parameters:

Table 3: Arrhenius kinetics for the HTL of microalgae [4]

Rate Constant	Pathway	Log10 (A_i , min ⁻¹)	Ea (kJ/mol)
k _{1,p}	Protein – AP	5.37	53.3

k1,c	Carbs – AP	4.15	57.9
k1,l	Lipids – AP	4.52	57.6
k2,p	Protein – BC	5.29	51.9
k2,c	Carbs – BC	5.25	78.6
k2,l	Lipids – BC	5.32	65.8
k3	BC – AP	3.41	65.6
k4	AP – BC	3.52	66.2
k5	AP – Gas	3.36	142
k6	BC - Gas	4.63	89.8

In Syed's [143] modelling for the direct liquefaction of lignocellulosic biomass, the three different components of lignocellulose (lignin, cellulose and hemicellulose) were considered each alone with its own kinetic model.

For cellulose, the kinetic model was adopted from Guang et al [152] following Arrhenius kinetics:

Cellulose → Glucose → Degradation products

With an activation energy of 201 ± 7 kJ/mol with a pre-exponential term of $6.83 \pm 2.42 \cdot 10^{16} \text{ min}^{-1}$.

For lignin decomposition, the following model was adapted from Matsumura [153]:

Lignin → Total organic compounds (TOC) + Gas + Char

For hemicellulose, the following model was adopted from Mazza [154]:

Hemicellulose → Xylo-oligomers → Xylose → Degradation products

5.3. Material Properties

The term “material properties” include the materials used in building the reactor, the chemical composition of the reactants and the products, the thermodynamic properties of the biomass-solvent slurry, the catalyst composition, etc. These properties should be known in order to implement them into the finite element software.

5.3.1. Biomass properties

Back to Ranganathan's work [144], the chemical composition of the microalgae used, *Nannochloropsis*, were taken from previous literature of Brown et al. (Hydrothermal Liquefaction and Gasification of *Nannochloropsis* [155]). The microalgae components were as follows:

Table 4: Microalgal properties reported by Brown et al.[17]

Constituent	Weight Percentage
Carbohydrates	56
Proteins	13
Lipids	20
Ash	11

The biomass used in the work of Syed [143] was lignocellulose, and the model components for this biomass are lignin, cellulose and hemicellulose, of respective densities 1520 kg/m^3 , 1500 kg/m^3 and 1800 kg/m^3 , and respective molecular weights of 260 g/mol , 162 g/mol , and 132 g/mol . The averaged density of the biomass was 1606 kg/m^3 , and the averaged molecular weight was 184 g/mol .

5.3.2. Solvent properties

In Ranganathan's work [144], the thermodynamic properties of the solvent, water at subcritical conditions, were estimated using the industrial formulations provided by the International Association for the Properties of Water and Steam, 1997. These properties were imported to COMSOL via user defined functions.

In Zhang's work [142], the temperature gradient was expected to exceed 100°C , the Boussinesq approximation is not applicable, thus, the density of water is assumed to follow a second order polynomial.

In addition, all the thermodynamic properties are evaluated at mean temperatures, and the solvent (water) is assumed to stay at the liquid phase, thus, the whole mixture was treated as homogeneous, single phase, with no phase change neither bubble formation. Finally, the properties of stainless steel, which consists the reactor, were taken directly from COMSOL.

Whereas Syed [143] extracted the thermodynamic properties of water solvent from the conventional thermodynamic tables of water, and inserted them via piece-wise and polynomial defined functions:

$$\mu = 0.00527 - 2.45 \times 10^{-5}T + 3.83 \times 10^{-8}T^2 - 1.97 \times 10^{-11}T^3$$

$$k = -2.596 + 0.0195T - 3.44 \times 10^{-5}T^2 + 1.8 \times 10^{-8}T^3$$

In Mekala's work [146], the density of carbon di-oxide co-solvent was estimated using Redlich Kwong equation of state [156], methanol solvent density and viscosity were extracted from the NIST data [157], and the methanol specific heat capacity was taken from a previous literature [158].

5.3.3. Mixture properties

In several studies, mixture models were used, combining both the biomass properties and the mixture properties.

Syed [143] model used mixture averaged parameters, in which the averaged velocity was defined as:

$$u_m = \sum_{k=1}^n \alpha_k \rho_k u_k / \rho_m \quad (40)$$

Where α_k represented the volume fraction of phase k , and n denoted the number of phases.

The averaged density of the mixture was defined using the following formula:

$$\rho_m = \sum_{k=1}^n \alpha_k \rho_k \quad (41)$$

And the mixture averaged dynamic viscosity took the following form:

$$\mu_m = \sum_{k=1}^n \alpha_k \mu_k \quad (42)$$

Finally, the mixture averaged effective conductivity k_{eff} was defined as:

$$k_{eff} = \sum_{k=1}^n \alpha_k K_k \quad (43)$$

5.4. Software Adaptation

The most common numerical method used to find a solution for the differential governing equations of hydrothermal liquefaction is finite element analysis. This process requires massive computation. Several software are available for this issue, including MATLAB, ANSYS Fluent, ANSYS CFX, and COMSOL Multiphysics. In MATLAB, the user must define the governing equations, the initial conditions, the domains and the boundaries. For this reason, it is easier to shuffle the work towards ANSYS or COMSOL Multiphysics. Each software has built-in governing equations, calibrated to be used in different coordinate systems; Cartesian, cylindrical and spherical. Each software enables graphical interfaces to facilitate the model definition and boundary conditions calibration. In a previous work done by Salvi et al. [159] for the simulation of microwave heating through ANSYS Fluent and COMSOL Multiphysics, the authors reported that both software gave good acceptable results which were validated. But it was noticed that COMSOL was simpler and more flexible in defining the model, although it needed more computational power. In addition, COMSOL Multiphysics is known for its ability to combine several physical phenomena in a single model, including heat transfer, fluid flow, stress analysis, chemical engineering, mass transport, etc, which are all essential for modelling the core of the HTL process. So, if a good computer machine is available, the best choice for the simulation of hydrothermal liquefaction of biomass would be COMSOL Multiphysics.

6. Conclusion

Hydrothermal liquefaction is an encouraging technology for converting biomass into biocrude. The quality and yield of biocrude are highly influenced by the reaction atmosphere, biomass characteristics, solvents and catalysts.

Reaction temperature differs from a biomass type to another; it also has different ranges for producing different products from the same biomass type. For each temperature range corresponding to a specific product, there exists an optimum value of temperature where the products yields are maximized. The temperature of the reaction is attained through a heating system, which is chosen based on the fluctuation demands and on the temperature ranges and limits. For example, relatively high temperatures are achieved using flue gases in large scale systems, but electric resistance heating may be enough while working in lab-scaled prototypes.

Although, to minimize the heat consumed by the system and increase the process's efficiency, the biomass-water mixture can be held at liquid phase by pressurizing the reactor, thus, removing the latent heat input component. Previous experiments showed that varying the reactions pressure have no significant impact on the products. This pressurizing can be obtained either by high pressure pumps, or by pressurized inert gases (nitrogen for example). In large scale systems, high pressure pumps would be more efficient due to the high cost of pressurized inert gases.

Another tip for decreasing the energy used by the system is the heat recovery technology, in which the hot products coming out from the reactor can be used to pre-heat the biomass slurry using a separate heat exchanger. Continuous reactors are of various types, but previous works showed that the plug flow cylindrical one dominates others by its simplicity, easy construction, large conversion rate and low pressure drop, which allows it to be easily up-scaled to industrial claims.

Concerning the biomass preparation before the HTL process, biomass must be pretreated before, in order to facilitate the pumpability and the reaction mechanism. Pretreatment methods decrease the

mixture's viscosity, and break the resistance walls protecting the biomass cells, ensuring a faster and more efficient process. This pretreatment is necessary for decreasing the residence time needed for the biomass to be transformed into. In continuous systems, retention time is illustrated by the biomass flow rate inside the system. Results of previous experiment showed that decreasing the flow rate increases the products yields till a maximum limit, at which the flow rate is called an optimum. Beyond this limit, the reactants are not favored to stay in the reactor to avoid side reactions decreasing carbon content in the liquid fuel produced.

Regarding the solvents, although water is the cheapest one to be used in hydrothermal liquefaction process, but due to its high critical conditions and its influence in the high oxygen contents in the products, some hydrocarbon solvents may be mixed with water to avoid these shortcomings. The use of solvents increases the products yields and improves their quality. Researchers use also catalysts to refine the products quality, by decreasing oxygen content and increasing products heating values. In this method homogeneous or heterogeneous catalysts are introduced in the reactor then removed and washed from the products mixture to be reused.

From the intensive reviews and studies previously mentioned, a suitable continuous hydrothermal liquefaction system may be a combination of:

1. High pressure pump (or series of pumps), capable to provide the biomass slurry with the required pressure before entering the reactor.
2. Continuous stirred tank reactor, followed by a plug flow cylindrical reactor, sensitive to temperature variation demands, used for laboratory scale or sized up to commercial industrial scale.
3. For the heating mode:
 - a. In a lab scale system, electric resistance is a good choice; it has quick response for varying demands, is clean and easy to control.

- b. In large scale reactors flue gases from a separate combustion chamber is a good choice. High temperatures can be achieved easily.
- c. An additional heat recovery system can be designed and built to preheat the biomass slurry by means of a heat exchanger that cools hot products leaving the system, which enhances neat energy ratio and decreases operating costs.

Chapter 2. Batch Reactor Model, Materials and Methods

1. Introduction

Research works were intensified on experimental understanding of the HTL process, covering their stages and subprocesses [8], [106], [160], [161]. Yet, commercializing such a process to produce significant amounts of high-quality fuels still needs lots of aspects to be covered in order to compete with other fuel sources.

Before designing, building and commercializing any system, numerical simulations and modelling are essential. Its risk-free environment and ability to tune the system's parameters before conducting any materialized step saves a lot of time and money. Recently, numerical simulations of hydrothermal liquefaction are applied in order to provide efficient shortcuts for optimizing the design and tuning the operating parameters to increase the products yields.

The majority of numerical studies on hydrothermal liquefaction processes were performed using continuous reactors. Modelling of such reactors can be achieved using steady state conditions for temperature and pressure, whereas in batch reactors, more complex phenomena should be taken into consideration, including the transient heating phase, the phase change of the material inside the reaction zone, etc.

However, modelling a batch reactor remains an essential step before proposing a new design for a commercial hydrothermal liquefaction system, especially that recent studies on such process showed that the most efficient system to be built is a hybrid system i.e. a continuous stirred tank reactor (CSTR) followed by a plug flow reactor (PFR) [160].

On the other hand, modelling, simulation, and validating a batch reactor model isn't an easy step. The complexity of the process replication in a closed pressurized medium remains a challenge to researchers, due to the relatively high computational power consumption needed to solve transient closed CFD systems accompanied with chemical reactions and mass transfer compared to steady state continuous systems simulations, in addition to the lack of accurate thermodynamic properties for the pressurized slurry, bio-oil and solvents in the full range of operation.

Several authors oriented their work towards the chemical kinetics of hydrothermal liquefaction processing, which can be adopted in modelling and designing new reactors. In her Ph.D. studies, Reem Obeid focused on the kinetics of hydrothermal liquefaction of different biomass species [162]. In another work, Obeid et al [163] focused on the kinetics of hydrothermal liquefaction of model macromolecules; lipids, carbohydrates, alkaline lignin, and proteins. However, experimental results showed that all the processes were producing a gaseous phase, except for the lipids processing. For this reason, as a first step, the hydrothermal liquefaction of lipids was selected to be studied, validated and modelled in the numerical model.

In this chapter, the batch reactor used in the lab for the hydrothermal liquefaction of biomass is presented. The experiments conducted are detailed, including their operating conditions, and the methods of products characterization. In addition, the approach made to build the simulation model is discussed, regarding the governing equations, material properties, assumptions and approximations, etc. The simulation model is validated following a three-step methodology. First, by heating an empty reactor and comparing the simulated and experimental temperature and pressure curves, then, by heating several solvents types and conditions (water, methanol and ethanol), and the last step is the validation of the chemical kinetics of hydrothermal treatment of main model macromolecules such as lipids, carbohydrates, protein and lignin. In this work, the kinetic modelling step was limited to lipids transesterification in methanol medium. This reaction was chosen because it has a well-known reactional mechanism that was established in literature and because its products remain in the liquid state. So following the step-by-step

validation process, this reaction is the simplest one to be modeled and used before building up more challenging reactions.

This methodology is illustrated in Figure 22.

In addition to the validation of lipids processing through methanol supercritical transesterification, an approach for the validation of another model macromolecules, cellulose, is discussed in this chapter, describing its methodology, and discussing its challenges.

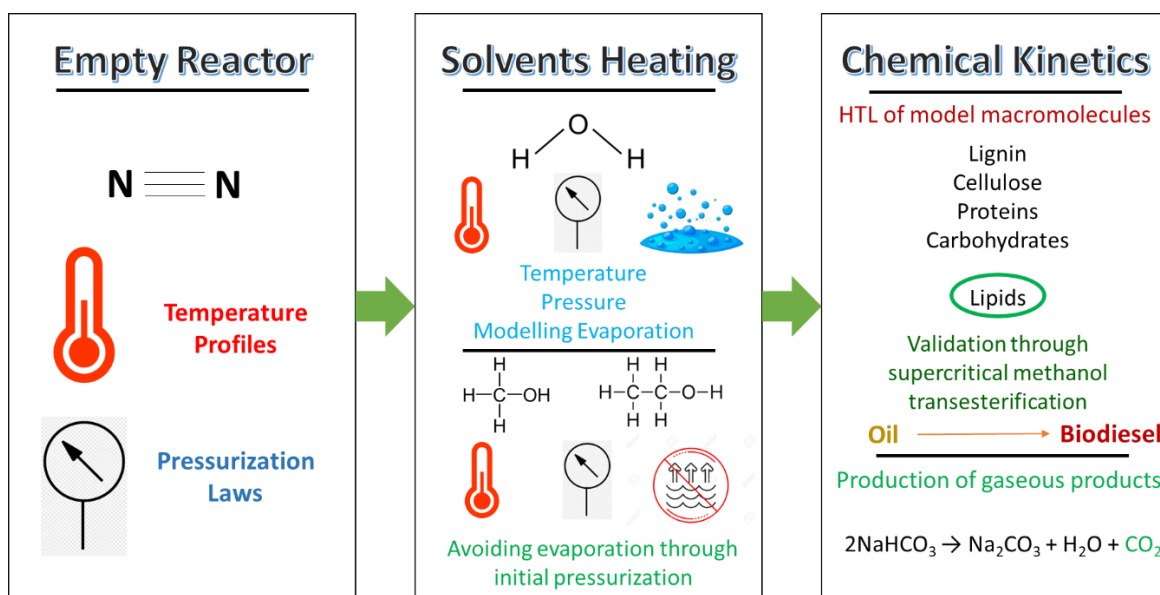


Figure 22: Step-by-step methodology utilized to build and validate the numerical model

2. Experimental Setup

Experiments were carried out at GEPEA Laboratory in the DSEE department of IMT Atlantique, Nantes. The hydrothermal reactor used is a cylindrical batch reactor made of stainless steel of 998 mL as volume, 35.95 cm of height, 3 cm of inner radius and 8.5 cm of outer radius.

The reactor is insulated using 5.2 cm insulation layer. The reactor's top part (cover) is fixed, the reactor's body slides relative to the cover, and the insulation slides independently from the reactor's body to accelerate the cooling process, as shown in Figure 23 **Error! Reference source not found.**

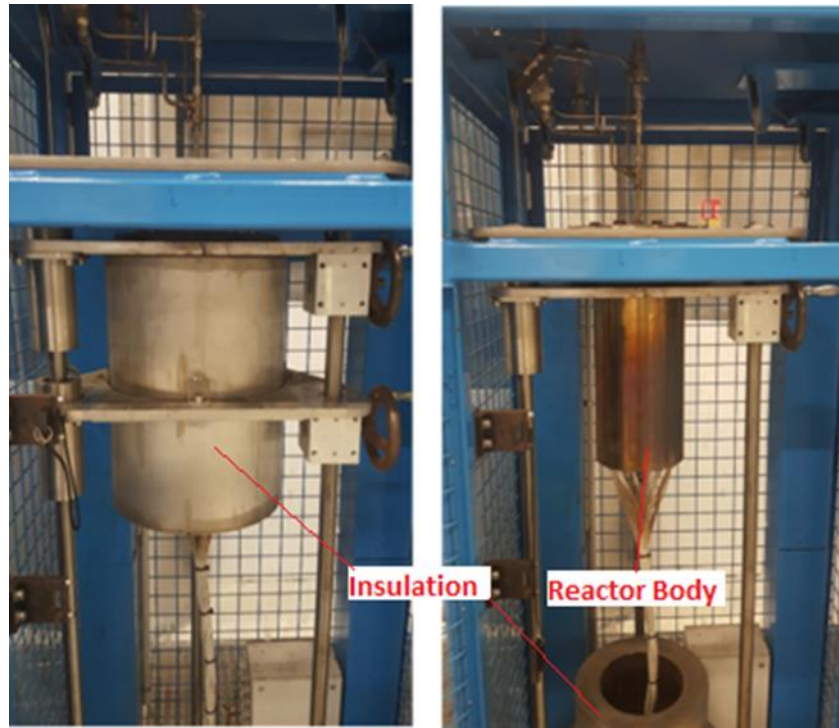


Figure 23: Batch reactor used for the hydrothermal liquefaction in the GEPEA Laboratory of DSEE department in IMT Atlantique

The heating power is provided to the reactor through electric resistance heaters built in its walls, capable to deliver up to 20 kW of heating power. Temperature is limited to a maximum of 450 Celsius degrees, after which the power is cut from the reactor through a circuit breaker, and the reactor handles a maximum pressure of 190 bars, after which a safety valve opens and vents it.

The reactor is equipped by a pressure transducer to measure the absolute instantaneous pressure inside the reaction zone. In addition, four thermocouples are installed at four different positions in the reactor, as shown in Figure 24. T_w is located at the bottom of the reactor measures the temperature of the reactor's metal body which is used to control the heat power supply. T_{in} is placed inside the inner volume of the reactor, measures the temperature of the reaction zone. T_3 is placed on the inner wall of the insulation; between the reactor and the insulation, and the thermocouple T_4 is placed on the outer surface of the insulation, at the same horizontal level with T_3 and T_{in} .

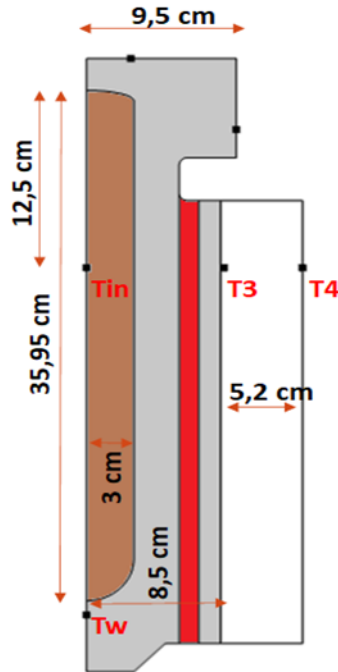


Figure 24: Reactor's axial cross-section

A gas feeding system is connected to the reactor. Before starting any experiment, the reactor is purged with nitrogen gas flowing at a rate of 0.1 L/sec (± 0.005) during 10 mins to remove oxygen and ensure an inert medium for any process. In addition to purging the reactor, the gas feeding system allows to pressurize the reactor with nitrogen.

A data acquisition system is connected to the reactor, to record the pressure (bars), temperatures (degree Celsius), and input power (Watts) during the experiment. The time stepping of this acquisition system can be varied. The most convenient time step for data recording was chosen to be one second. This helps in the comparison with simulation results later on.

Several experiments were conducted using the reactor, starting from the simplest one, heating the empty reactor, to check the heat diffusion inside the system, and the pressurization of gases inside the reaction zone, passing to solvents heating, finalizing with a full hydrothermal liquefaction process, represented by the supercritical methanol transesterification of rapeseed oil. Since the major gas product from HTL processes is CO_2 , the simplest reaction producing carbon dioxide is studied; decomposition of sodium bicarbonate.

2.1. Empty Reactor Heating (Nitrogen Heating)

The reactor is purged with nitrogen gas, then, the reactor is closed at atmospheric pressure, sealed, and turned on. Nitrogen is heated in the closed medium, thus, according to thermodynamics laws, it will undergo a pressure rise. The results are collected from the data acquisition system.

2.2. Solvents Heating

2.2.1. Water Heating

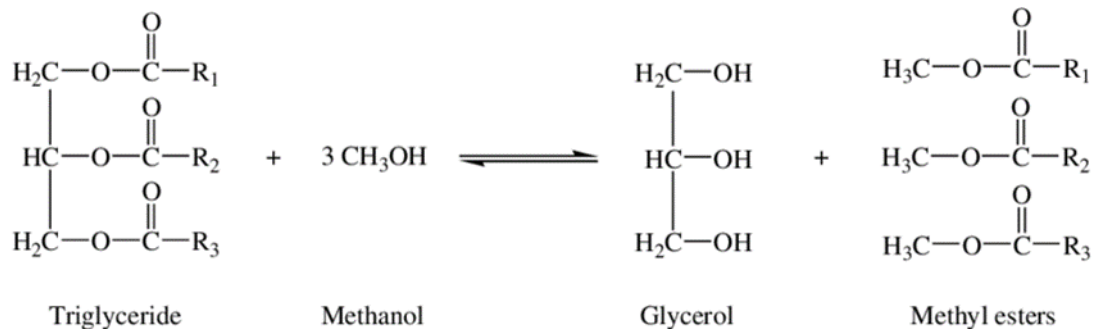
Two experiments regarding water heating were conducted. In the first experiment, 300 mL of water are introduced into the reactor at room temperature, the reactor is purged with nitrogen, closed and sealed, and the heaters are turned on. In the second experiment, the same volume of water is used, the reactor is closed and sealed, and purged with nitrogen. But, before turning on the heaters, the reactor is pressurized with nitrogen gas to 42.7 bars, ensuring a one phase liquid water at a temperature up to 300 Celsius degrees.

2.2.2. Methanol and Ethanol Heating

Methanol and Ethanol are purchased from Thermo Fisher Scientific, France, having respective densities of 792 kg/m³ and 789 kg/m³, and molar masses of 32.04 g/mol and 46.07 g/mol respectively. In each experiment, 300 mL of the solvent are introduced into the reactor, then, the reactor is washed with nitrogen gas, closed and sealed, pressurized with nitrogen to 47 bars, ensuring a liquid phase while heating it inside the reactor from room temperature to the critical point. Finally, the heaters are turned on.

2.3. Supercritical Methanol Transesterification of Rapeseed Oil

Supercritical methanol transesterification experimental parameters are adapted from Kusdiana and Saka's work [164], in which they found that to maximize the products' yields, the optimum ratio of methanol to oil should be 42:1. The transesterification reaction is represented as follows [164]:



Rapeseed oil was purchased from a local store. Its density is 915 kg/m³, and its molar mass is 882 g/mol. To obtain a ratio of 42:1 of methanol to oil, 100 grams of rapeseed oil, corresponding to 0.11338 moles were added to 152.4 grams of methanol, corresponding to 4.7625 moles, with a total volume of 300 ml.

The mixture was stirred using a magnetic stirrer at 600 rpm during 10 minutes and introduced to the reactor. The reactor was closed, sealed, and purged then pressurized with nitrogen, to reach 47 bars, a starting pressure enough to ensure a single-phase liquid methanol throughout the whole experiment, which is the core concept of hydrothermal liquefaction processing. Finally, the heaters are turned on.

A reference experiment was done, leaving the reactor operating for more than six hours to ensure complete conversion of colza oil into biodiesel. After finishing the experiment, the reactor is left to cool, then the products are collected in a rotary evaporator to remove all the methanol from the mixture. The remaining products are placed in a separating funnel for about an hour, a sufficient time to separate completely the products. It was noticed that two layers appeared clearly in the funnel after separation, the upper being biodiesel, and the lower being glycerol.

After that, three different experiments were performed, aiming to stabilize the inner temperature of the reactor above 270 Celsius degrees. The residence time in the first experiment was one hour, in the second it was two hours, and in the third it was three hours. Layer 1 of each experiment's products is supposed to be a mixture of biodiesel and unreacted colza oil. The quantifying analysis of produced

biodiesel and unreacted oil in each experiment was done using Gambill's formula for the viscosity of a liquid-liquid mixture [165]:

$$\nu^{1/3} = y_a \nu_a^{1/3} + y_b \nu_b^{1/3} \quad (44)$$

Where ν represents the kinematic viscosity, and y represents the mass fraction.

3. Reactor Modelling and Implementation into COMSOL

In this work, COMSOL Multiphysics finite element software is used to model a batch reactor for the hydrothermal liquefaction of biomass. The model replicates the batch reactor present in GEPEA Laboratory, IMT Atlantique, Nantes. This model is validated step by step by comparing the numerical and experimental results, starting from heat diffusion, passing to the pressurization of the reactor, transitioning to applying chemical reactions in transient and steady state phases, and producing new species. The thermochemical process experimented and simulated in this work is the supercritical methanol transesterification of rapeseed oil, transforming the triglycerides (lipids) into methyl esters (biodiesel) and glycerol. The steps for implementing the batch reactor into COMSOL Multiphysics is listed and discussed. This includes the reactor's geometry, power input, pressurization of the reaction zone, mesh size influence, boundary conditions, and the calibration of material properties.

3.1. Reactor's Geometry

The dimensions of the reactor taken from the designer's manual are implemented into COMSOL using 2D-axisymmetric coordinates, in which an axial cross-section of the reactor is drawn as shown in Figure 24. In this figure, the brown zone represents the reaction zone, in which the reaction takes place. The grey zone represents the heating zone imbedded in the reactor. Finally, the insulation is represented by the white zone.

At every second of the experiment's time, the reactor's acquisition system records the input power (Watts) which is extracted and imported into COMSOL as an interpolation function for the power source. Thus, experimental power is applied accurately to the simulation model.

3.2. Isothermal Domain Interface

An isothermal domain interface was adopted in the reaction zone due to the low expected temperature gradient that would be obtained in the mixture. In this interface homogeneous properties (temperature, pressure, density, viscosity, etc) are defined among its volume. Fluid inside the reactor can be treated as one block of uniform properties in case of empty reactor heating, and as two isothermal domains (two blocks) in case of solvent and nitrogen heating. The reaction zone is heated by the inner walls of the reactor through convective heat transfer, which is also included in the isothermal domain assumption. A convective heat transfer coefficient was proposed and calibrated using several CFD model setups to meet the required performance. This assumption established itself using much less computational resources with satisfying results' accuracy.

3.3. Power Zone Assumption

The reactor is fitted with cylindrical heaters imbedded in its metallic walls. However, modelling these heaters in 2D-axisymmetric coordinates is not possible. For this reason, an assumption was adopted, transforming the heating zone from separate individual heaters into a volume heating zone. This volume zone emits the same amount of power, and it is located at the same radial distance. Figure 25 shows the transformation from individual heaters to the volume heating zone.

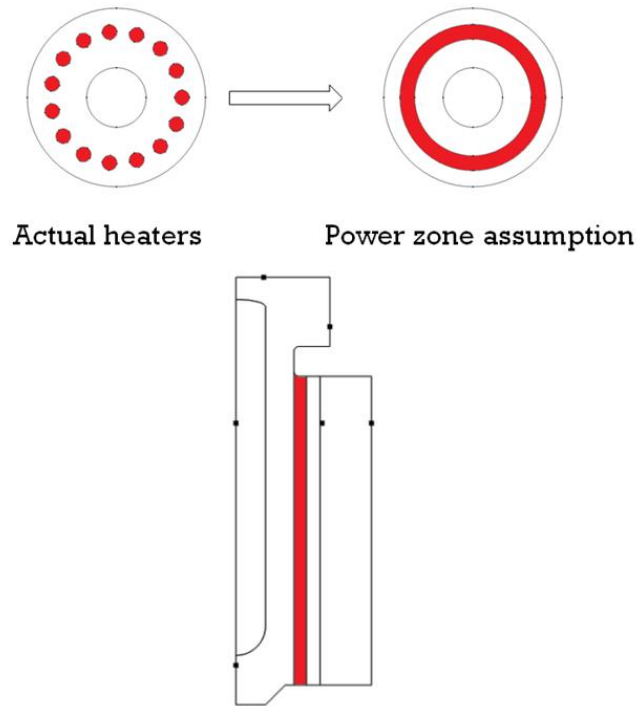


Figure 25: Individual heating to power zone assumption

The reactor's acquisition system records the input power (Watts) which is extracted and imported into COMSOL as an interpolation function for the power source. The power was imported in terms of volumetric heat source, the heating volume having a hollow cylindrical shape was calculated and appeared to be equal to 1.6438 L. The experimental power from the acquisition system was divided by this volume to obtain the volumetric power.

To further ensure the accuracy of the power zone assumption, a comparison model was built using COMSOL, in which the actual heaters are modelled and operated, and compared to the case where the power zone assumption is used. The comparison was done in 2D and 3D coordinates as shown in Figure 26.

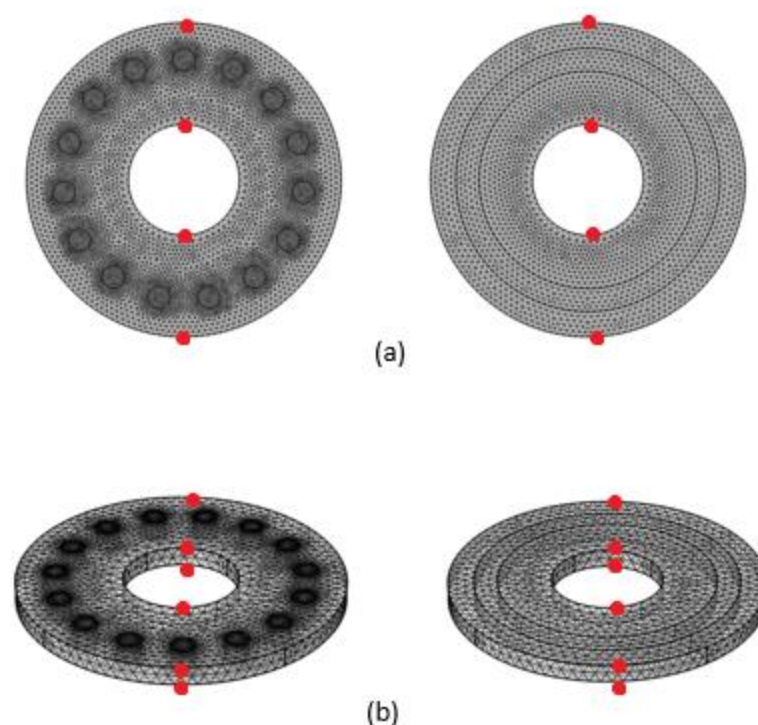


Figure 26: Real heaters model vs power zone assumption model mesh

The red dots represent the temperature across the inner wall and the outer wall of the reactor, which are the key parameters of heating and cooling the reactor. The temperature profiles of the red dots, considered to be critical points at which the temperature may differ due to this approximation, were compared for both: real heater model and power zone assumption model, in 2D (a) and 3D (b) coordinates. The maximum relative temperature error between the models is 0.085%, which is considered negligible. Thus, the power zone assumption is strongly valid in the simulation model.

3.4. Pressurizing the Reactor's Medium

Referring to thermodynamics' laws, an increase of temperature in a closed volume yields an increase in pressure too. In the case of a batch reactor, the total pressure is the sum of three different partial pressures; purging gas pressure, solvent vapor's pressure, and pressure obtained from production of new gaseous species.

3.4.1. Purging gas pressure

The increase in the Nitrogen gas pressure can be modelled following two different laws; ideal gas law and real gas law. Both laws were adapted and compared to know which one is most suitable for our study.

Ideal gas law

The ideal gas law states that

$$P_i = \rho RT \quad (49)$$

Where P_i (Pa) is the partial pressure following the ideal gas law, ρ (kg/m^3) is the density of gas, R ($kJ/(kg.K)$) is the gas constant and T (K) is the absolute temperature [166].

Real gas law

Van der Walls equation describing the real gas behavior states that

$$\left[P_r + a \left(\frac{n}{V} \right)^2 \right] \left(\frac{V}{n} - b \right) = RT \quad (50)$$

Where P_r (Pa) is the partial pressure following the real gas law, a ($Pa.m^6/mol^2$) represents the intermolecular forces correction, n (mol) is the number of moles, V (m^3) is the occupied volume, and b (m^3/mol) represents the correction for the volume occupied by the gas particles [167].

3.4.2. Solvents' vapor pressure

When a liquid is heated in a closed volume, it undergoes an isochoric process. In such process under the given conditions, the absolute pressure in the reactor follows the saturation pressure of the liquid throughout the whole experiment [168]. Thus, the solvents' vapor pressure will be the difference between the absolute pressure inside the reactor and the partial pressure of the purging gas.

Calculating the quantity of liquid evaporation using partial pressure

In an isochoric process, a portion of the liquid evaporates, the produced vapor pressurizes the medium, and due to the presence of a two-phase fluid, the medium's pressure will always be equal to the vapor's saturation pressure. This is applicable in the case of the batch reactor under study.

In the case of water heating starting from atmospheric pressure, the vapor's partial pressure defined and explained in the above section can be used for calculating the number of moles of the water vapor resulting in this pressure using re-arranged Van Der Waals equation:

$$(ab)n^3 + (-av)n^2 + (Pb + RT)(V^2)n - PV^3 = 0 \quad (51)$$

The above equation is a third-degree polynomial having the following form:

$$p_1n^3 + p_2n^2 + p_3n + p_4 = 0$$

Thus, for each instant, the above third-degree polynomial should be solved to calculate the number of moles of water vapor, meaning that the number of equations to be solved exceeds thousands. For this reason, MATLAB software was used to solve these equations numerically. After calculating the number of moles, the mass of the evaporated water is calculated by multiplying the number of moles by the molar mass of water.

Generalizing the evaporation correlation for any volume of water in the reactor

An approach was studied to generalize the correlation describing the evaporation of water in a control volume. This correlation serves to estimate the evaporation rates of water without performing an experiment. For this reason, seven experiments of water heating were conducted, and the correlation was reshaped in order to link the mass of evaporated water instead of the number of moles. Two experiments were conducted using 300 mL of water, three using 500 mL, and two using 750 mL. The results were exported, and the coefficients p_1 , p_2 , p_3 , and p_4 of each of the seven third degree polynomials were tabulated

for generalizing the correlation (Table 5). We assume the following abbreviations for the function representing the correlation for each experiment:

- F1: heating 300 mL of water, trial 1.
- F2: heating 300 mL of water, trial 2.
- F3: heating 500 mL of water, trial 1.
- F4: heating 500 mL of water, trial 2.
- F5: heating 500 mL of water, trial 3.
- F6: heating 750 mL of water, trial 1.
- F7: heating 750 mL of water, trial 2.

Table 5: Coefficients of the 3rd degree polynomials describing the seven different experiments

Function	p ₁	p ₂	p ₃	p ₄
F1	1.62E-09	-1.63E-06	0.000545	-0.06089
F2	1.72E-09	-1.75E-06	0.000597	-0.06791
F3	1.20E-09	-1.22E-06	0.000409	-0.04575
F4	1.19E-09	-1.20E-06	0.000403	-0.04512
F5	1.19E-09	-1.21E-06	0.000407	-0.04573
F6	5.34E-10	-5.25E-07	0.000172	-0.01866
F7	5.77E-10	-5.75E-07	0.000191	-0.02111

As discussed previously, the mass of the evaporated water is directly linked to the available gaseous phase volume inside the reactor. Thus, the coefficients of each polynomial were divided by the available volume corresponding to the experiment it describes:

- F1 and F2: available volume $v_1 = 0.000998 - 0.0003 = 0.000698 \text{ m}^3$
- F3, F4 and F5: available volume $v_2 = 0.000998 - 0.0005 = 0.000498 \text{ m}^3$
- F6 and F7: available volume $v_3 = 0.000998 - 0.00075 = 0.000248 \text{ m}^3$

Let $p_i' = p_i / v_i$, applicable for all the coefficients, with p_i' the new coefficient value to be considered.

These values are represented in Table 6 below.

Table 6: Calibrated coefficients of the 3rd degree polynomials describing the seven different experiments

Function	p ₁ '	p ₂ '	p ₃ '	p ₄ '
F1/ available volume	2.31E-06	-0.00233	0.781232	-87.235
F2/ available volume	2.46E-06	-0.00251	0.855731	-97.2923
F3/ available volume	2.42E-06	-0.00244	0.820884	-91.8675
F4/ available volume	2.39E-06	-0.00241	0.809036	-90.6024
F5/ available volume	2.4E-06	-0.00242	0.816667	-91.8273
F6/ available volume	2.15E-06	-0.00212	0.692742	-75.2419
F7/ available volume	2.33E-06	-0.00232	0.769758	-85.121

Table 6 shows satisfying agreement in the coefficients of the new functions, the constants. But, to make sure that this is applicable over the temperature range used in the experiments (280 – 573K), Figure 27 reveals the plot of the function of temperatures varying from 280 to 573K.

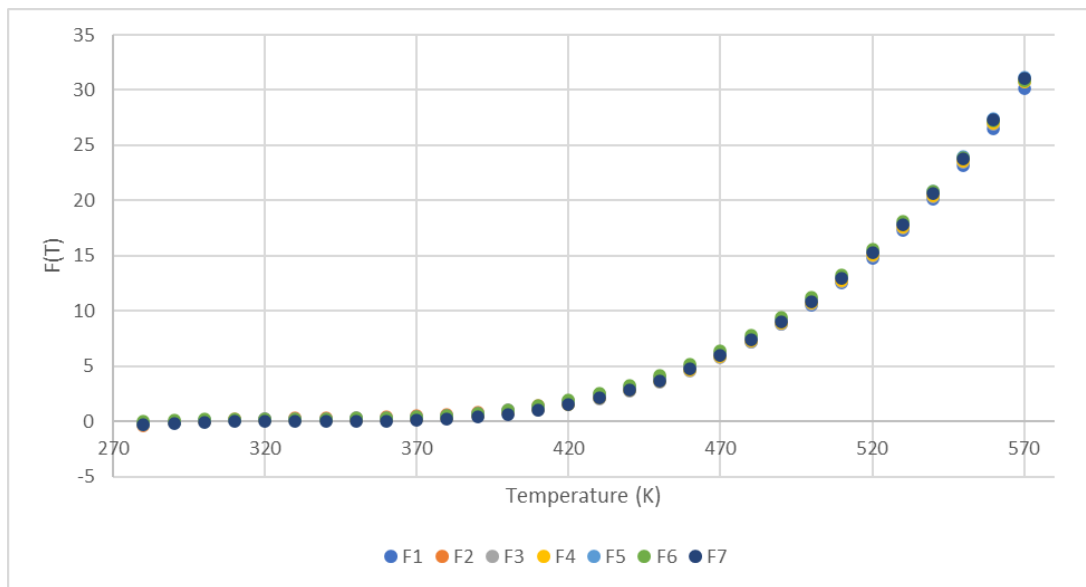


Figure 27: $F(T)$ versus temperature for the seven different obtained correlations

Figure 27 shows satisfying agreement among the obtained correlations, with a maximum relative error below 5%. The value of each coefficient is averaged, with:

$$P_1' = 2.35 \times 10^{-6}$$

$$P_2' = -0.00236$$

$$P_3' = 0.792293$$

$$P_4' = -88.4553$$

And new function obtained will be:

$$\frac{\text{mass of evaporated water (kg)}}{\text{available gaseous volume (m}^3\text{)}} = 2.35 \times 10^{-6} T^3 - 0.00236 T^2 + 0.792293 T - 88.4553$$

Where T is expressed in Kelvins.

The final averaged correlation (F) is plotted versus the case correlations (F1 to F7) in Figure 28. The averaged correlation is in perfect agreement with the other single-case correlations describing the results of each experiment. Thus, the averaged correlation is assumed valid and accurate to use.

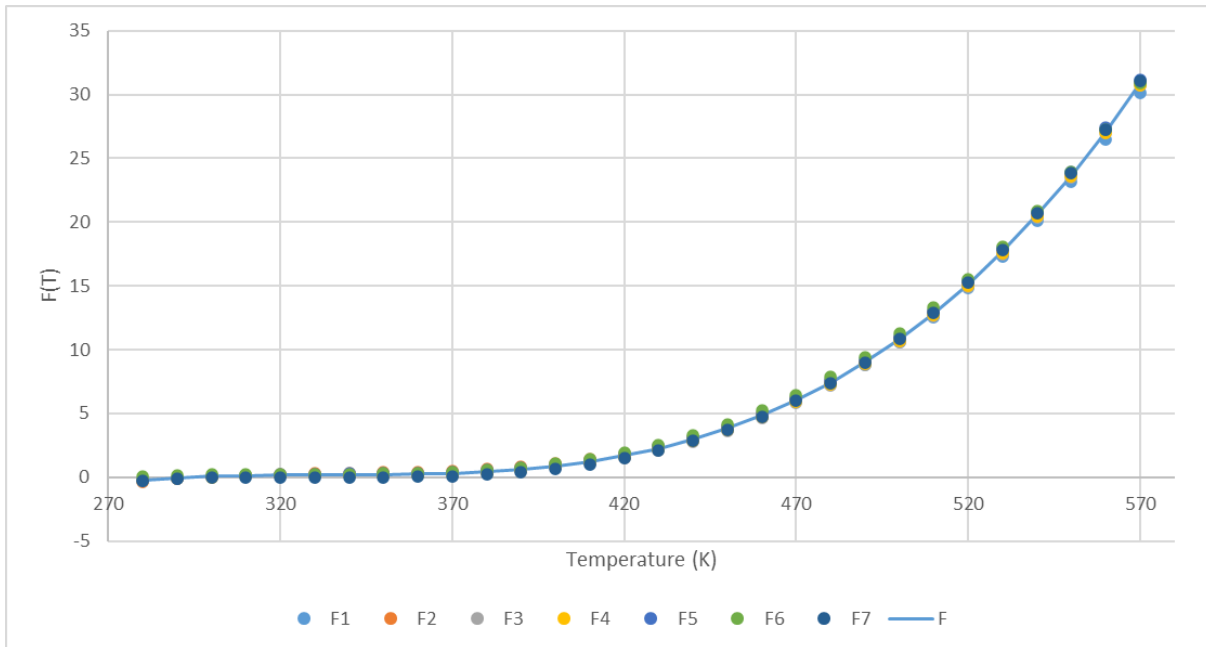


Figure 28: Averaged Correlation F versus the other correlations

3.4.3. Carbon dioxide partial pressure

Carbon dioxide tends to follow the real gas law instead of the ideal gas law due to its high compressibility ratio. Thus, the pressure of carbon dioxide gas in the reactor is calculated using Van Der Waals equation described in section 3.4.1.

3.5. Governing Equations

For the analysis of thermochemical conversion of biomass, finite element software adopts three major governing equations: conservation of mass (continuity), conservation of momentum, and conservation of energy.

The conservation of momentum equation has the following vector form:

$$\rho \frac{\partial \vec{u}}{\partial t} + \rho(\vec{u} \cdot \nabla) \cdot \vec{u} = \nabla \cdot [-p \cdot \vec{I} + \mu(\nabla \vec{u} + (\nabla \vec{u})^T)] \quad (52)$$

Where ρ is the density of the mixture (kg/m^3), μ is the dynamic viscosity ($kg/m.s$), and u is the velocity vector (m/s).

The conservation of energy equation has the following vector form:

$$\rho c_p \left(\frac{\partial T}{\partial t} + \vec{u} \cdot \nabla T \right) = \nabla \cdot (k \nabla T) + \dot{q} \quad (53)$$

Where c_p is the specific heat at constant pressure, k represents the thermal conductivity of the material, and \dot{q} represents the amount of generated or absorbed energy per unit volume. The equation describing the heat sink contributing in \dot{q} in the above equation, due to the evaporation of liquid solvents is given by:

$$\dot{q} = \frac{dQ_s}{dt} = \dot{m}_{evap} \times L_i \quad (54)$$

Where Q_s represents the heat sink energy absorbed by the system due to evaporation (J), \dot{m}_{evap} represents the evaporation rate of species i , and L_i represents the specific heat of vaporization of species i .

The continuity equation used by COMSOL in the case of species transport through diffusion and convection has the following vector form:

$$\frac{\partial c_i}{\partial t} + \nabla \cdot \vec{J}_i + \vec{u} \cdot c_i = R_i \quad (55)$$

Where c_i denotes the concentration of species i (mol/m^3), \vec{J}_i is the mass flux relative to the mass averaged velocity ($m^{-2}s^{-1}$), R_i represents the reaction rate term, and ω_i is the mass fraction of species i .

The reaction rate term, or net production rate R_i , used in the above equation is evaluated using Arrhenius kinetics for chemical reactions. The expression for the reaction rate term R_i can take many forms depending on the order of the reaction taking place. For a first order kinetic reactions, the rate R_i of the reaction is expressed through the following form

$$R_i = k[A] \quad (56)$$

Where k represents the reaction rate constant (1/s), and $[A]$ represents the concentration of species A.

Kusdiana and Saka [164] reported different values for the supercritical methanol transesterification reaction rate constant over a range of different temperatures. Since the methanol to oil ratio was very high (42:1), the reaction is assumed to follow first order chemical kinetics, and the values of $\ln(K)$ were plotted versus $(1/T)$ for the linearization of the results as shown in Figure 29.

The derived correlation has a good fitting, with $R^2 = 0.9546$, thus, it can be implemented into COMSOL Multiphysics as first order Arrhenius Kinetics in the following form:

$$\ln K = -\frac{8331.1}{T} + 8.8481$$

$$K = e^{-8331.1/T} \times e^{8.8481}$$

Comparing the derived formula with

$$K = Ae^{-E/RT}$$

Yields $A = 6961.1/\text{sec}$, and $E = 69.27 \text{ kJ/kg}$.

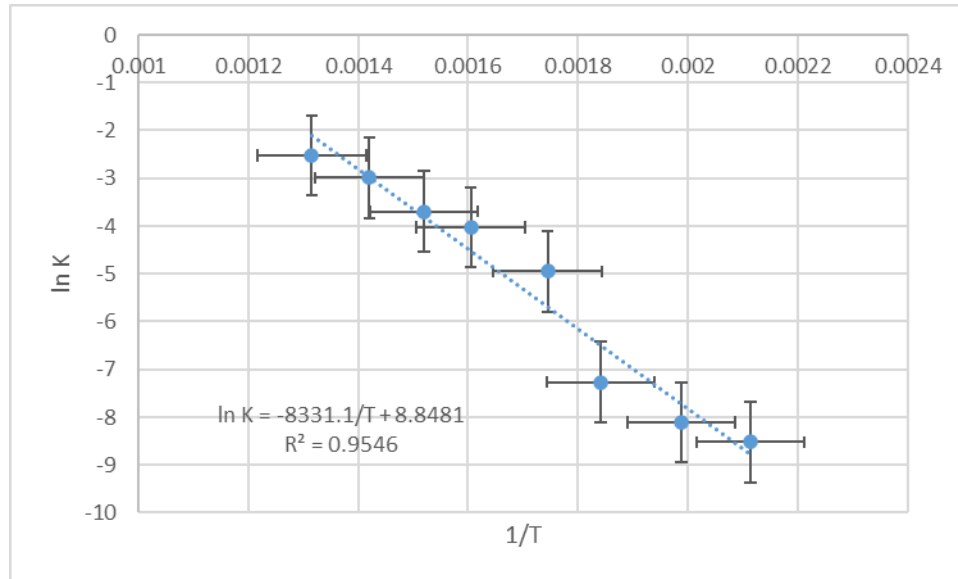


Figure 29: Linearized kinetics reported by Kusdiana et al as pseudo first order

3.6. Material Properties

The reactor is made of stainless steel of 316 L [169], with a density of 8000 kg/m^3 , heat capacity of 510 J/kg.K , and thermal conductivity varying function of temperature as shown in Table 7.

Table 7: Thermal conductivity of stainless steel 316L [169]

T (°C)	k_{st} (J/kg. K)
20	13.5
100	15
300	18.5
500	21.5

Nitrogen and water properties are chosen from COMSOL’s materials’ library [170]. Methanol and Ethanol thermodynamic properties are obtained through NIST material library [171]. The insulation’s material was not specified in the reactor’s designer’s manual, thus, the ranges for these properties were taken from a previous work [172], and a sensitivity study was performed to fully calibrate them. Insulation’s

heat capacity was fixed at 2500 J/kg. K, and its density was fixed at 350 kg/m³. The thermal conductivity of the insulation material is shown in Table 8.

Table 8: Thermal conductivity of the insulation material

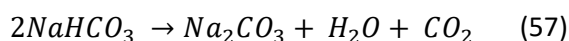
T (°C)	k _{ins} (J/kg. K)
20	0.06
200	0.15
800	0.23

4. Validation of Other Chemical Reactions

In addition to the validation of the supercritical methanol transesterification process, an approach of validating other model macromolecules was studied. Obeid et al [163] studied the kinetics of hydrothermal processing of different model macromolecules, including lipids, proteins, carbs, etc. For the carbohydrates model, the hydrothermal liquefaction of microcrystalline cellulose was experimented. However, it was noticed that such reaction produces a noticeable portion of gases. Going back to the batch reactor in this work, the production of gaseous species pressurizing the reaction medium maybe an excellent indicator to monitor the reaction progress with time, thus, validating its kinetics experimentally and numerically. For this reason, it was easier to start with a simpler chemical reaction producing only one gaseous product; decomposition of sodium bicarbonate.

4.1. Decomposition of Sodium Bicarbonate

Sodium bicarbonate, or baking soda, is a chemical solid that undergoes a decomposition reaction if it is heated to a temperature above 90 Celsius degrees to form three compounds; sodium carbonate, water and carbon dioxide [173]. The stoichiometric equation of sodium bicarbonate decomposition is as follows:



The decomposition reaction of sodium bicarbonate will be conducted experimentally in the lab's reactor. This approach will help in strengthening the COMSOL's model, in which the reaction kinetics will

be implemented and the quantity of products will be recorded during the reaction time. This step is intended to act as an intermediate approach between solvents heating and full hydrothermal liquefaction reactions, since this simple reaction is expected to produce only one gaseous compound (carbon dioxide), and tracking its quantity versus time will be feasible in the reactor. Once this reaction is validated experimentally and numerically, we can shift toward full hydrothermal liquefaction reactions.

4.2. Kinetics of Sodium Bicarbonate Decomposition

The kinetics of sodium bicarbonate thermal decomposition were studied and reported by several researchers. Our main goal is to adapt one kinetic model for this reaction based on the experimental results achieved in the laboratory.

Matthew Ball et al. studied the thermal decomposition of sodium bicarbonate in a temperature range of 360 – 500 K, over a range of partial pressures of carbon dioxide, moreover, the effect of water vapor has been studied [174]. Experiments were carried using a Stanton Redcroft TG750 thermobalance and a potentiometric recorder. Results showed that before reaching 440 K, the reaction follows contracting-cube kinetics with an activation energy of 32 kJ/mol, and a frequency factor of 10/sec. At this temperature, it was found that the presence of water vapor or carbon dioxide had some effects on the kinetics, which may be considered negligible compared to the overall behavior of the kinetic model. Moreover, the results revealed that at temperatures below 390 K, the reaction follows first order kinetics. In nitrogen, the activation energy is 64 kJ/mol with a frequency factor of 100000/sec. At high partial pressures of carbon dioxide, the activation energy is increased to 130 kJ/mol with a frequency factor of $10^{13.5}$ /sec.

Wu and Shih [175] studied the intrinsic kinetics of the thermal decomposition of sodium bicarbonate by non-isothermal thermogravimetric analysis in the temperature range of 360 – 450 K. Experiments were carried in a Perkin-Elmer TGS-2 thermogravimetric analysis apparatus using three different heating rates in flowing nitrogen. Results showed a first order dependence kinetics with an activation energy of 105.8 kJ/mol and a pre-exponential factor of 6.7×10^{12} /min.

Wang Hu et al. studied the kinetics of sodium bicarbonate particles decomposition using a thermal gravimetric method [176]. Results showed that the kinetics follow the first order behavior. Isothermal runs were conducted at four different temperatures; 373, 393, 423 and 473 K. Another approach was conducted, using the temperature rise method for calculating the rate constants at different heating rates.

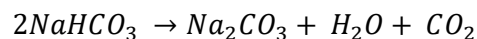
However, a wide range of different values were reported for the reaction kinetics. For this reason, it was recommended to conduct a thermogravimetric analysis of the decomposition of sodium bicarbonate in the laboratory, in which a previous kinetic model can be validated, or a new kinetic model can be suggested.

4.3. Thermogravimetric Analysis of Decomposition of Sodium Bicarbonate

Sodium bicarbonate powder was purchased from Honeywell Research Chemicals, France, with a 99.7% purity. 10.2 mg of sodium bicarbonate were placed inside the apparatus at room temperature, then, heated to 50 degrees Celsius and kept for few minutes in order to make sure to remove all moisture contents. After that, the reactants were heated at a rate of 0.3 K/s to reach 423K, and kept for 30 minutes. The results are compared with previously reported kinetics to select the most compatible kinetic model.

4.4. Decomposing Sodium Bicarbonate in the Batch Reactor

Three experiments were conducted on solid sodium bicarbonate decomposition. In each experiment, 30 g were placed in a light mesh, and the reactor was purged with nitrogen flowing at 0.1 L/min during 10 minutes. The first experiment's operating temperature was 473 K, the second was 423 K, and the third was 383 K. Recalling the stoichiometric equation (9) of the decomposition reaction:



$$n_{CO_2} = \frac{n_{NaHCO_3}}{2} = \frac{m_{NaHCO_3}/M_{NaHCO_3}}{2} = \frac{30/84.01}{2} = 0.17855 \text{ moles}$$

Where n represents the number of moles, m represents the mass, and M is the molar mass. Thus, when the reaction is finished, 0.17855 moles of carbon dioxide should be found in the reactor.

For calculating the instantaneous number of moles obtained in each experiment, the following procedure was followed:

- The partial pressure of nitrogen gas is calculated using the ideal gas law

$$P_{N_2} = \rho_{N_2} \times R_{N_2} \times T$$

Where P_{N_2} is the partial pressure of nitrogen (Pa), ρ_{N_2} is the density of nitrogen at the starting conditions of the experiment (1.174 kg/m³), R_{N_2} is the nitrogen gas constant (296.8 J/kg. K), and T is the absolute temperature (K).

- The partial pressure of carbon dioxide gas is calculated by subtracting the nitrogen's partial pressure from the total pressure inside the reactor

$$P_{CO_2} = P - P_{N_2}$$

Where P_{CO_2} and P are the partial pressure of carbon dioxide and the total pressure inside the reactor respectively, measured in Pascals.

- As long as the partial pressure of carbon dioxide is calculated, the number of moles of carbon dioxide can be determined using the following Van der Waals equation:

$$\left[P_r + a \left(\frac{n}{V} \right)^2 \right] \left(\frac{V}{n} - b \right) = RT$$

5. Conclusion

The objective of this chapter is to describe the methodology used to build a numerical model using COMSOL Multiphysics, in order to simulate the hydrothermal liquefaction processes occurring in a batch reactor. For this reason, an experimental campaign was conducted on a 1 L batch. In addition, a simulation model was built to be tested and validated later after comparing the simulated results to the experimental ones. The methodology used is based on a step-by-step process, where the reactor was heated with only

nitrogen gas inside it to calibrate the model's parameters and material properties, and to verify the pressurization law. Moreover, liquid solvents heating experiments; water and hydrocarbon solvents heating were conducted. The experiments of water heating help in calibrating the evaporation phenomenon in the simulation model, converging the simulation results towards the experimental results. The experiments involving hydrocarbon solvents heating (methanol and ethanol) help in calibrating the simulation model when operating in the supercritical state.

In addition, the process of supercritical methanol transesterification of rapeseed oil was used to ensure the validity of the simulation model when dealing with chemical reactions. Supercritical methanol transesterification was selected since it does not produce any gaseous products, thus, it can be assumed as an intermediate step before proceeding with more complex hydrothermal liquefaction processes.

Finally, an approach for testing the model beyond the supercritical transesterification of methanol was explained and discussed. A simple reaction, decomposition of sodium bicarbonate, producing only one gaseous product (carbon dioxide) was studied experimentally, in the batch reactor and using TGA analysis.

The next step is to compare the experimental results obtained in the laboratory to the simulation results obtained from running the COMSOL's model. The upcoming chapter, Results and Discussions, will present a full step-by-step comparison for the results and discuss the validity of the simulation model.

Chapter 3. Batch Reactor Model, Results and Discussions

1. Introduction

In this chapter, the results of the conducted experiments in the batch reactor, presented in Chapter II, are compared to the numerical results obtained through COMSOL's model. A step-by-step comparison is stated and discussed, following the methodology detailed in the previous chapter, where first, we compared the experimental and simulated temperature profiles and pressure curves of the empty reactor heating experiment. Then, the pressurization laws and the evaporation models proposed are validated using the solvents heating experiments and simulations results. After that, supercritical methanol transesterification results are compared and validated for all experiments. Finally, the results and advancements in the modelling of the decomposition of sodium bicarbonate are presented and discussed, including the status, the challenges and the obstacles.

2. Empty Reactor Heating

The first step in the methodology presented in the previous chapter was to heat the empty reactor. This experiment is the first step for calibrating and tuning the model's parameters for optimizing its results and eliminating the simulation errors.

2.1. Heat Diffusion

The results of the first simulation of nitrogen heating experiment (empty reactor) were compared to the experimental results obtained in the laboratory. High errors were observed between the experimental and the simulated temperatures, where the maximum error reached 13.08% in the inner thermocouple, 45.1% in the third thermocouple and 12.5% in the fourth thermocouple.

Because of these high error values and in order to converge the simulation model to the real one, several modifications were applied, including:

- Introducing surface-to-surface radiation
- Sweeping the surfaces' emissivity, and choosing an optimum of 0.7
- Calibrating the convective heat transfer coefficient for the isothermal domain, and choosing an optimum of $6 \text{ W/m}^2\text{K}$ as an average value regarding the reaction zone – heating wall temperature difference.
- Tuning the insulation properties, including: the addition of a steel layer as a cover to the insulation, the addition of a clearance between the reactor and the insulation, and, calibrating the heat capacities, thermal conductivities, and densities
- Adding forced convection phenomenon on the outer surface of the reactor as per the experimental setup

After integrating all the previous steps, the results were adjusted, and the experimental versus simulation temperature profiles at different positions across the reactor are shown in Figure 30.

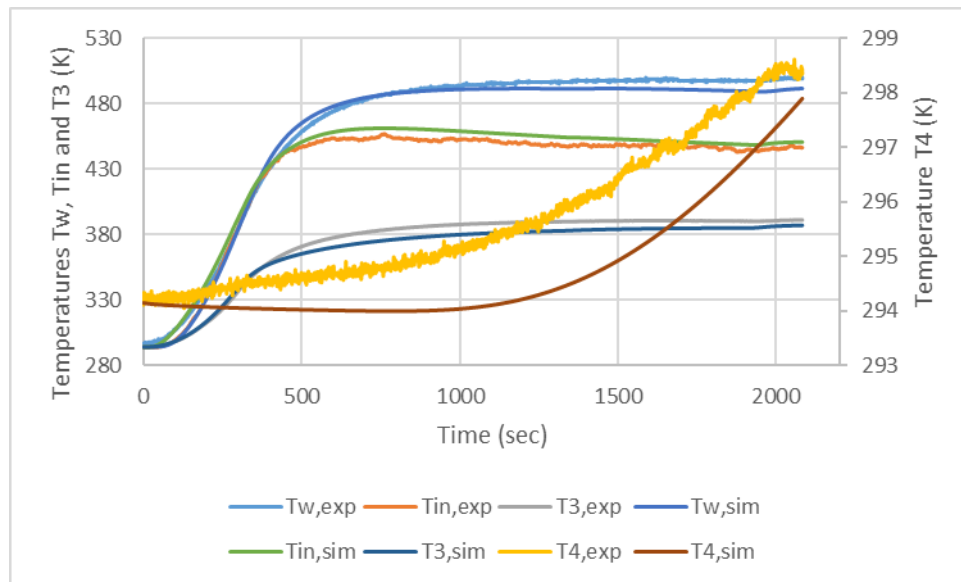


Figure 30: Experimental versus simulation temperature profiles for the nitrogen heating experiment

Results are satisfactory, all the curves behave in the same manner during the transient heating phase and the steady state phase, with a maximum error of 3.38% for the wall temperature, 3.98% for the inner temperature, 2.14% for the third thermocouple and 0.59% for the fourth thermocouple. The results are considered in good agreement for the given error values.

2.2. Pressurization

Before heating the empty reactor, it is purged with nitrogen, thus, the reactor is not literally empty, it contains only nitrogen gas at atmospheric conditions. Figure 31 shows the variation of the nitrogen's experimental pressure, the nitrogen's simulation pressure following the ideal gas law, and the nitrogen's simulation pressure following the real gas law function of the inner temperature.

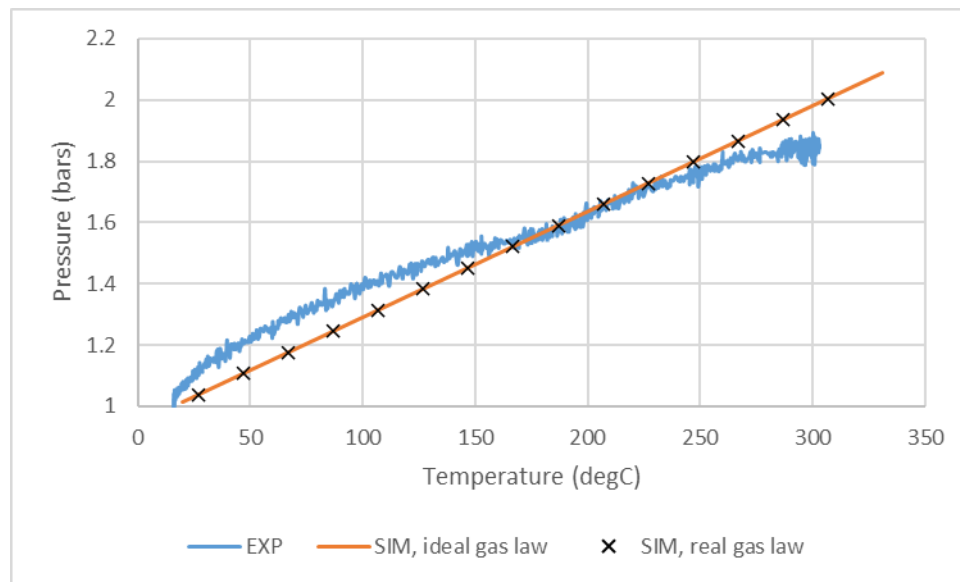


Figure 31: Experimental pressure and simulation pressures using ideal and real gas laws plotted versus the inner temperature of the reactor

According to the plotted data, for the reactor's operating range of temperature (up to 400 degC), there is no difference between adopting the real gas law or the ideal gas law for nitrogen pressurization. This is clearly stated in the error between the two sets of values, where the maximum error is always less than 0.07%. Such an agreement between the two laws is due to the fact that the intermolecular forces

between nitrogen gas molecules are very weak compared to other gases, that's why nitrogen gas can be treated as an ideal gas in this operating range.

However, when comparing simulated and experimental pressures, it is noticed that the experimental pressure deviates from the numerical pressure at low temperatures (below 150 degC), causing a maximum error of 8.88%, after which the error decreases, then, at high temperatures (above 300 degC), the experimental pressure curve deviates again, but this time it goes under the simulation pressure, with a maximum error of 7.54%.

The deviation of the experimental curve at the beginning of the heating phase can be related to the fact that the inner thermocouple has a high heat inertia (capacity) compared to the quantity of nitrogen inside the reactor, which means that at the beginning of the heating phase, the thermocouple is colder than nitrogen, thus, using the thermocouple's reading at this stage for plotting the PT diagram will generate a curve higher than the actual value.

Whereas, the deviation of the experimental curve at higher temperatures has a different reason. Temperature T_{in} is not the actual temperature of nitrogen inside the reactor; it is also influenced by the radiation energy absorbed from the reactor's walls. At high temperatures, the radiation effect increases dramatically, thus the temperature of the thermocouple is higher than the nitrogen's temperature, thus, using the thermocouple's reading at this stage for plotting the PT diagram will generate a curve lower than the actual value.

3. Liquid Solvents Heating

In this section, the inner experimental and simulated inner temperatures inside the reactor, along with the experimental and simulated internal pressures will be compared and discussed for the water, methanol, and ethanol heating experiments.

3.1. Water Heating

Figure 32 and Figure 33 show respectively the experimental and simulated inner temperatures and internal pressures of the water heating experiment, starting from atmospheric pressure, but without considering the evaporation phenomenon.

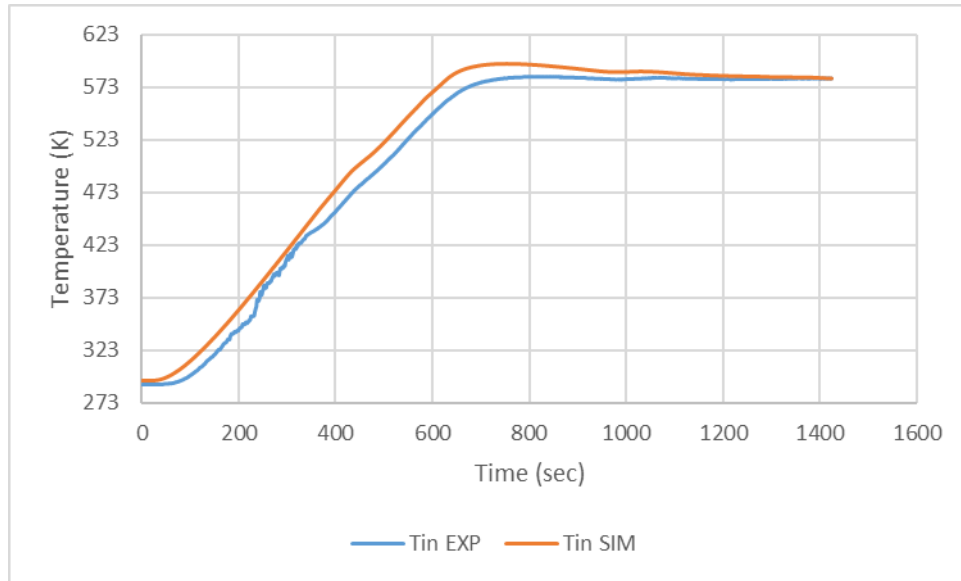


Figure 32: Experimental vs simulation inner temperature for the water heating experiment, starting from atmospheric pressure and neglecting the evaporation phenomenon

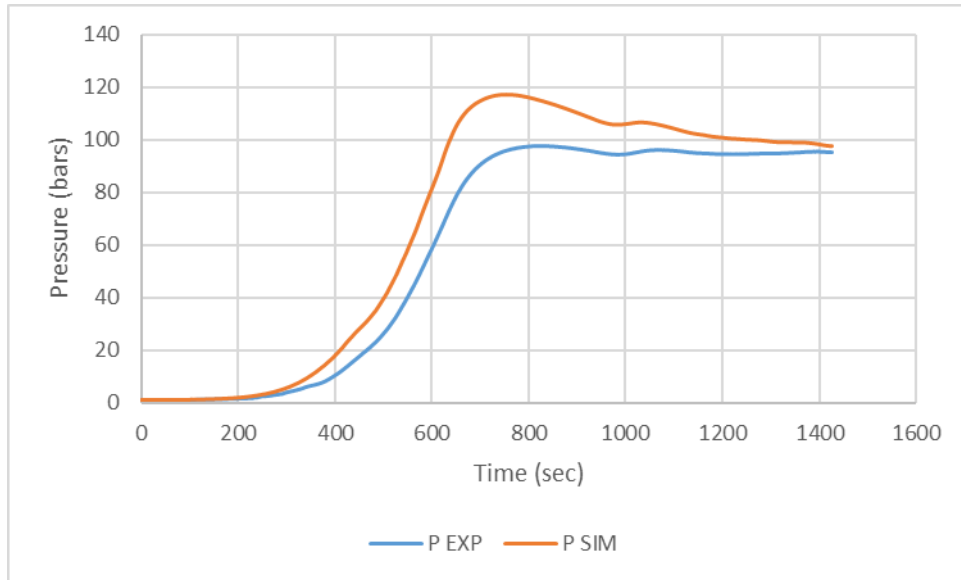


Figure 33: Experimental vs simulation internal pressure for the water heating experiment, starting from atmospheric pressure and neglecting the evaporation phenomenon

Although, the maximum error percentage in the temperature curve is 6.5%, but the graphical results seem acceptable. However, this small error in the temperature curve creates a large error in the pressure comparison results, due to the highly sensitive relation between the temperature and the pressure at elevated values. The maximum error in the pressure results exceeded 30%, which is not acceptable. The simulated temperature is higher than the experimental temperature, causing the simulated pressure to be also greater than the experimental pressure. For this reason, evaporation was modelled and integrated in the simulation model, and the latent heat absorbed by quantity of evaporated water improved the results and sharpened their accuracy. Figure 34 and Figure 35 show respectively the experimental and simulated inner temperatures and internal pressures of the water heating experiment, starting from atmospheric pressure, and considering the evaporation phenomenon.

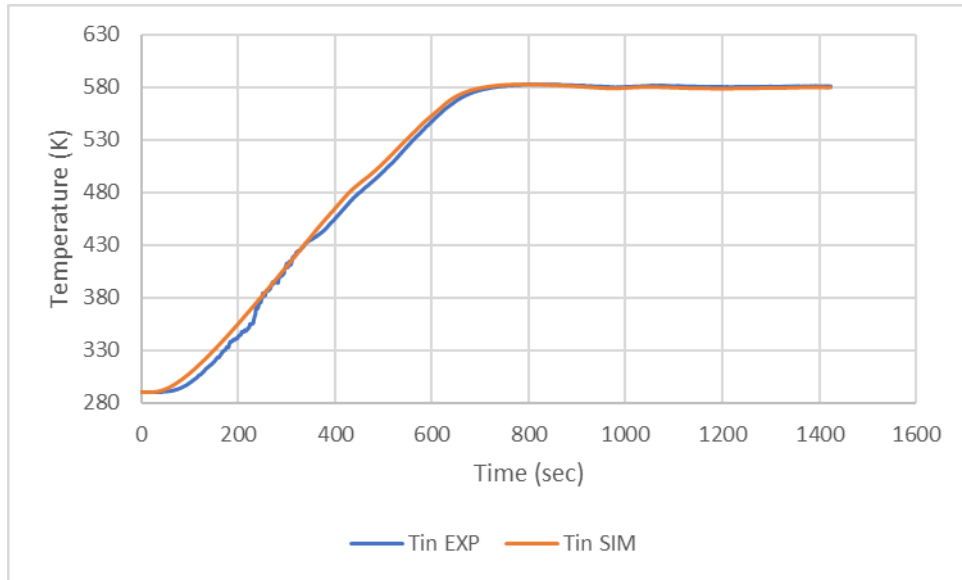


Figure 34: Experimental vs simulation inner temperature for the water heating experiment, starting from atmospheric pressure and taking the evaporation phenomenon into account

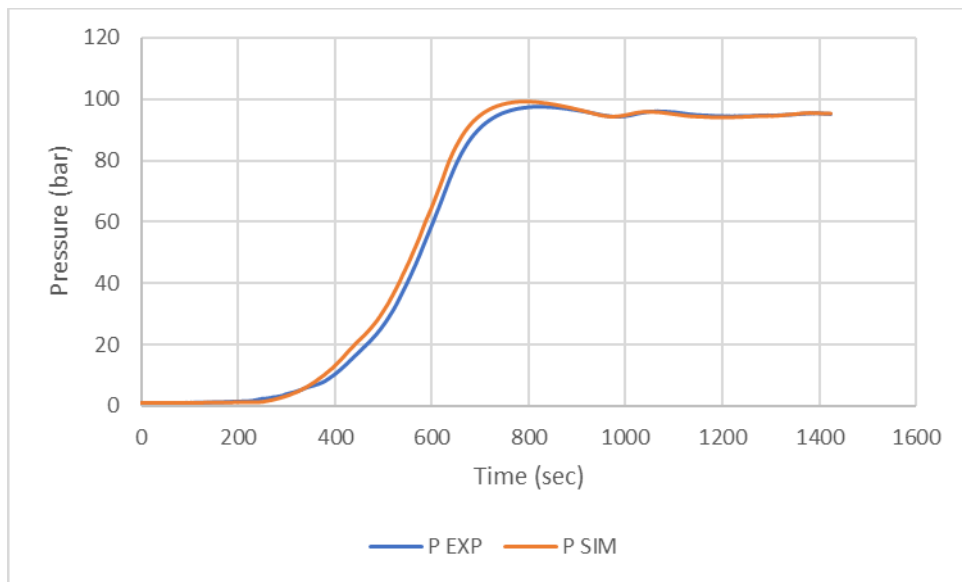


Figure 35: Experimental vs simulation internal pressure for the water heating experiment, starting from atmospheric pressure and taking the evaporation phenomenon into account

Both temperature and pressure curves revealed satisfactory results. The transition heating phase is starting approximately at the same instant for both experimental and simulated curves. And, the rate of temperature increase has the same value in both curves, around 0.4 K/s, revealed in the same curve inclination from the beginning of heating till reaching the stabilized temperature phase. The maximum error in temperature occurred at $t = 220$ seconds, with a relative value of 4.5%, but it diminished quickly, to reach

less than 0.5% in the steady state phase. Regarding the pressure curves, the same behavior is noticed for both experimental and simulated pressures, with a little deviation for time ranging between 300 and 800 seconds, caused by the temperature deviation in the heating phase. However, both curves converge after 800 seconds, for a relative error less than 2%.

Figure 36 and Figure 37 show respectively the experimental and simulated inner temperatures and internal pressures of the water heating experiment starting from nitrogen-pressurized medium.

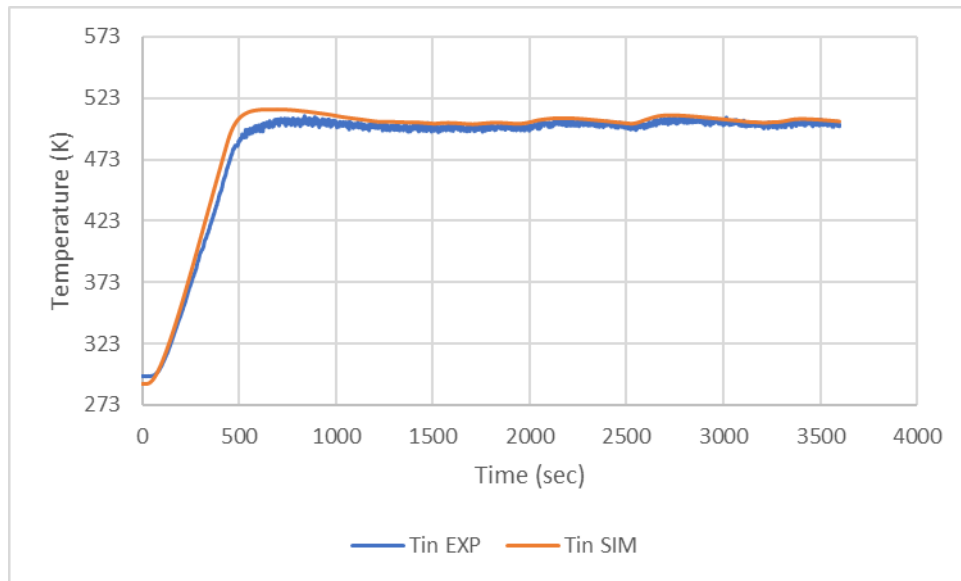


Figure 36: Experimental and simulated inner temperature in the water heating starting from nitrogen-pressurized medium

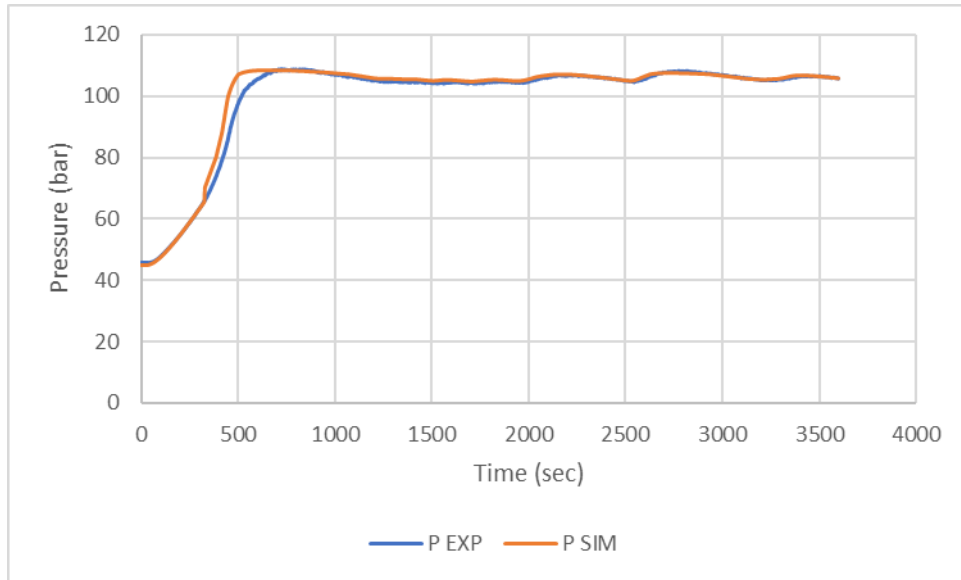


Figure 37: Experimental and simulated internal pressures in the water heating starting from nitrogen-pressurized medium

The temperature curve shows a good agreement between experimental and simulated temperatures, where the maximum error remained below 5% during the heating phase, and below 1% in the stabilized temperature phase. Regarding the pressure curves, it is shown that the beginning of the pressurization follows approximately a linear behavior. This is referred to the fact that pressurized nitrogen is controlling the medium's pressure, which increases linearly with temperature. However, beyond 80 bars, the experimental pressure and temperature lag a little beyond the numerical ones. This may be explained by the fact that a little portion of water is evaporated, absorbing latent heat enough to deviate the results. However, the stabilized relative error between the experimental and simulated pressures remained below 2%.

3.2. Methanol and Ethanol Heating

Figures 38 to 41 show respectively the experimental and simulated inner temperatures and internal pressures of the methanol and ethanol heating experiments starting from nitrogen-pressurized medium.

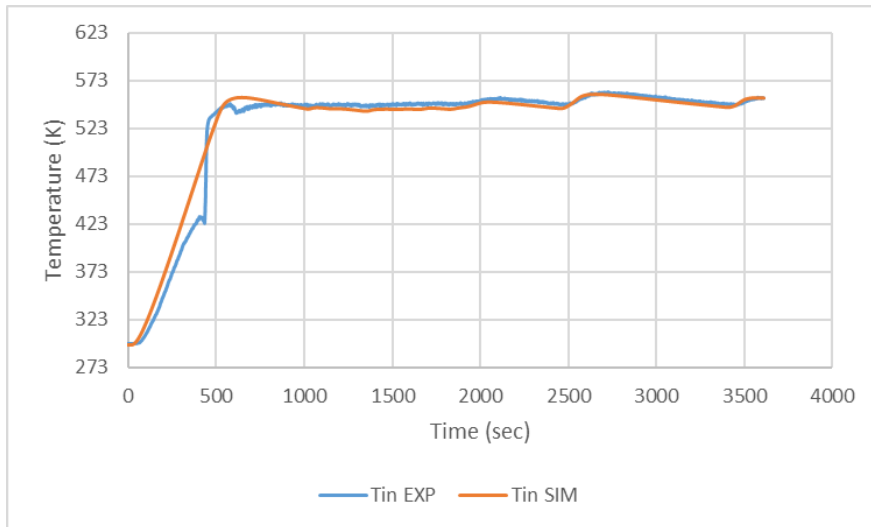


Figure 38: Experimental and simulated inner temperature in the methanol heating starting from nitrogen-pressurized medium

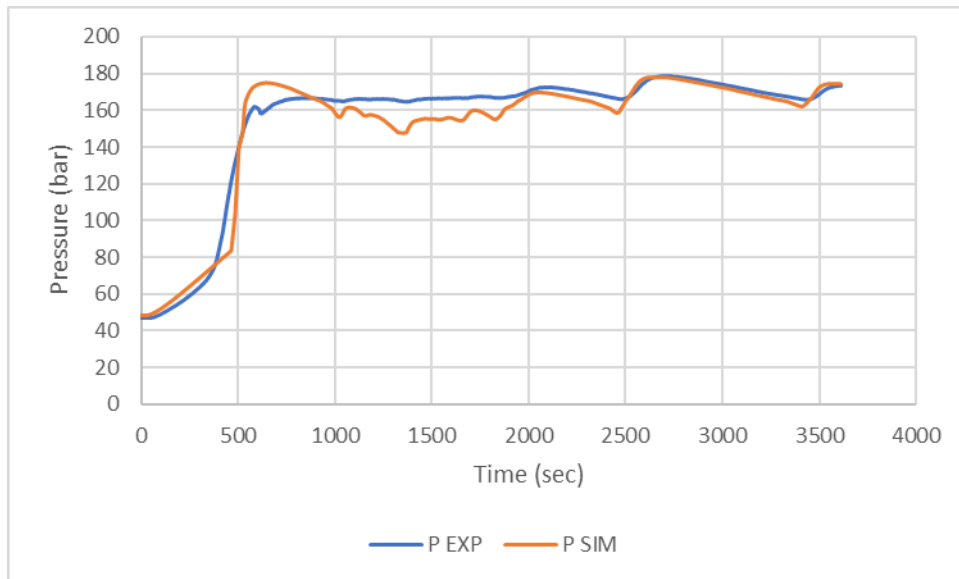


Figure 39: Experimental and simulated internal pressures in the methanol heating starting from nitrogen-pressurized medium

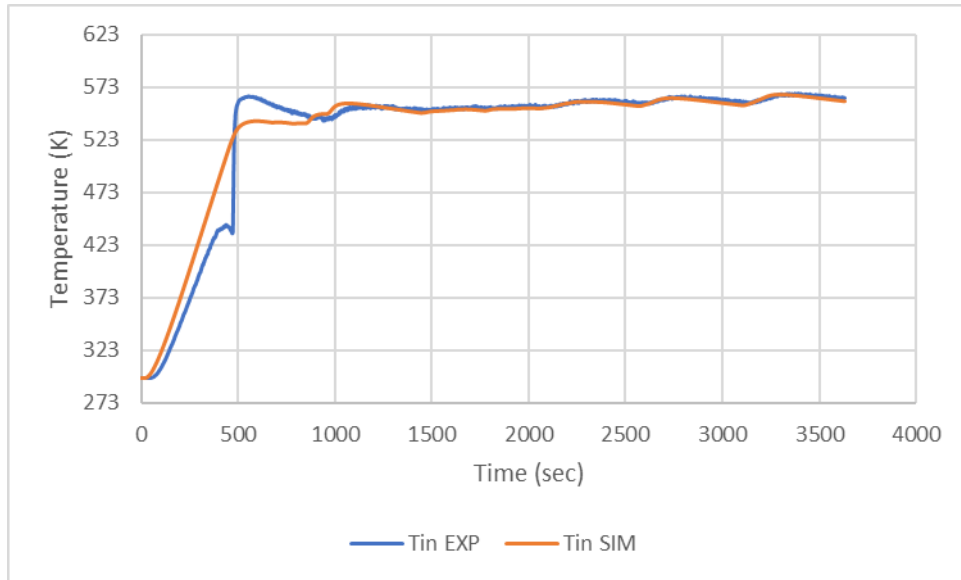


Figure 40: Experimental and simulated inner temperature in the ethanol heating starting from nitrogen-pressurized medium

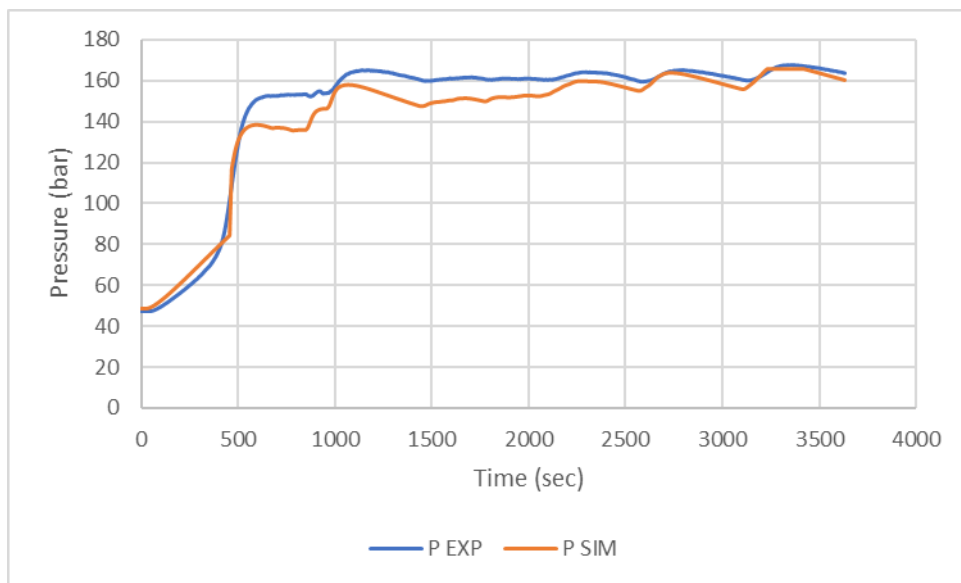


Figure 41: Experimental and simulated internal pressures in the ethanol heating starting from nitrogen-pressurized medium

In both experiments, the simulated temperature curves increase linearly to reach the steady state temperature. However, the experimental temperature experiences a lag in the heating phase, after which the temperature jumps suddenly and then converges to the simulated temperature. Although the bump between the two curves caused an instantaneous error of 16% in methanol and 20% in ethanol, the steady state error remains below 1% for both experiments. The pressure curves experience an approximately linear behavior upon reaching the critical pressure, after which it increases dramatically to reach a steady state behavior.

The fluctuations between the experimental and the simulated curves are due to the high sensitivity of pressure-temperature relation for supercritical methanol at elevated temperatures, in which a two-degree temperature difference will cause a deviation in the pressure value, which may exceed 5 bars. However, as prementioned, the aim of pressurizing the medium is to keep the methanol in a monophasic, and as long as the fluctuations are occurring without changing the state of methanol (staying in the supercritical state), and as long as the temperature curves are converged, then we can proceed to the next step.

4. Supercritical Methanol Transesterification

After ensuring that the model is verified totally from empty reactor performance till the liquid solvents heating including pressurization, the last step is to verify that the model's behavior is valid for supercritical methanol transesterification of rapeseed oil.

The experiments were conducted in methanol solvent, which behavior is validated in the previous section. However, to ensure that the key component of chemical transformation, the medium temperature, is valid experimentally and numerically, the temperatures of the three transesterification experiments done for 1 hour, 2 hours and 3 hours are compared, and the results were quite satisfying. The results of the three experiments are plotted in Figures 42 - 44:

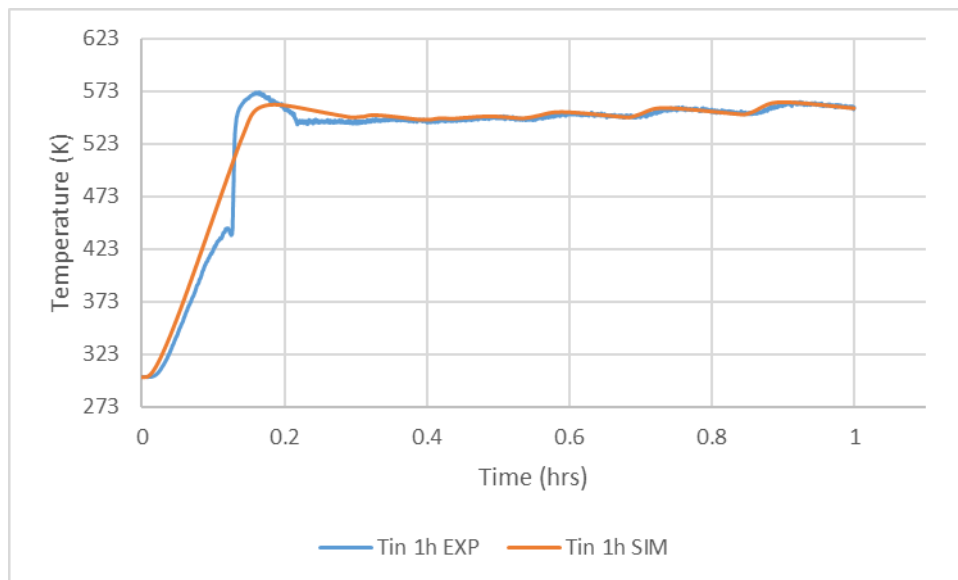


Figure 42: Experimental and simulated inner temperature of the reactor in the one-hour transesterification experiment

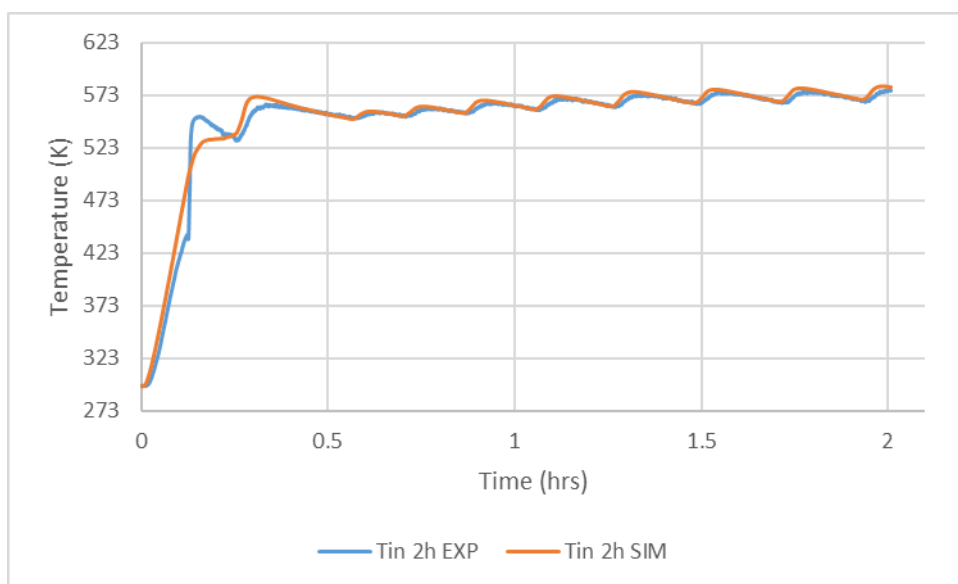


Figure 43: Experimental and simulated inner temperature of the reactor in the two-hour transesterification experiment

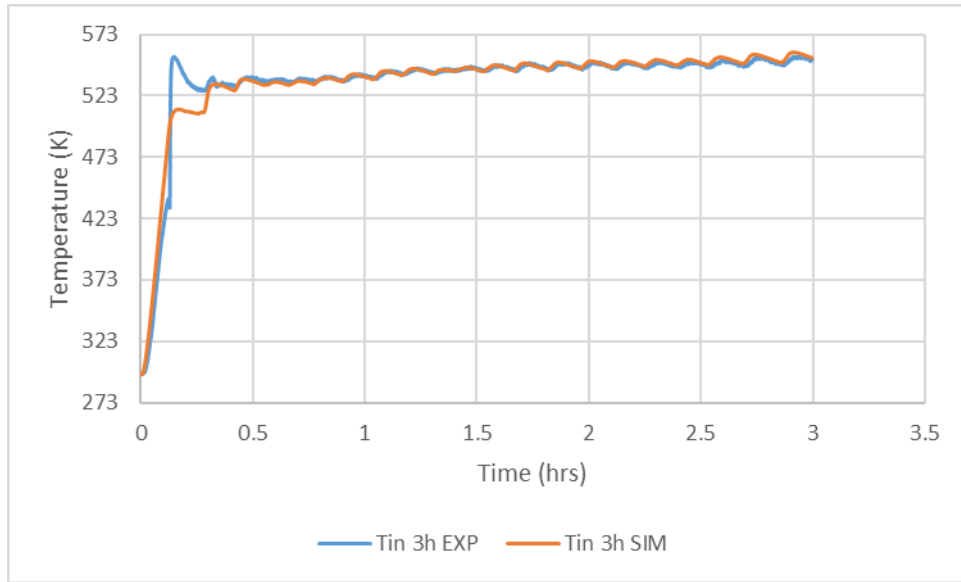


Figure 44: Experimental and simulated inner temperature of the reactor in the three-hour transesterification experiment

The simulated temperature variation is in good compatibility with the experimental one inside the reactor. Errors were almost null in the steady state phase, after the temperature exceeds 523K, the temperature at which the kinetics of the supercritical methanol transesterification becomes noticeable, referring to Kusdiana and Saka’s work [164].

The quantity of produced biodiesel was calculated using Gambill’s relation as stated previously (equation 44), where the kinematic viscosity of a liquid-liquid mixture is used to determine the mass fraction of each liquid in the mixture, which is used to calculate the conversion to biodiesel. The results are tabulated below:

Table 9: Viscosity of the supercritical transesterification products, and the conversion of each experiment

Experiment	Dynamic Viscosity (mPa.s)	Kinematic Viscosity (mm ² /s)	Biodiesel Mass Fraction	Conversion
1-hour	6.29	6.989	0.8104	0.928
2-hour	6.01	6.678	0.8265	0.935
3-hour	4.52	5.022	0.9214	0.972

The calculated values of the conversion for each experiment are plotted in comparison with the simulated conversion curve. The results are shown in Figure 45:

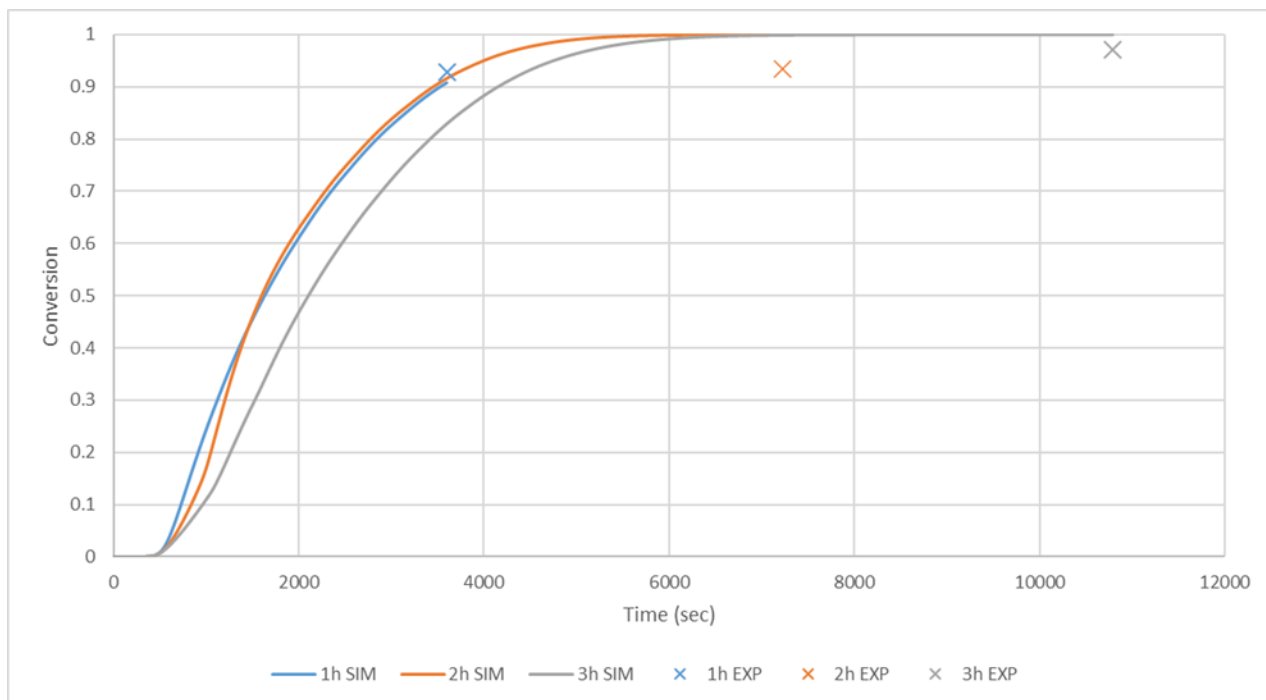


Figure 45: Numerical conversion curve, with the final products' experimental conversion points

The results are quite satisfactory, with errors of 2.47%, 5.88% and 1.85% respectively for the 1-hour, 2-hours and 3-hours experiments. It is noticed that the conversion in the three-hour experiment lags behind the first and the second, which is due to the fact that in this experiment, the temperature did not reach the values reached in the first two experiments as explained previously. The heaters were turned on, aiming for 300 Celsius degrees, the temperature stabilized around 270 and increased gradually to 280 throughout the experiment, slowing down the rate of the reaction, which is strongly temperature dependent.

5. Decomposition of Sodium Bicarbonate

Sodium bicarbonate decomposition was selected as a simple chemical reaction producing only one gaseous product; carbon dioxide. This criterion helps the calibration of the simulation model for the production of gaseous products, allowing us to improve it to simulate full hydrothermal liquefaction reactions of model macromolecules producing several gas compounds products. In this section, the results of decomposition of sodium bicarbonate in the thermogravimetric analyzer and batch reactor will be presented and discussed.

5.1. TGA Analysis of Sodium Bicarbonate Decomposition

Figure 46 shows the variation of temperature of the sodium bicarbonate sample under study versus its mass loss.

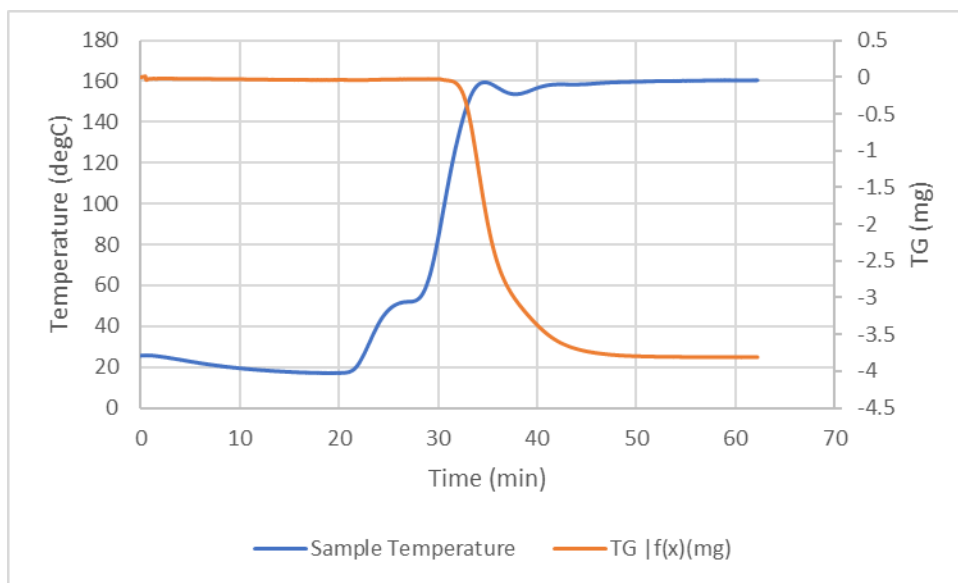


Figure 46: TGA analysis of sodium bicarbonate decomposition

The results show that the decomposition of sodium bicarbonate starts after the temperature exceeds 110 Celsius degrees, which complies with all of the previously reported kinetics. The kinetic analysis of the results is divided into two parts, the first one is based on the temperature rise method, and the second part is based on the isothermal method. Results were compared to the reported kinetics, and it was found that the most compatible kinetic model with the decomposition of sodium bicarbonate is that proposed by Hartman et al [177].

Figure 47 shows a comparison of the conversion calculated through the TGA analysis (X TGA) versus the conversion calculated through the application of Hartman's kinetic model (X).

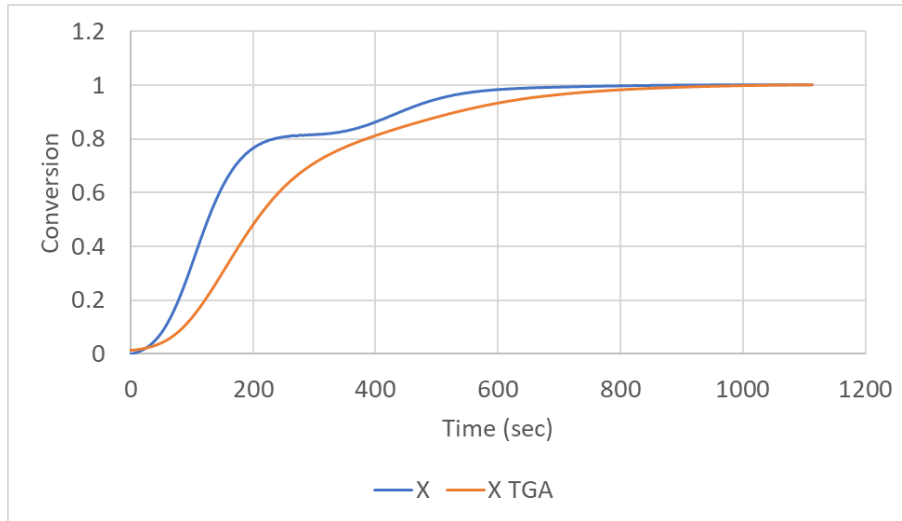


Figure 47: Comparison of the conversion of decomposition of sodium bicarbonate using Hartman's model and TGA results

The reaction starts at the same instant for curves, and it reaches 99% conversion after about 800 seconds for both models. Thus, this model can be considered valid, and its Arrhenius kinetic parameters can be used in COMSOL for modelling the decomposition of sodium bicarbonate in the batch reactor.

5.2. Decomposition of Sodium Bicarbonate in the Batch Reactor

Figures 48-50 show respectively the reaction progress through the production of carbon dioxide versus the inner temperature of the reactor in the three experiments conducted on sodium bicarbonate decomposition inside the reactor at three different temperatures; 473, 423 and 373 K.

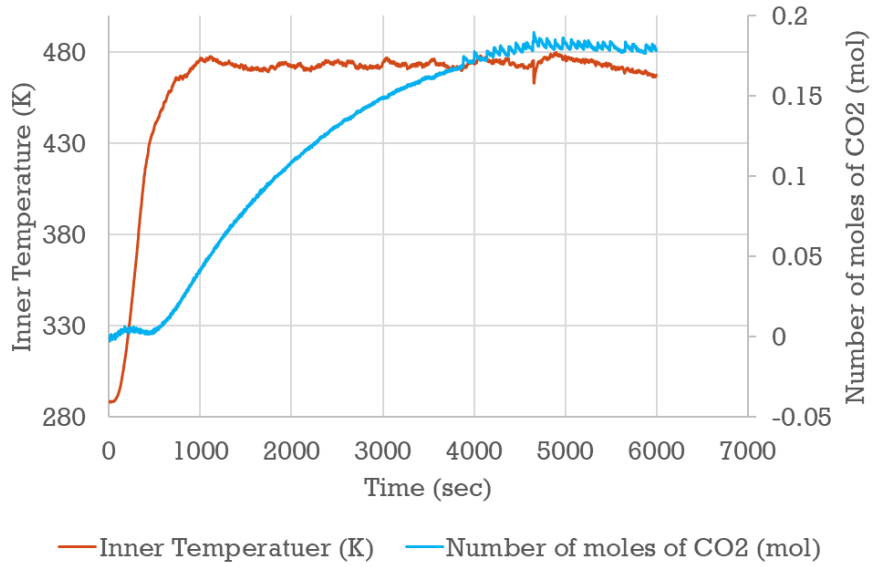


Figure 48: Inner temperature of the reactor and the instantaneous number of moles of produced carbon dioxide in the 473K sodium decomposition experiment

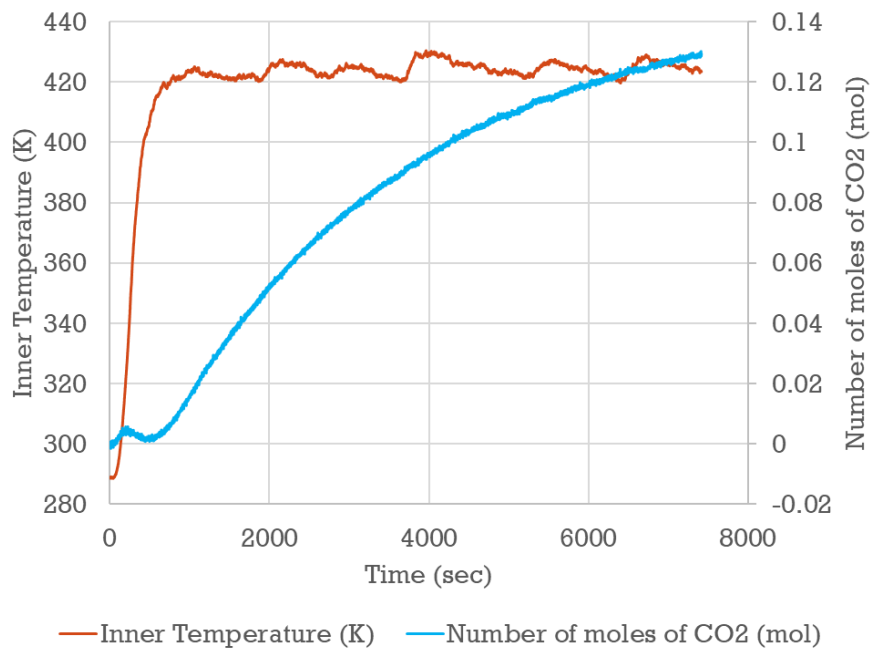


Figure 49: Inner temperature of the reactor and the instantaneous number of moles of produced carbon dioxide in the 423K sodium decomposition experiment

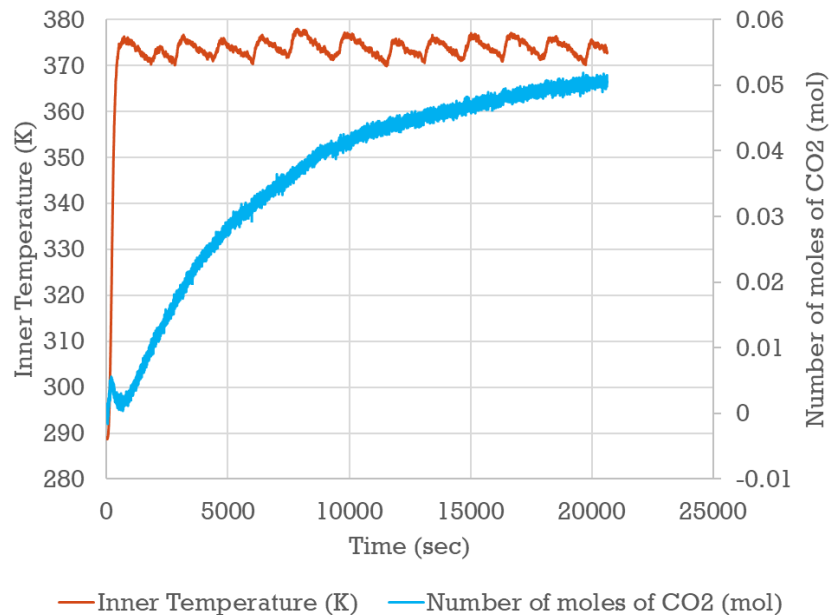


Figure 50: Inner temperature of the reactor and the instantaneous number of moles of produced carbon dioxide in the 373K sodium decomposition experiment

In the first experiment, the reaction is considered completed since the number of moles of produced carbon dioxide reached its final value (0.1785 moles). However, in the second and third experiments, the carbon dioxide indicator showed that the reaction was not completed, although according to the chemical kinetics, it should be ending by the given time.

However, before simulating this chemical reaction in COMSOL, it was noticed that the carbon dioxide quantity is not stabilized in the reactor, even after the reaction ends. For this reason, the data acquisition system was intentionally left operating to record the pressure values after the reaction ends and the reactor cools down, to check what is happening inside the reactor. Figure 51 shows the temperature and pressure curves from the beginning of the sodium bicarbonate decomposition experiment until cooling down and stabilizing.

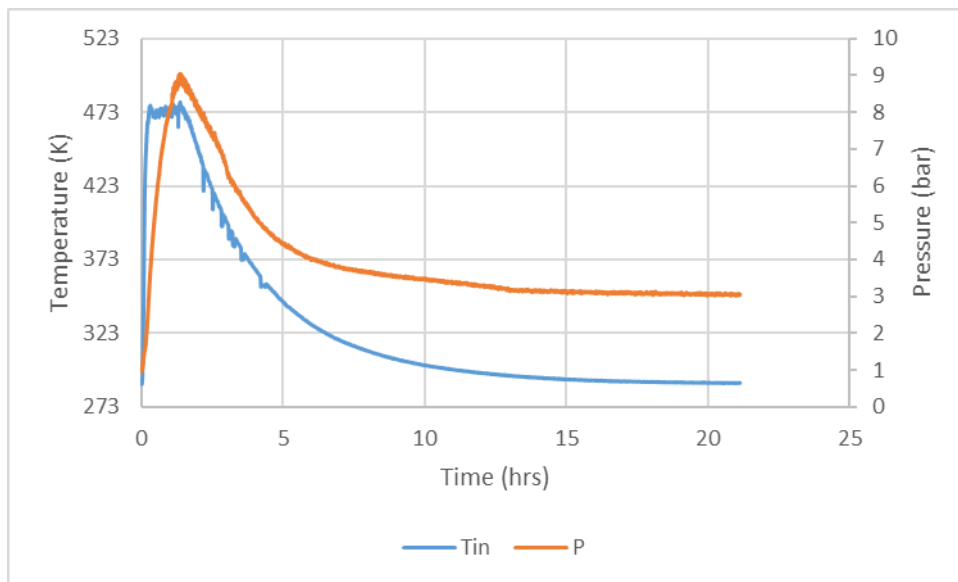


Figure 51: Temperature and pressure curves for the sodium decomposition experiment after cooling down and stabilizing

It is noticed that after turning off the heaters, the reactor cools down, and the temperature decays to its ambient value. Following the temperature drop, the pressure also drops, but not to the atmospheric value, and this is due to the fact that the produced carbon dioxide pressurizes the medium. Figure 52 shows the number of moles of carbon dioxide produced in the experiment calculated through the partial pressure of carbon dioxide.

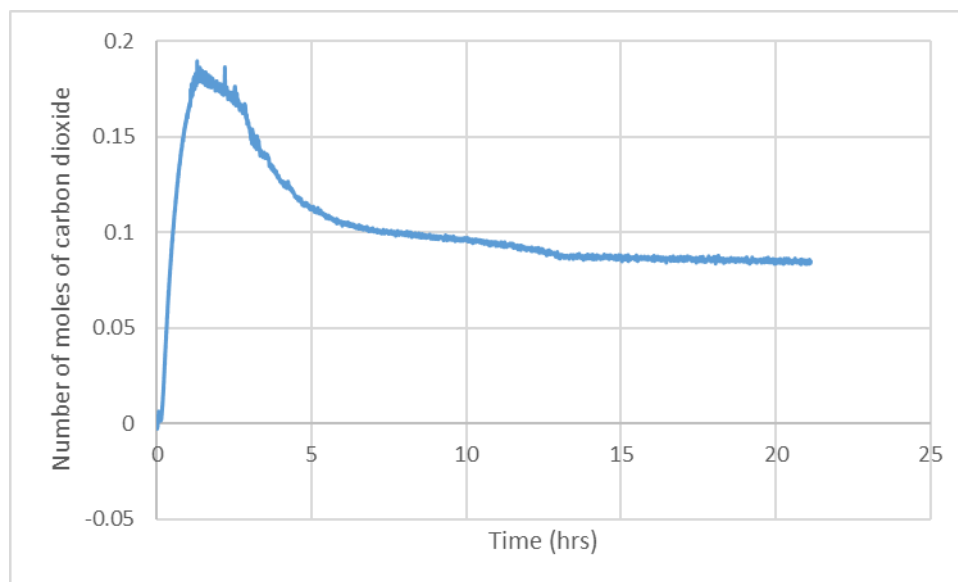


Figure 52: Variation of number of moles occupying the gaseous volume in the reactor throughout the experimental time and cooling time

After turning off the heaters, and upon the cooling down of the reactor, the number of moles of carbon dioxide decreases from 0.1785 moles to about 0.08 moles. This is referred to the fact that the produced carbon dioxide gas is dissolving in the water produced by the reaction, especially that at elevated pressures, the solubility of carbon dioxide in water increases dramatically. In 2018, Materials journal published an article titled “Effective capture of carbon dioxide using hydrated sodium carbonate powders” [178]. Results showed that sodium carbonate (Na_2CO_3) powders with 30 wt.% water can achieve a very high carbon dioxide absorption capacity of 282 mg/g within 60 mins, 90% of it achieved during the first 16 mins, so the process is fast. Since the products of sodium bicarbonate decomposition are carbon dioxide, water and sodium carbonate, then we will already have hydrated sodium carbonate in the product phase which absorbs a relatively high quantity of CO_2 . The absorption of carbon dioxide produced from the reaction causes a pressure drop inside the reactor due to the decreasing in the number of moles of gaseous carbon dioxide. This phenomenon prevents using the pressure variation in the reactor as an indicator for the reaction progress over time.

6. Results Validity

Among the previously reported results for the simulation and modelling of the HTL process, there is no work exactly similar to our model. However, researchers have reported results regarding the simulation of hydrothermal liquefaction in continuous reactors, or the simulation of other processes in a batch reactor. In all cases, the same phenomena are studied; heat transfer, pressurization, mass transport, etc. This section will compare the relative errors between experimental and simulated results for the previous works conducted and for this work.

In his study of simulating a tubular reactor for the hydrothermal liquefaction of biomass, Zhang [142] plotted the wall temperature profile across the axial direction of the reactor. The simulation results are compared to the experimental results, where the relative error percentage reached a maximum of 15% at the midpoint of the reactor before converging to less than 2% at its outlet. In another work, Ranganathan built a simulation model for the hydrothermal liquefaction of microalgae in a continuous reactor [179]. He compared his CFD model's temperature across the reactor to the experimental temperature, where the maximum relative error percentage remained below 10% at the reactor's midpoint, before converging to less than 1% at its outlet. Moreover, Mazloun et al. [180] modelled a batch plastic pyrolysis reactor. Results showed that the all-maximum temperature error across the reactor remained below 4%. Chen et al [181] simulated the hydrothermal liquefaction process in a coil reactor, and compared the mass fraction results of the reactants and the products based on experiments carried on a batch reactors. Results showed a good agreement, where the results converged to less than 5% error after 10 minutes.

Compared to the above reported works, the relative errors between the simulated and experimental results in our work, are in the range of the accepted values, where the maximum error in temperature remained below 4%, and diminished to less than 2% in the steady state regimes. Moreover, the final chemical conversion error remained below 6% for all the experiments conducted. Thus, our model can be considered validated.

7. Conclusion

The aim of this work is to build a numerical model simulating a batch reactor used for the hydrothermal liquefaction of biomass. The goal is achieved by conducting several experiments on a 1 L batch reactor, and developing the simulation model in parallel with each experiment, comparing step-by-step the experimental and numerical results.

The work plan started by conducting an empty reactor heating study, in which the maximum error between the experimental and simulated data were less than 4%. Ideal and real gas laws were investigated numerically to predict the gas behavior inside the reactor, and it was noticed that both laws are applicable in the full experimental range of operation, and the maximum error remained below 9%. Solvents heating experiments were conducted, the errors between simulated and measure temperatures were always acceptable, and the pressure was noticed to follow the saturation pressure of the solvents induced when starting from atmospheric pressure. Whereas, when starting with a nitrogen pressurized medium, the pressure follows the nitrogen's partial pressure as long as it is larger than the instantaneous solvent's vapor pressure, whereas at the moment where evaporation takes place, the medium's pressure follows the solvent's pressure again.

Supercritical methanol transesterification was selected as the first step of chemical process to be modelled and validated. The reaction kinetics were adopted from previous works studying the process over a wide range of pressure and temperature conditions [164]. The comparison of experimental and simulation results showed great compatibility, where the errors between simulated and measured temperatures were almost negligible, and the errors between experimental and simulated conversion remained below 6%, regardless of the reaction conditions (temperature and time). The validity of this built numerical model is achieved, and the model can be used for numerically tuning and calibrating hydrothermal processes, and it can be the base of building and designing a continuous reactor for the same processes.

In addition to validating the model using the supercritical methanol transesterification of rapeseed oil, an approach was made to validate other model macromolecules, starting with cellulose, which produces significant gaseous products. To simplify the procedure, a simple reaction was subjected to testing, the decomposition of sodium bicarbonate. However, tracking the reaction kinetics through monitoring the pressure inside the reactor was doubted due to the high solubility of carbon dioxide in water and hydrated sodium carbonate product.

Further validation of the model can be done by intensively studying the solubility of carbon dioxide in water at a wide range of temperatures and pressures, to predict the instantaneous amount of dissolved carbon dioxide, and thus, obtaining the real undoubtable quantity of the gas inside the reactor, and making sure that the results will be accurate and hard based.

Now, after validating the simulation model for the supercritical methanol transesterification of rapeseed oil, the final step in this project can be initiated, and the results can be used to design a continuous reactor for the same process, based on the same thermo-physical and chemical phenomena studied and validated.

Chapter 4. Design of a Continuous System for the Supercritical Methanol Transesterification of Rapeseed Oil

1. Introduction

The final goal of this work is to design a system for the hydrothermal liquefaction of biomass. As a first step a reactor type should be chosen. Batch reactors are known for their basic design; simple fabrication and modification processes, and, their ability to handle various types and qualities of biomass [182], in addition to the small instrumentations and less supporting equipment needed compared to continuous reactors [183]. On the other hand, continuous reactors dominate in terms of process comparisons, safety when it comes to handling hazardous material and utilizing high pressures, ability to perform faster reactions, and setting a route for scaling up the process [184]. For these reasons, in this work, the choice settled on designing a continuous hydrothermal liquefaction system meant to be manufactured and used in research centers, where the processes can be studied, tuned, optimized, and scaled-up to commercialization.

In this chapter, the detailed steps followed to design a continuous hydrothermal liquefaction system are listed and discussed, including the material selection, geometry preferences, operating parameters and process optimization. The reactor is designed and calibrated using the results of the supercritical methanol transesterification presented and discussed in the previous chapters.

2. Plug Flow Reactor, PFR

A plug flow reactor, or PFR, is the simplest continuous reactor that can be built. It consists of a hollow cylinder, in which reactants enter from one side, heat up and react before exiting from the other

side. PFRs are known for their ability to handle high pressures and temperatures, ensuring fast processes, including homogeneous and heterogeneous reactions [185].

2.1. Materials Selection

The biofuel produced from the hydrothermal liquefaction of biomass contains some acids [186], which induces corrosion in the material flowing over. In addition, the process conditions of hydrothermal liquefaction are quite high, with temperatures elevating up to 450 Celsius degrees, and pressures up to 250 bars creating internal stresses in the material. Thus, the reactor's material should be corrosion resistive, in addition to its ability to handle the critical atmosphere of the process. Stainless steel has been established as an excellent material for building chemical reactors. Many researchers [187]–[191] used stainless-steel in hydrothermal liquefaction experiments, handling temperatures up to 400 Celsius degrees and pressures up to 250 bars. Thus, the reactor is chosen to be built of stain-less steel AISI 316L, with the following mechanical and thermal properties shown in Table 10 [192]:

Table 10: Mechanical and thermal properties of AISI 316L stainless-steel

Material property	Symbol (Unit)	Value
Young's modulus	E_{st} (GPa)	193
Yield stress	σ_{y_st} (MPa)	205 @ 293 K 170 @ 673 K
Thermal expansion coefficient	α_{st} ($10^{-6} K^{-1}$)	17.5 @ 673.15 K
Poisson's ratio	ν_{st}	0.25
Density	ρ_{st} (kg/m^3)	8000
Heat capacity at constant pressure	C_{p_st} (J/(kg.K))	510
Thermal conductivity	k_{st} (W/(m.K))	13.5 @ 300 K 15 @ 373.15 K 18.5 @ 673.15 K

An insulation layer is used to cover the reactor's body, for safety issues, and in order to decrease the heat power lost from the system, increasing its overall efficiency. The insulation material selected is the glass wool, its thermal properties are predefined in COMSOL's material library and represented in Table 11 [170]:

Table 11: Thermal properties of glass wool insulation

Material property	Symbol (unit)	Value
Density	ρ_{ins} (kg/m ³)	22
Heat capacity at constant pressure	C_{p-ins} (J/(kg.K))	850
Thermal conductivity	k_{ins} (W/(m.K))	0.035 @ 300 K 0.065 @ 450 K 0.09 @ 600 K 0.107 @ 700 K

2.2. Geometry

The reactor has a cylindrical shape, defined by three parameters; length L , inner radius r_i , and outer radius r_o , where the thickness e of the reactor's wall is defined by the difference between the inner and the outer radii $e = r_o - r_i$.

2.2.1. Inner radius selection

The inner radius is a critical parameter to select when designing a plug flow reactor. The smaller the inner radius is, the faster the slurry will achieve the desired temperature. On the other hand, thin reactors suffer from the slurry clogging inside it, especially for highly viscous slurries and slurries containing significant portion of solid content. Thus, a compromise must be made, choosing an inner radius small enough to enhance the fast thermal homogenization of the flowing slurry, but not too small in order to prevent the slurry clogging.

In the case of supercritical methanol transesterification, heated oil, biodiesel and glycerin have relatively low viscosities (less than 30 mPa.s), and the slurry contains no solid particles, thus the clogging problem is not an issue. But the designed reactor is built for hydrothermal liquefaction processes, and should not be limited to supercritical methanol transesterification only. Thus, previous works were investigated to select the smallest inner radius allowing different slurries to pass through without clogging issues.

The Pacific Northwest National Laboratory [193] is a well reputed research center, in which there are several process developments units used for studying and optimizing processes. One of these units is a continuous flow reactor utilized by Elliott et al in several works [50], [54], [194]. The pumping system consists of 3/8 and half inch pipes, and the reactor is a 1-inch stainless-steel tube. In another work, Anastasakis et al [102] studied the hydrothermal liquefaction of biomass in a novel pilot plant. The system consisted on a reactor of half inch internal diameter.

Since the above reactors were able to handle microalgal and lignocellulosic biomass with significant solid content without any clogging problems, the inner radius of the reactor to be designed was chosen to be 1 cm (2 cm internal diameter).

2.2.2. Outer radius selection

After fixing the inner radius at 1 cm, the outer radius will define the thickness of the reactor. The thickness is a critical parameter in designing the system. Thick-walled reactors are known for their ability to handle high internal pressures, whereas thin-walled vessels are more efficient in heat transfer due to the low temperature gradient across the wall's thickness. For these reasons, a compromise must be made, choosing the minimum thickness that can handle the reaction's pressure.

When a hollow vessel is filled with a pressurized liquid, internal stresses are created across the walls of the vessel. Three normal stress components are resulted from such a phenomenon; axial, circumferential, and radial [195], shown in Figure 53 below:

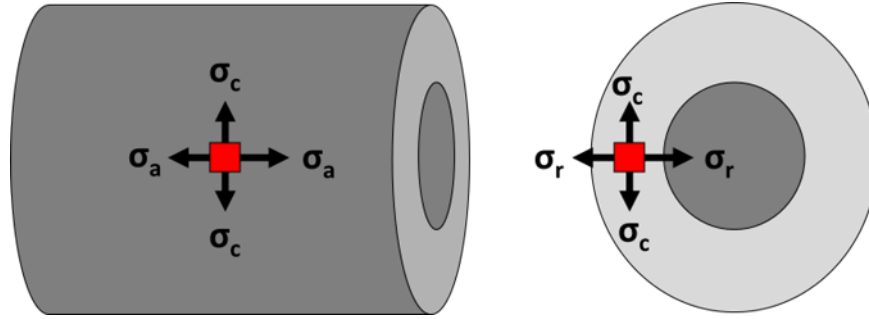


Figure 53: The three stress components presented in a thick-walled vessel under pressure

Stress in axial direction

The stress in axial direction at any point in the vessel can be expressed as:

$$\sigma_a = (p_i r_i^2 - p_o r_o^2) / (r_o^2 - r_i^2) \quad (58)$$

Where:

σ_a : stress in axial direction (MPa)

p_i : internal pressure in the vessel (MPa)

p_o : external pressure outside the vessel (MPa)

r_i : internal radius of the vessel (mm)

r_o : external radius of the vessel (mm)

Stress in circumferential direction (hoop stress)

The stress in circumferential direction – hoop stress – at any point in the vessel can be expressed as:

$$\sigma_c = [(p_i r_i^2 - p_o r_o^2) / (r_o^2 - r_i^2)] - [r_i^2 r_o^2 (p_o - p_i) / (r^2 (r_o^2 - r_i^2))] \quad (59)$$

Where:

σ_c : stress in circumferential direction (MPa)

Stress in radial direction

$$\sigma_r = [(p_i r_i^2 - p_o r_o^2)/(r_o^2 - r_i^2)] + [r_i^2 r_o^2 (p_o - p_i)/(r^2 (r_o^2 - r_i^2))] \quad (60)$$

Where:

σ_r : stress in radial direction (MPa)

Resultant stress

According to Von Mises theory [196], a material may yield even if none of the principal stresses acting on it reaches the yielding stress. He defined a virtual stress component, Von Mises stress σ_{VM} , which is the resultant stress taking into consideration the effect the interaction between all the principal stresses in a finite element. When checking if a material reaches its yielding limit, Von Mises stress should be calculated and compared to the yield stress of the material, using the following equation:

$$\sigma_{VM} = \sqrt{\frac{1}{2} [(\sigma_1 - \sigma_2)^2 + (\sigma_1 - \sigma_3)^2 + (\sigma_2 - \sigma_3)^2]} \quad (61)$$

Where σ_1 , σ_2 , and σ_3 represent the three principal stresses inside the finite element.

Table 12 represents the stress components in a cylindrical tube of the selected inner radius (10 mm) and a suggested outer radius of 13 mm. The values of the stress components are determined on the inner and the outer radius of the tube in order not to miss the maximized value of Von Mises stress. The internal pressure is fixed at 250 MPa, which is the maximum pressure achieved in hydrothermal processing.

Table 12: Stress components and Von Mises stress in the cylindrical tube with an internal pressure of 19 MPa

Position	σ_a (MPa)	σ_c (MPa)	σ_r (MPa)	σ_{VM} (MPa)
$r = r_i$	36	97	-25	105
$r = r_o$	36	72.1	-0.1	62.52

The reactor is made of AISI 316L stainless-steel, with a yield stress of 170 MPa at 400 °C. A safety factor is set at 1.5 regarding the maximum allowable stress inside the reactor.

$$F.S = \sigma_{y_{st}}/\sigma_{allowable} \quad (62)$$

With a safety factor of 1.5, the maximum allowable stress inside the reactor should not exceed 113 MPa, which is acceptable for 105 MPa, the maximum Von Mises stress obtained at $r = r_i$.

2.2.3. Thermal Expansion Analysis

The thermal expansion coefficient of AISI 316L stainless-steel is $17.5 \times 10^{-6} \text{ K}^{-1}$, which means that at a temperature difference of $dT = 400 \text{ K}$, the elongation of the reactor's material is defined as:

$$\frac{dL}{L} = \alpha_{st} \times dT \quad (63)$$

Thus, dL/L is equal to $7 \times 10^{-3} \text{ mm/mm}$.

Assume the reactor is fixed, and the supports are preventing it from any expansion or relaxation, then the stress applied on the reactor's material to prevent it from moving is calculated using Hooke's Law:

$$\sigma = E \times \epsilon \quad (64)$$

Where $\epsilon = dL/L = 7 \times 10^{-3} \text{ mm/mm}$, thus the stress in the materials reaches 1351 MPa, much larger than its yielding stress.

Avoiding these dramatic values of stress can be done by placing the reactor on a roller support without pinning it or attaching it to any fixed part. Flexible tubes can be utilized for connecting the reactor to the pumping unit, and for leading the products to the separation unit.

2.2.4. Length Selection

The previously selected parameters including inner and outer radii will remain constant disregarding the flow rate of the slurry or the temperature of the reactor. However, the length of the reactor remains the flexible term, that will be chosen in later sections depending on the flow rate, temperature, and species conversion inside the reactor.

2.3. Fluid Flow inside the Reactor

Studying the fluid flow inside the reactor is an essential step for better understanding the behavior of the biomass slurry and the liquid products. In this section, the volumetric flow rate of the slurry will be discussed, passing to the flow velocity inside the reactor which defines the type of flow, whether it is laminar or turbulent, in order to predict and enhance the heat transfer between the reactor walls and the reactants flowing inside.

2.3.1. Volumetric flow rate

Lab-scale reactors are not intended to produce significant amounts of biofuel, that's why their volumetric flow rates are limited to few liters per hour. Billing et al [197] designed a continuous hydrothermal liquefaction unit with a volumetric flow rate up to 6 L/hr, whereas Elliott's reactor was capable to deliver up to 3 L/hr [194]. Another smaller unit tested by Patel and Hellgrat delivered only 0.24 L/hr [198].

In this work, three different volumetric flow rates are proposed; 2.5, 5 and 10 L/hr. For each flow rate, the reactor's length required to ensure 99% conversion is calculated.

2.3.2. Mean velocity inside the reactor

The average velocity of the slurry inside the reactor is calculated using the following equation:

$$u_{av} = Q/A_c \quad (65)$$

Where:

u_{av} : mean velocity inside the reactor (m/s)

Q : volumetric flow rate (m³/s);

A_c : reactor's inner cross-sectional area (m²); $A_c = \pi r_i^2 = 3.14159 \times 10^{-4} \text{ m}^2$.

Table 13 represents the average velocity for each of the pre-selected volumetric flow rates.

Table 13: Average flow velocities calculated from the selected flow rates inside the reactor

Q (L/hr)	Q (m ³ /s)	u_{av} (m/s)
2.5	6.94444×10^{-7}	2.21×10^{-3}
5	1.38888×10^{-6}	4.42×10^{-3}
10	2.77777×10^{-6}	8.84×10^{-3}

2.3.3. Type of flow

A fluid flowing inside a pipe can undergo laminar, transition, or turbulent flow phenomena. It is important to study and specify the type of flow inside the reactors for better understanding the slurry's behavior and calibrating the system for enhancing the heat transfer depending on the flow type. The parameter defining the type of flow is Reynolds number, defined as the ratio of the inertial forces to the viscous forces [199, p. 2], calculated through the following formula:

$$Re = \frac{\rho u D}{\mu} \quad (66)$$

Thus, to determine Reynold's number, it is required to determine the viscosity of the slurry first, containing rapeseed oil and methanol. In 1959, Gambill [165] proposed the following equation for estimating the kinematic viscosity of a two liquid mixture:

$$v^{1/3} = y_a v_a^{1/3} + y_b v_b^{1/3} \quad (67)$$

Where v represents the kinematic viscosity, expressed in mm²/s, and y represents the mass portion of the liquid in the mixture.

Applying Gambill's formula to the inlet slurry, with a molar ratio of methanol to oil of 42:1, equivalent to 1.525:1 mass ratio, gives a kinematic viscosity value of 7.445 mm²/s, equivalent to a dynamic viscosity of 6.261 mPa.s. The following table represents the Reynolds number at the inlet conditions for the preselected volumetric flow rates inside the reactor.

The density of the mixture is calculated by dividing the total mass by the total volume using the following formula:

$$\rho = \frac{m_{oil} + m_{methanol}}{V_{oil} + V_{methanol}} \quad (68)$$

Applying the above equation to the inlet slurry yields a mixture density of 841 kg/m³.

Table 14 represents the Reynolds number on the inlet conditions on the different preselected flow rates inside the reactor.

Table 14: Reynolds number at the inlet conditions for the selected flow rates

Q (L/hr)	Re
2.5	2.969
5	5.937
10	11.868

The flow at the inlet conditions is laminar, since the Reynolds number is less than 2000 [200].

2.4. Reactor's Length Estimation

As mentioned previously, the inner and outer radii are fixed parameters, and the length of the reactor will be selected according to each volumetric flow rate, ensuring 99% reaction completion. Figure 54 represents the basic operation of a simple plug flow reactor:



Figure 54: Basic operation mechanism of a plug flow reactor

The reactor is designed based on the results of the supercritical methanol transesterification process in a batch reactor, in which the kinetic model was chosen to follow a pseudo first order form. The governing equation of first order reaction occurring in a plug flow reactor is given by [201]:

$$\frac{dF_A}{dV} = r_A \quad (69)$$

Where:

$F_A = Q \times C_A$ is the molar flow rate of species A, and C_A is the concentration of species A.

r_A : reaction rate of species A

Rearranging equation 69 yields:

$$\frac{dQC_A}{dV} = r_A = -kC_A$$

Where Q remains constant throughout the reactor's length

Recalling the definition of conversion, $C_A = (1 - x)C_{A0}$

Therefore:

$$V = \frac{Q}{k} \ln\left(\frac{1}{1-x}\right) = \pi r_i^2 L \quad (70)$$

Q is constant, and to ensure a complete reaction inside the reactor, the desired conversion x is chosen to be 0.99. and the inner radius is designed to be 0.01 m. However, the reaction rate constant k is temperature dependent, and the conditions along the reactor's length are not isothermal, thus, COMSOL Multiphysics was used for simulating the heat and mass transfer, fluid flow and chemical reaction kinetics to estimate the reactor's length needed for 99% conversion at different heating temperatures: 400, 350, 300 and 270 Celsius degrees.

The reactor was modelled in COMSOL Multiphysics in 2D-axisymmetric coordinates, the inner radius is fixed at 1 cm, with a wall thickness of 3 mm, a heating volume representing an electric resistance

heater is introduced in the reactor, and an insulation layer of 5 cm thickness is covering the outside walls of the reactor. Figure 55 shows the cross-sectional view of the reactor's geometry.

The first run was calibrated at a heating temperature of 400 Celsius degrees. The length of the reactor needed to achieve 99% conversion at this heating temperature is selected to be 1.42 meters after many iterations done at a flow rate of 2.5 L/hr. Figure 55 and Figure 56 represent respectively the temperature profile across the reactor's 3D body, and the axial centerline temperature along the reactor's length.

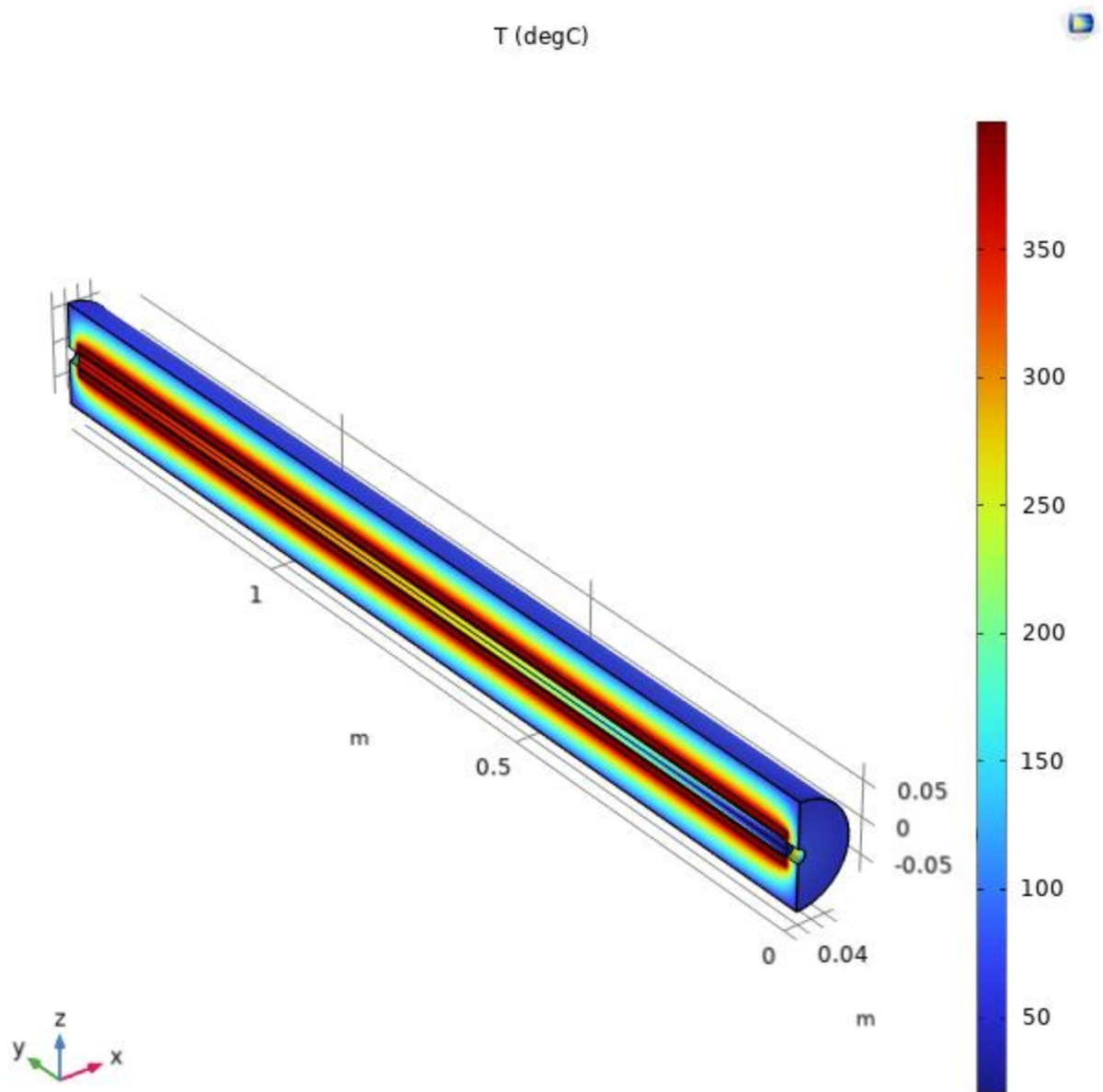


Figure 55: Temperature profiles across the 3D model of the reactor

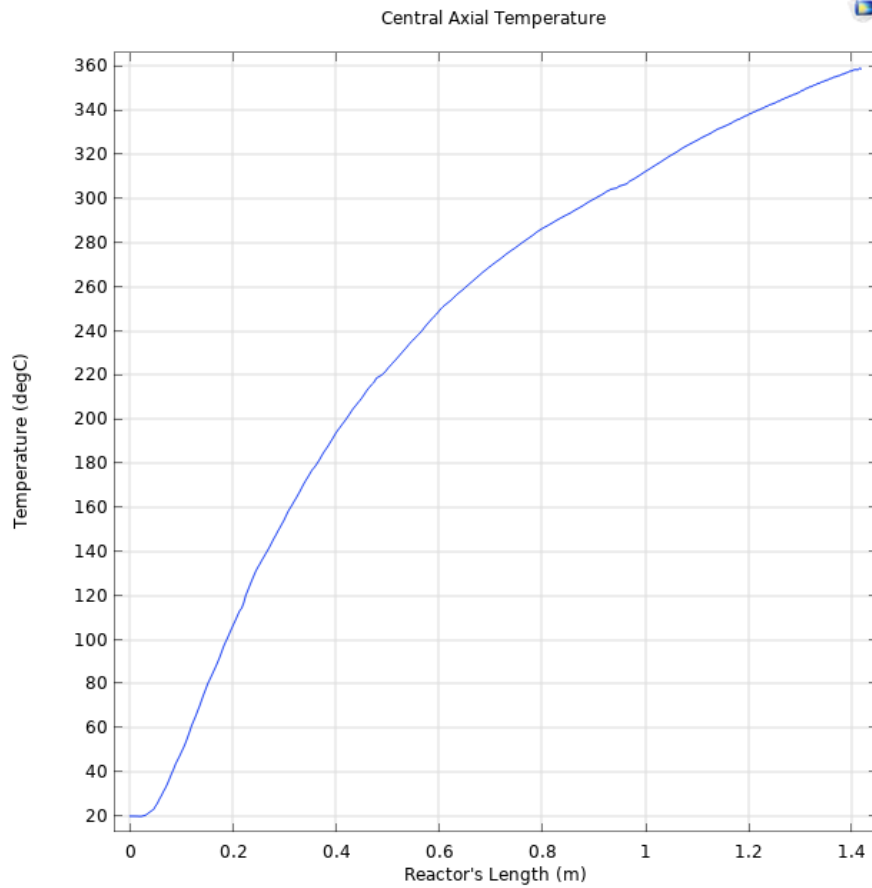


Figure 56: Centerline axial temperature along the reactor's length

It is noticed that the temperature of the slurry was maximized at the reactor's outlet at a value of 360 Celsius degrees approximately, so the slurry did not reach the heating temperature which is 400 Celsius degrees.

Figure 57 and Figure 58 represent respectively the conversion across the reactor's inner zone and the centerline axial conversion along the reactor's length.

Conversion

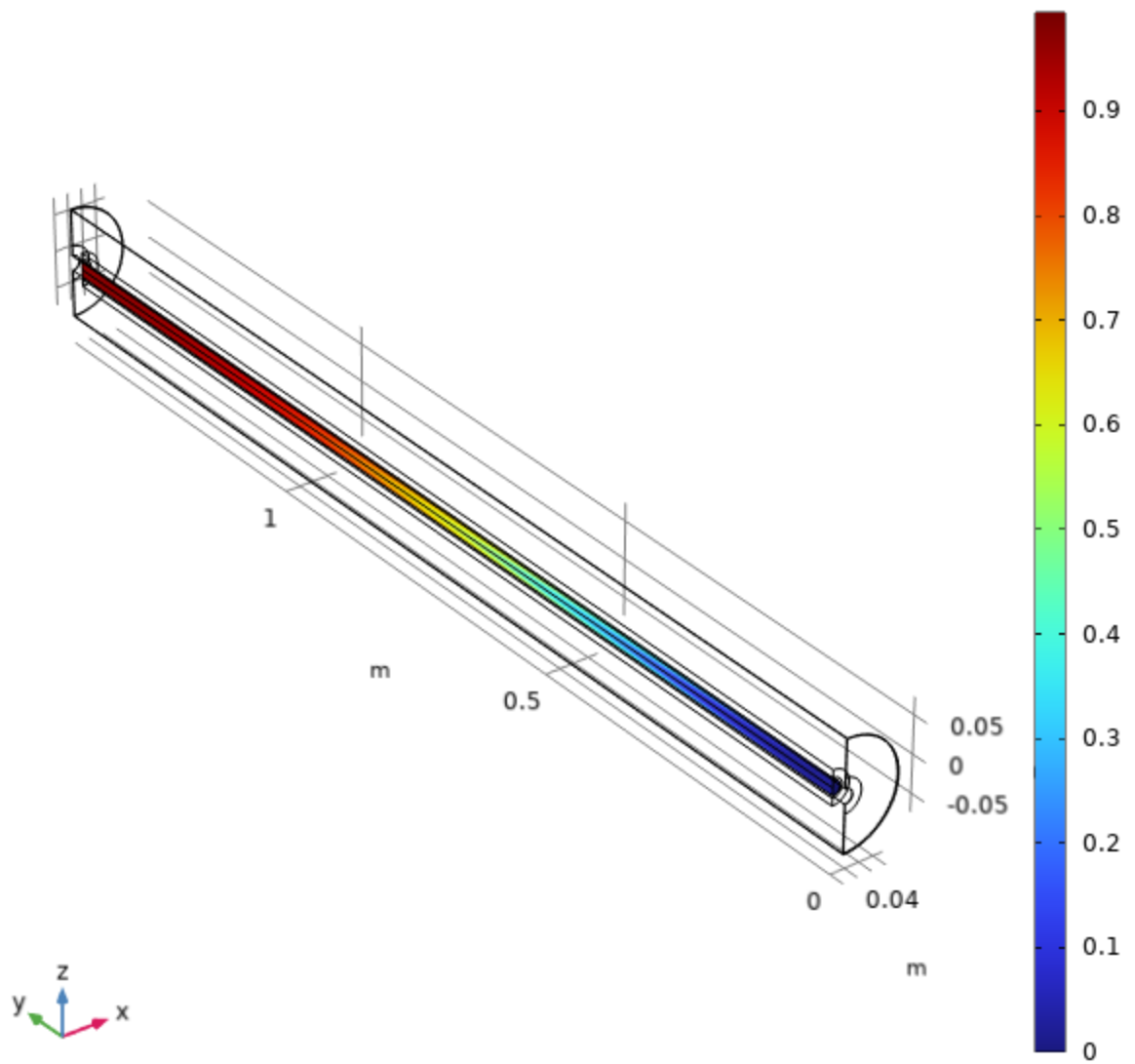


Figure 57: Reaction conversion inside the reactor's inner zone

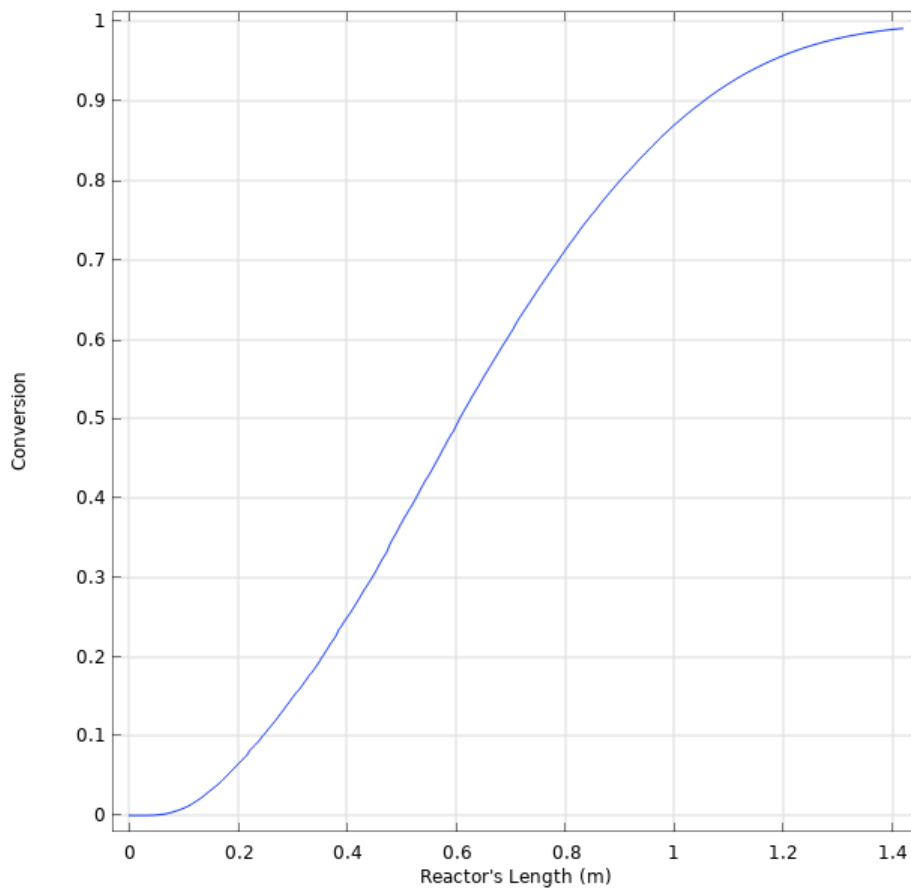


Figure 58: Centerline axial conversion along the reactor's length

The same procedure was repeated at different heating temperatures, Table 15 represents the required length of the reactor to achieve 99% conversion at a volumetric flow rate of 2.5 L/hr for the different heating temperatures used.

Table 15: Required length to achieve 99% conversion at different temperatures

Heating Temperature (°C)	Length to achieve 99% conversion (m)
400	1.42
350	2.2
300	4.3
270	8

It is obvious that as the heating temperature decreases from 400 to 270 Celsius degrees, the required reactor's length to achieve 99% conversion increases from 1.42 to 8 meters, which completely makes sense. As the temperature decreases, the reaction rate constant also decreases, and the reaction needs more time to complete.

After figuring out the required length for 99% at $Q = 2.5$ L/hr, an approach was initiated for estimating the required length for the same conversion at higher flow rates; 5 and 10 L/hr. For this reason, consider Nusselt number, which is defined as the ratio of convective to conductive heat transfer, defined by the following formula:

$$N_u = hD/K \rightarrow h = N_u D/K \quad (71)$$

Where:

h : convective heat transfer coefficient (W/m² K)

D : diameter of the pipe

K : conductive heat transfer coefficient (W/m.K)

In addition, Nusselt's number can be expressed by the Dittus-Boelter correlation using the following formula [202]:

$$N_u = 0.023Re^{4/5}Pr^n \quad (72)$$

Where Pr represents Prandtl number, defined as the ratio of momentum diffusivity to thermal diffusivity, and n is a calibration constant, equal to 0.4 for heating, and 0.3 for cooling.

When varying the volumetric flow rate inside the reactor, the diameter and the conductive heat transfer coefficient remain constant, therefore:

$$\frac{h_2}{h_1} = \frac{N_{u2}}{N_{u1}} = \frac{0.023Re_2^{4/5}Pr^n}{0.023Re_1^{4/5}Pr^n}$$

Prandtl number is considered constant since the momentum diffusivity and thermal diffusivity don't vary in both cases, meaning that:

$$\frac{h_2}{h_1} = \left(\frac{Re_2}{Re_1}\right)^{4/5} = \left(\frac{u_2}{u_1}\right)^{4/5} \quad (73)$$

Now, consider two reactors having the same radii, operating at the same temperature and pressure conditions, where the only difference is the volumetric flow rate of the slurry. To achieve the same 99% conversion, the two reactors should be subjected to the same convective heat flux per unit volume of the reactor, as shown in the following equation:

$$\frac{q_1''}{V_1} = \frac{q_2''}{V_2}$$

$$\frac{h_1(T_{heating} - T_{in})}{A_c \times L_1} = \frac{h_2(T_{heating} - T_{in})}{A_c \times L_2}$$

Where the heating temperature is the same in both reactors, and the inner temperature is considered to be the same in both reactors at each relative section. Then:

$$\frac{L_2}{L_1} = \frac{h_2}{h_1} = \left(\frac{u_2}{u_1}\right)^{4/5}$$

Although COMSOL Multiphysics utilized full CFD simulations to calculate the exact length of the reactor, but this is done only using trial and error, which required a huge number of simulation iterations sweeping the reactor's length. The above equation is based on empirical correlations, which has lower accuracy than COMSOL, but it helps in limiting the huge number of iterations, as it gives an idea about the narrow range of which the reactor's length is found in. So, instead of sweeping the length of the reactor over a wide set of values to find the exact solution, the value of L_2 calculated from the above equation is treated as a first assumption, and the exact length of the reactor is found using quite a lower number of iterations.

Table 16 shows the estimated reactor length at the different reaction temperatures for a volumetric flow rate of 5 L/hr, at which $L_2/L_1 = (u_2/u_1)^{4/5} = 2^{0.8} = 1.74$, and a flow rate of 10 L/hr, at which $L_2/L_1 = (u_2/u_1)^{4/5} = 4^{0.8} = 3.03$, and the exact lengths figured out by COMSOL Multiphysics:

Table 16: Predicted and exact length of the reactor at $Q = 5$ L/hr and 10 L/hr

Heating Temperature (°C)	L_1 (m) @ 2.5 L/hr	L_2 (m) @ 5 L/hr = $1.74 \times L_1$	L_2 (m) @ 5 L/hr (COMSOL)	L_2 (m) @ 10 L/hr = $3.03 \times L_1$	L_2 (m) @ 10 L/hr (COMSOL)
400	1.42	2.47	2.51	4.30	4.42
350	2.2	3.83	3.88	6.67	6.86
300	4.3	7.49	7.59	13.04	13.40
270	8	13.93	14.12	24.25	24.93

The length of the reactor was calculated based on 99% conversion, for three different volumetric flow rates, and in each flow rate four different heating temperatures were used. The lengths calculated vary between 1.42 meters at a flow rate of 2.5 L/hr and 400 Celsius degrees heating temperature, to 24.93 meters at a flow rate of 10 L/hr and 270 Celsius degrees heating temperature.

3. Continuous Stirred Tank Reactor, CSTR

The essential feature of a continuous stirred tank reactor, also known as the perfectly mixed flow reactor, is the assumption of complete uniformity of concentration and temperature through the reactor [203]. In this section, the reactor to be fulfilling the need is considered to be a CSTR, and it will be sized based on 99% conversion, for three different flow rates; 2.5, 5 and 10 L/hr, each at four different operating temperatures; 270, 300, 325 and 350 Celsius degrees.

3.1. Steady State Governing Equation

As a consequence of the complete mixing, a CSTR also operates isothermally, which means that at steady state, it is not necessary to consider mass and energy balances simultaneously [203]. The design equation is written using the following form:

$$C_{A0} - C_A = \tau r_A \quad (74)$$

Where τ represents the residence time, expressed in seconds, needed by the reactants to achieve the required concentration C_A , and r_A represents the reaction rate, given by the following formula:

$$r_A = kC_A = A_f e^{-\frac{E_a}{RT}} C_A$$

Where:

A_f : frequency factor (s^{-1})

E_a : activation energy (J/mol)

R : universal gas constant (8.3145 J/mol.K)

T : temperature (K)

Rearranging equation (74) gives:

$$\tau = \frac{C_{A0} - C_A}{A_f e^{-\frac{E_a}{RT}} C_A}$$

Recall that:

$$C_A = (1 - x)C_{A0}$$

Which gives:

$$\tau = \frac{C_{A0} - C_{A0}(1 - x)}{A_f e^{-\frac{E_a}{RT}} C_{A0}(1 - x)}$$

$$\tau = \frac{x}{A_f e^{-\frac{E_a}{RT}} (1 - x)} \quad (75)$$

3.2. Reactor Sizing

Equation (75) describes the residence time as a function of reaction temperature and required conversion. As the conversion tends to 1, the residence time tends to infinity, that's why it is not favored to use a unique CSTR as the only reactor in a hydrothermal liquefaction system. This is cleared in Table 17, where the residence time to achieve 0.99 conversion is calculated for the four different operating temperatures.

Table 17: Residence time required to achieve 99% at the different operating temperatures

T = 350°C	T = 325°C	T = 300°C	T = 270°C
2.53 hr	4.42 hr	8.12 hr	18.12 hr

By definition, the volumetric flow rate is the volume of liquid flowing per unit time, and since it is constant in continuous reactors, it can be written as:

$$Q = V/\tau$$

$$V = Q \times \tau \quad (76)$$

Applying equation (76) for the three selected flow rates; 2.5, 5 and 10 L/hr at the different heating temperature gives the minimum volume in Liters of the CSTR needed to ensure 99% conversion under the relevant conditions. The results are presented in Table 18:

Table 18: Minimum CSTR volume (L) required for 99% conversion at different reaction conditions

Q (L/hr)	T = 350°C	T = 325°C	T = 300°C	T = 270°C
2.5	6.32	11.1	20.3	45.3
5	12.6	22.1	40.6	90.6
10	25.3	44.2	81.2	181

3.3. Reactor Start-up

Although CSTRs are considered continuous reactors, but they need a significant time to achieve the steady state conditions. For this reason, a COMSOL simulation comparison was done to figure out the optimum initial concentrations for achieving the steady state conditions in the lowest possible time interval. This simulation involves the process only, without any interference from the geometry of the reactor. It treats the CSTR as an ideal reactor to determine the characteristic time for the reactor startup.

The first approach was starting the CSTR with no reactants inside it (solvent reactor), and injecting the reactants slurry with a flow rate of 2.5 L/hr at $t = 0$. The results are shown in Figure 59.

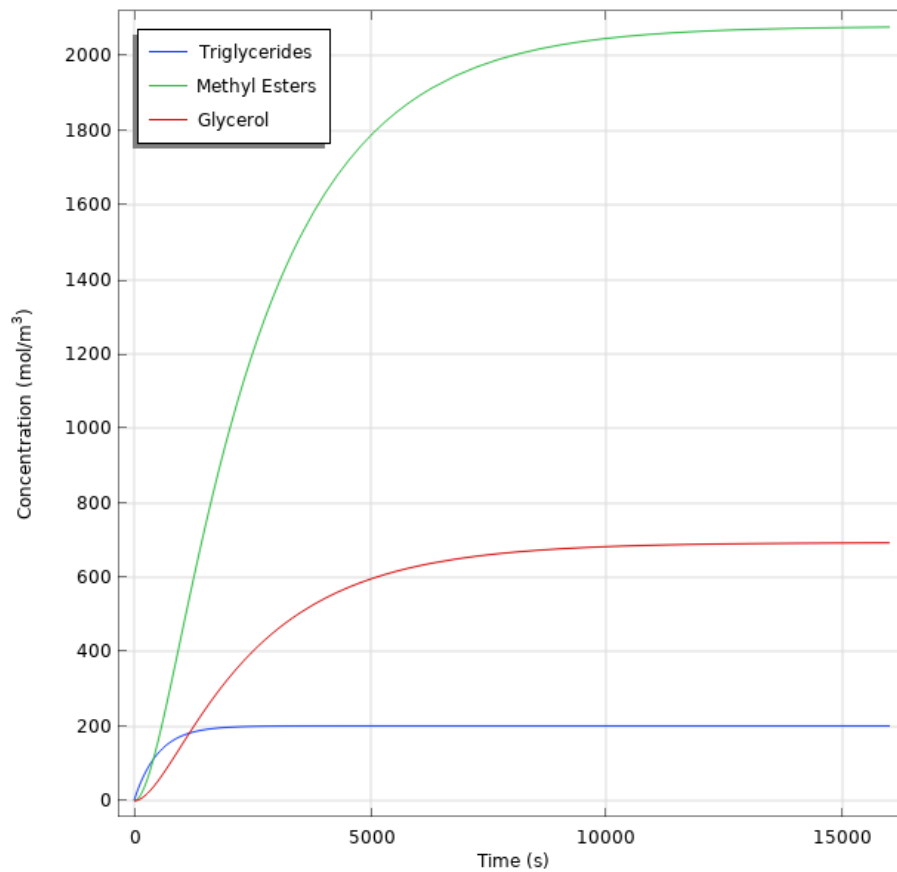


Figure 59: Starting up the CSTR with zero initial concentration

It is noticed that the time needed by the CSTR to reach the steady state conditions for the products (methyl esters and glycerol) exceeds 4 hours. This is due to the fact that the reaction rate directly proportional to the concentration of the reactants (triglycerides), and since the starting conditions ensure a zero-reactant initial concentration, then the reaction rate takes significant time to build up to its steady state value.

The second approach was starting the CSTR filled completely with the reactants slurry (methanol + rapeseed oil), with the same flow rate and temperature as the first approach. The results are shown in Figure 60.

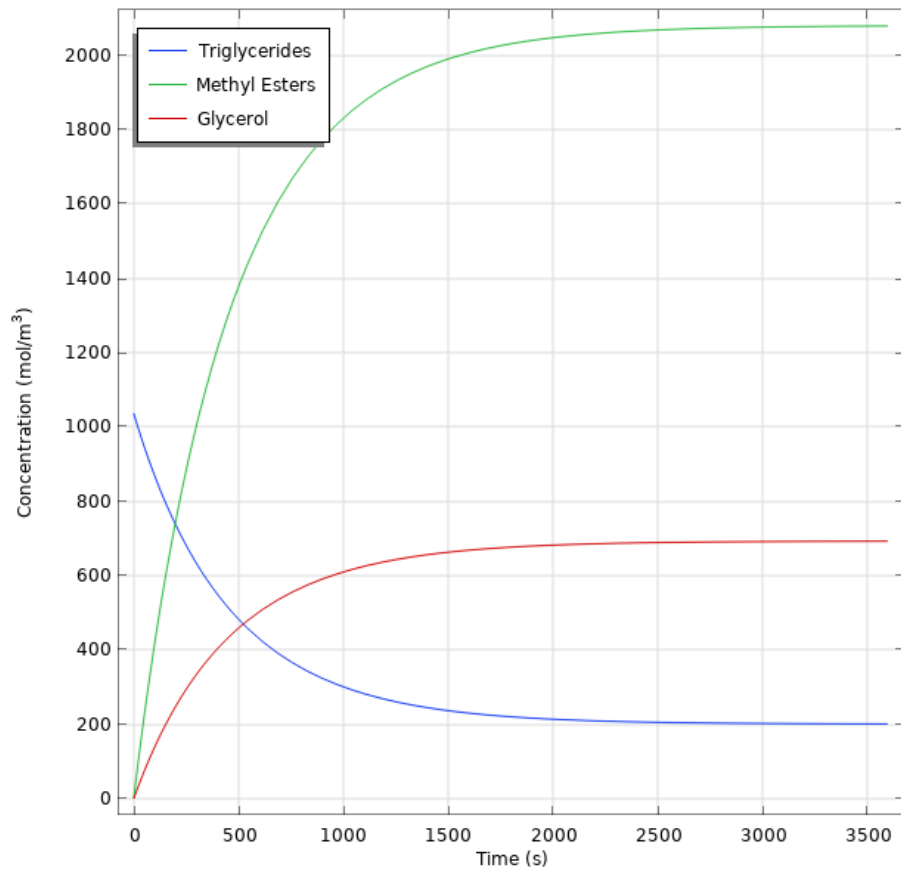


Figure 60: Starting up the CSTR with the reactant's slurry inside it

It is noticed that the time needed by the CSTR to reach the steady state conditions decreased dramatically from more than four hours to less than an hour (about 3500 seconds). This time diminishing is due to the same reason that links the reaction rate to the concentration. Thus, when starting up a continuous stirred tank reactor, it is recommended to stuff it with the biomass slurry before turning it on rather than heating the solvent alone without inserting the biomass slurry.

4. Hybrid System

Referring to the previous designs, it was noticed that the plug flow reactor doesn't need a big inner volume to ensure 99% conversion. The longest reactor was that operating at 10 L/hr and 270 Celsius degrees, with a relatively high length of 24.93 meters, corresponding to 7.83 L volume. For CSTRs, it is

noticed that the issue is not the length of the reactor, but its volume, where the largest reactor operating at 10 L/hr at 270 Celsius degrees has a volume of 181 L.

A compromised design can be a combination of a CSTR and PFR in series, where the CSTR ensures a primary conversion through heating the reactants during a defined time, after which the reaction continues in the PFR to the desired final conversion. This combination decreases significantly the volume of the CSTR and the length of the PFR, decreasing the size and the energy consumption of the whole reaction unit. This combination was previously studied by different researchers, including Elliott et al [50] and Billing et al [197], and was established as an efficient system, ready for scaling up and commercializing the continuous reactors for the hydrothermal liquefaction process.

In this section, a hybrid combination of CSTR and PFR in series will be selected for achieving 99% conversion at the preselected flow rates, 2.5, 5 and 10 L/hr, each for four different temperatures; 270, 300, 325 and 350 Celsius degrees. Two broad approaches will be studied; the first one is using the CSTR for 80% conversion and completing the rest in the PFR, and the second one is using the CSTR for 90% conversion and completing the rest in the PFR.

4.1. Sizing Methodology

The residence time needed for the reactants in the CSTR is calculated using equation (75):

$$\tau = \frac{x_1}{A_f e^{-\frac{E_a}{RT}}(1 - x_1)}$$

Where x_1 represents the desired conversion in the CSTR, which is 0.8 in the first approach and 0.9 in the second approach. After which the reactor's volume is calculated using equation (76):

$$V = Q \times \tau$$

The reactor's length needed for the reaction in the PFR is calculated using equation (70):

$$V = \frac{Q}{k} \ln\left(\frac{1}{1-x_2}\right) = \pi r_i^2 L$$

Where x_2 represents the desired local conversion in the PFR, required to provide a global conversion $x = 0.99$. In this case, no need for COMSOL Multiphysics to do a finite element analysis to figure the reaction rate constant k , since the slurry enters the PFR at the same temperature that it exits the CSTR, and the temperature is held constant in the reactor.

First Approach: 80% CSTR - 19% PFR

In this approach, the CSTR should convert 80% of the slurry, and the rest is finalized by the PFR. Table 19 summarizes the CSTR volume and the PFR length for the three selected flow rates at four different heating temperatures.

Table 19: CSTR volume (L) and PFR length (m) for achieving a final 99% for all the different volumetric flow rates and operating temperatures

Q(L/hr)	T = 350°C		T = 325°C		T = 300°C		T = 270°C	
	V _{CSTR} (L)	L _{PFR} m						
2.5	0.255	0.61	0.447	1.06	0.82	1.95	1.83	4.36
5	0.511	1.22	0.893	2.13	1.64	3.91	3.66	8.73
10	1.02	2.44	1.79	4.26	3.28	7.82	7.32	17.45

Second Approach: 90% CSTR – 9% PFR

In this approach, the CSTR should convert 90% of the slurry, and the rest is finalized by the PFR. Table 20 summarizes the CSTR volume and the PFR length for the three selected flow rates at four different heating temperatures.

Table 20: CSTR volume (L) and PFR length (m) for achieving a final 99% for all the different volumetric flow rates and operating temperatures

Q(L/hr)	T = 350°C		T = 325°C		T = 300°C		T = 270°C	
	V _{CSTR} (L)	L _{PFR} m						
2.5	0.57	0.468	1.00	0.818	1.84	1.50	4.11	3.35
5	1.15	0.936	2.01	1.64	3.69	3.00	8.23	6.71
10	2.30	1.87	4.02	3.27	7.38	6.00	16.47	13.41

Based on the results shown in this section, a combination of a CSTR of 1.02 L volume and a PFR of 2.44 m length will be used to operate at a 10 L/hr maximum flow rate and a temperature of 350 Celsius degrees.

4.2. CSTR Dimensions

The CSTR should handle 1.02 L of reactants, thus, it will be designed with an internal volume larger than 1.02 L.

Different types of mixers can be used in the CSTR; anchors, propellers, flat blade turbines, paddles, and helical screws. However, Holland and Chapman [204] found that flat-blade turbines are the most efficient mixers for liquids with viscosities ranging from 1 to 10⁴ mPa.s. Thus, a flat-blade turbine will be considered as CSTR's mixer. For heavy biomass slurries having viscosities larger than 10⁴ mPa.s, helical impellers can be used, withstanding viscosities exceeding 10⁶ mPa.s.

Trambouze et al [205] studied the dimensions and the positioning of the flat-blade turbine mixer inside the CSTR. The standard design providing the most efficient performance is illustrated in Figure 61:

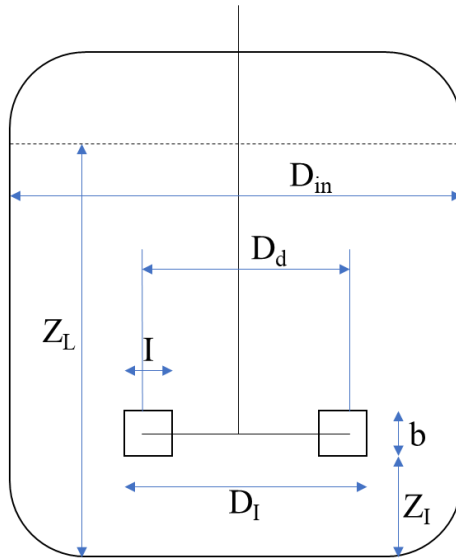


Figure 61: Standard Dimensions of a CSTR

Where:

D_{in} : internal diameter of the CSTR

D_I : impeller's diameter, $D_I / D_{in} = 1/3$

D_d : impeller's disc diameter, $D_d / D_I = 3/4$

b : impeller blade width, $b / D_I = 1/5$

I : impeller blade length, $I / D_I = 1/4$

Z_I : impeller distance from tank's bottom, $Z_I / D_I = 1$

Z_L : static liquid depth, $Z_L / D_{in} = 1$

Since $Z_L / D_{in} = 1$, then the liquid's depth inside the CSTR should be equal to its inner diameter. The volume of the liquid should be 1.02 L, then:

$$1.02 \times 10^{-3} = \frac{\pi}{4} \times D_{in}^2 \times D_{in}$$

Thus, $D_{in} = 109.1$ mm, and $Z_L = 109.1$ mm

In addition, $D_I = D_{in} / 3 = 36.37$ mm, therefore $Z_I = 36.37$ mm.

Moreover, the impeller's blade's width is $b = 36.37 / 5 = 7.27$ mm, and its length is $l = 36.37 / 4 = 9.09$ mm.

The CSTR differs from PFR in terms of metal body execution. The PFR can be built as one part, whereas the CSTR should be able to be opened and closed, for maintenance reasons, and for the installation of the mixer. Thus, it should be held by bolts. In addition, electrical resistance heaters should be embedded inside its walls. Thus, the thickness design of the CSTR is inspired by the batch reactor of the GEPEA laboratory, with a wall thickness of 6 cm, capable of holding the bolts and the heaters, without being affected by the stress concentrations resulting from the geometry change, caused by the hollowed parts to place the bolts and the heaters.

A design is proposed, where the wall thickness of 6 cm, with 10 heaters, 8mm diameter and 2 kW Watts each, providing a total heating power of 20 KW. In addition, ten M10 100 bolts, with a diameter of 10 mm each and a length of 100 mm are distributed across the CSTR's wall. To make sure this structure will support the maximum pressure inside the CSTR, which is limited at 25 MPa, COMSOL is used to study the stress concentrations along the cross-sectional area of the reactor. The results showing Von Mises stress distribution are shown in Figure 62:

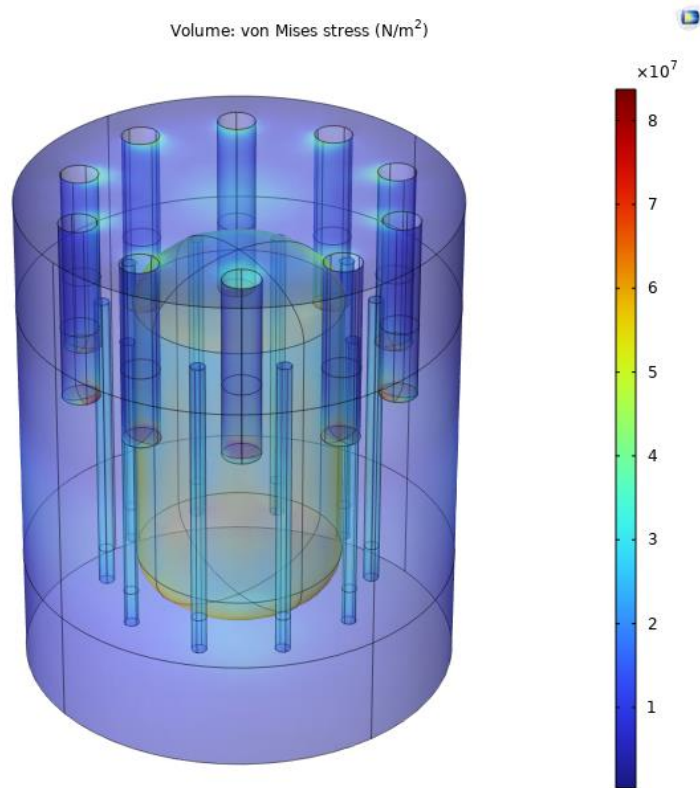


Figure 62: Von Mises stress distribution across the CSTR's wall when subjected to 25 MPa internal pressure

Based on the above results, the maximum stress caused by the holes in the walls yielding to stress concentrations attains a maximum of 85 MPa, which is less than the maximum allowable stress for the stainless steel at high temperatures, 113 MPa. Thus, the design can withstand the required pressure and temperature.

4.3.CSTR Agitation

After choosing the type and the dimensions of the CSTR's mixer, this section will present the mixing speed of the CSTR's impeller to ensure a well-mixed reaction medium. Russinova and Kresta [206] studied the relation between the mixing time and the residence time, and, their effect on the homogeneity of the fluids inside the CSTR. Their experiments and simulations revealed that a well-mixed CSTR should have a mean residence time at least 10 times larger than the mixing time. When this ratio drops below 10, the CSTR deviates from their ideal model, and as this ratio increases above 15, the

reactor approaches the ideal conditions. For this reason, the ratio of the mean residence time to the mixing time in the CSTR will be fixed at 20. Let t_{mix} denote the mixing time inside the CSTR, then:

$$t_{mix} = \frac{\tau}{20} = \frac{V/Q}{20} = \frac{367.2}{20} = 18.36 \text{ s} \quad (78)$$

Norwood and Metzner [207] found a correlation linking the mixing time in a CSTR to the impeller's revolution speed, which is applicable for six flat blade turbine:

$$N \times t_{mix} \times \left(\frac{D_I}{D_T}\right)^2 = 5 \times N_{FR}^{\frac{1}{6}} \times \left(\frac{Z_L}{D_T}\right)^{0.5}$$

$$N_{FR} = \frac{N^2 D_I}{g} \quad (79)$$

Where N represents the revolution speed of the impeller, and N_{FR} represents Froude's number; the ratio of inertial to gravitational forces. Solving the above equation gives a rotational speed of $N = 0.9468$ revolutions per second or 56.8 rpm.

4.4. Pumping System

Continuous hydrothermal processing of biomass requires an accurate selection of the pumping system. The HTL process utilizes different biomass feedstocks with different viscosities, densities, solid particles, etc.

For a specific application of the transesterification process design, Burt Process Equipment suggested a specialized pump for the transesterification process involving high viscosity oils, aggressive chemicals and alcohols. The Grundfos ATEX – approved pumps, with the NBG/NKG end suction, which is ISO 2858 compliant is the ideal choice for such processes [208]. The DMH variant of these pumps operate at pressures up to 200 bars, and delivers a variable flow rate from 0.2 L/hr up to 1000 L/hr. Thus, it is the perfect choice for the hybrid system design when it comes to transesterification.

However, our work tends to create a continuous system capable of processing different kinds and biomass with a wide range of characteristics. The PNNL laboratory reported different types of pumping systems that can be utilized for the continuous hydrothermal liquefaction units they build [209]. According to their tests and analysis, PNNL team suggested few pumps, that can be utilized according to the system's requirements:

1. Piston pump, designed by Putzmeister Group, Germany. With a twin screw feeder to ensure a wide variety of HTL-type biomass. This pump can deliver a continuous 130 bars flow, at a maximum temperature of 105 °C, able to deliver 45% solid content slurries with a maximum particle size of 8 mm [210]
2. Diaphragm (hose) pump, designed by FELUWA Group, Germany, delivering a continuous 320 bars flow, at a maximum temperature of 200 °C, up to 15% solid content slurries with a maximum particle size of 7.5 mm [211].
3. Lobe (specialized chopper) pump, designed by Zeilfelder Pumpen, Germany, delivering a continuous 250 bars flow, at a maximum temperature of 450 °C. This pump has many unique features regarding its operating temperature, allowing it to operate as an HTL booster pump, and, its ability to run backwards, allowing it to be used for an energy recovery process. This pump is able to deliver up to 18% solid content slurries, with a maximum particle size just exceeding 10 mm [212].

All of the prementioned pumps can be purchased with a wide range of flow rates, from small lab scale bench systems, to the commercialized scale.

4.5. Separation System

The product stream exiting the reactor at 350 °C is a mixture of biodiesel, excess methanol, and glycerol. In this section, a simple system consisting of a pressure regulator and a flash drum will be used to

separate methanol from other species, after which the liquid products can be separated by decantation due to their different densities.

The outlet stream has a pressure of 190 bars, which cannot be directly vented or opened to the atmosphere. For this reason, a pressure regulator (pressure reducing valve PRV) must be installed. Usually, simple pressure regulators cannot handle this huge pressure difference. A three-stage regulator ensures a stable outlet pressure, with the ability of handling large inlet pressures [213]. For example, the PRD4HP is a three – stage regulator provided by BESWICK Engineering, capable of accurately reducing very high inlet pressures, up to 3000 psi (206 bars), down to 0 to 40 psi (0 to 2.75 bars), depending on the variant selection [214].

In the outlet stream, methanol is in supercritical phase, while the glycerol and biodiesel (methyl esters) are in the compressed liquid region [215]. Fluids passing through the pressure regulator undergo an isenthalpic throttling process, where the enthalpy is given by $h = u + Pv$. For biodiesel and glycerol in their compressed liquid states, the specific volume v is very small, such that the product Pv can be neglected compared to the internal energy u . This assumption assumes that there is no change in the internal energy for liquid – liquid throttling, thus the temperature is not affected. On the other hand, methanol undergoes an isenthalpic throttling process, from 190 bars to 1 bar. At 350 Celsius degrees and 190 bars, the enthalpy of supercritical methanol is equal to 1380 kJ/kg. At 1 bar, the temperature of methanol corresponding to 1380 kJ/kg enthalpy is 213 Celsius degrees. Thus, methanol is throttled from the supercritical state to the superheated state. However, this is not the final pressure of methanol, since the biodiesel and glycerol temperatures are not affected during the throttling process, they are still at 350 Celsius degrees, and there will be a heat transfer phenomenon between these liquids and methanol to achieve stabilized temperature. Assuming T_f is the final temperature of the mixture, then the energy gained by methanol is:

$$Q_1 = m_{\text{methanol}} C_{p_{\text{methanol}}} (T_f - 213)$$

Which is the same energy loss from biodiesel and glycerol, equal to:

$$Q_1 = m_{biodiesel+glycerol} C_{p_{biodiesel+glycerol}} (350 - T_f)$$

Solving the above equations for an average heat capacity of 1.9 J/g.K for methanol and 3 J/g.K for biodiesel and glycerol gives a final temperature of 289 Celsius degrees. At this temperature, biodiesel and glycerol are still in the liquid phase, while methanol regains its supercritical state.

A heat exchanger can be used after the pressure regulator, where the temperature of the stream is decreased to 220 Celsius degrees to ensure that methanol is in the superheated vapor state, then the stream can be introduced into a separation column, where glycerol and biodiesel are collected as liquids, and separated by decantation, and methanol is passed through the heat exchanger and pumped again into the system in a closed loop. Applying energy balance on the heat exchanger leads to a decrease of the methanol temperature. Given that the transesterification process needs 3 moles of methanol per one mole of colza oil, and given that the molar ratio used in this setup is 42:1, then there will be excess of 39 moles of methanol which can be recirculated in the system decreasing the operating cost.

4.6. Final System Representation

After designing and optimizing the continuous system for the transesterification process regarding its components and operating parameters, Figure 63 shows a schematic representation of the planned design to be executed:

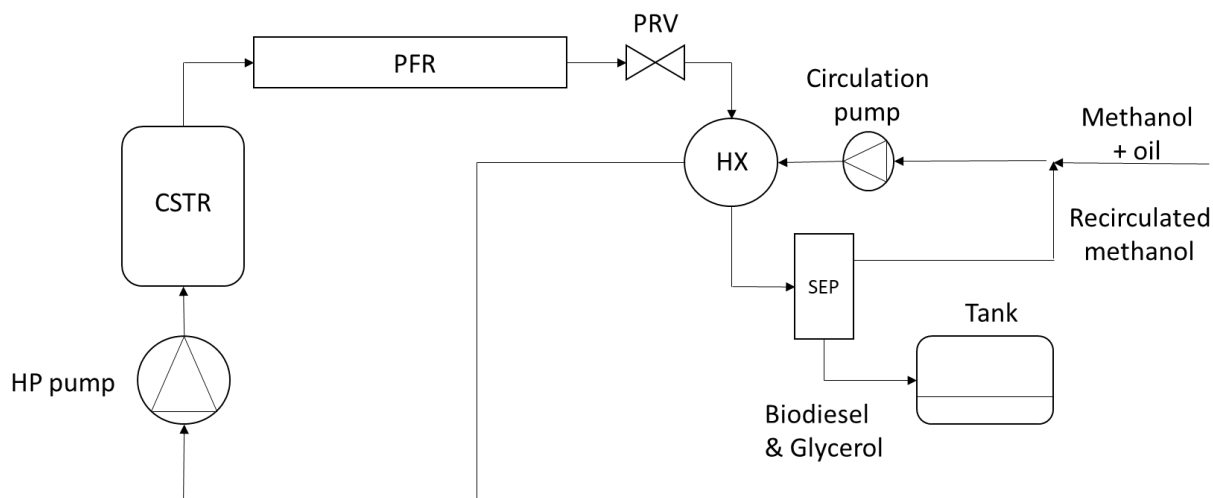


Figure 63: Schematic representation of the continuous system

Rapeseed oil and methanol enters the high-pressure pump HP, after which they are pumped to the CSTR followed by the PFR. The products consisting of biodiesel, glycerol and remaining methanol exit the PFR at 350 Celsius degrees, and enter the three-stage pressure relief valve PRV, in which they undergo an isentropic expansion from 190 bars to 1 bar, and cool to a temperature of 289 Celsius degrees. After that, the mixture enters the heat exchanger HX where it is cooled to 100 Celsius degrees, and the methanol is in superheated vapor state. The mixture enters the separator, where the liquid biodiesel and glycerol are extracted to a tank and separated by decantation, and the methanol vapor is mixed with fresh methanol and oil and enters the CSTR again. Recovering excess methanol and using it in the system again saves 39 moles of methanol per 1 mole of rapeseed oil.

5. Conclusion

In this chapter, the methodology of designing a continuous system for the hydrothermal liquefaction of biomass was explained. The system was designed aiming for 99% conversion for the supercritical methanol transesterification of rapeseed oil, which was discussed in the previous chapter. The first step was designing a standalone plug flow reactor. After that a design of a standalone continuous stirred tank reactor was presented. Standalone reactors did not show promising results. The length of the PFR and the volume of the CSTR were too high for a lab scale system. Therefore, a hybrid system (CSTR – PFR)

was proposed, and a specific system was designed for a volumetric flow rate of 10 L/hr, operating at 350 Celsius degrees, where 80% of the reaction's conversion occur in the CSTR, and the PFR finalized the 19% rest. The reactors were designed using stress analysis to handle the reaction's elevated pressures. The internal diameter of the PFR was selected based on previous works, reported without clogging issues in different types of biomass slurries. The CSTR was designed based on standard dimensions, with a stirrer operating at the conditions allowing us to treat the reaction medium as a homogeneous zone. Moreover, a pumping system is selected, optimized for the supercritical methanol transesterification. And a separation system with integrated heat recovery system was designed to separate the products and recirculate excess methanol in the system to decrease the operating cost, increasing the overall efficiency of the system.

Conclusions and Perspectives

The main goal of this thesis was to design a continuous system for the hydrothermal liquefaction of biomass, which can be scaled up for commercialization, to produce significant amounts of biofuels. This target is achieved through a step-by-step workplan, based on building and validating a numerical model for a batch hydrothermal liquefaction reactor, then, using the results of this model and the previous reported works on continuous reactors to design a full continuous hydrothermal liquefaction system.

For this purpose, first, a study is done on the continuous systems for the hydrothermal liquefaction of biomass, including the various system components; reactor, pumping system, separation system, heating system, and, the effects of reaction parameters. Moreover, a survey on the previous works done on the simulation and modelling of the hydrothermal liquefaction process is presented. In addition, the transition from batch to continuous processing is discussed.

The next step was to build and validate a simulation model for the batch processing of HTL. For this reason, a 1L batch reactor for the hydrothermal liquefaction of biomass is studied. Several experiments are conducted, starting from the simplest ones; empty reactor heating, ending with a full chemical reaction experiment. In parallel, a simulation model is built using COMSOL Multiphysics and tested for each experiment. The experimental results are compared to the simulation results achieved by the model.

For the heat transfer mechanism, the relative error between the experimental and simulated results remained below 4%, and for the chemical process validation, the reaction's conversion relative error between the experimental and the simulation results remained below 6%. Compared to previous reported works dealing with numerical simulations of reactors [179]–[181], [216], where their relative errors ranged between 2% and 15%, the simulation model of batch reactor built in our work is considered validated.

After its validation, the simulation model's phenomena can be used to propose a new design for a continuous system for the hydrothermal liquefaction of biomass. Several setups are studied; a standalone

PFR, standalone CSTR, and a hybrid system consisting of both types in series. Results showed that a standalone PFR is relatively too long, and the volume of the standalone CSTR is relatively large. However, when these reactors are connected in series, the same results can be achieved with much smaller sizes. A pumping system capable of withstanding the slurry demands is designed, and a separation system integrated with a heat recovery system is proposed to optimize the process. The final system is intended to operate at a temperature of 350 Celsius degrees, a pressure of 190 bars, and to handle a flow rate up to 10L/hr. The designed CSTR has a 1.02 L internal volume, while the PFR has a 1 cm internal diameter and a 2.44 meters length.

In addition to being an endothermic process, HTL is based on heating large amounts of solvents, usually water, having very high heat capacity especially with increasing temperatures. Thus, it is essential to perform an energy balance of this process [134]. Previous energy balances in batch HTL reactor did not show promising results in terms of thermal efficiency and total energy efficiency [217]. Usually, the thermal efficiency is calculated by taking into consideration the average yields and heating values of the reactants and the products, and the total energy efficiency is calculated by taking into account, in addition to the up mentioned parameters, the energy consumption by the heaters during the process and the feeding pump power when utilized. Increasing the overall efficiency of the system depends mainly on utilizing the energy input and circulating it in heat recovery devices to extract the maximum benefit before it goes as waste heat. For this reason, several aspects should be addressed:

- Electrical resistance heating is used in this system, since the reactor is designed at a lab-scale for research purposes. However, when scaled up, electrical resistance heating is not the best choice. Usually, large industrial applications involving large amounts of heat energy utilize hot flue gases for heating purposes. Due to the relatively low temperature ranges of HTL, waste gaseous hot streams of industrial sites can be used to feed this type of reactors.
- One strategy to minimize the energy input to the system, reducing the overall operational cost, is to utilize solar energy for heating the biomass, or even preheating it. This approach was adapted by

Xiao et al [40] by using a custom solar parabolic trough collector, designed to be operated on a pressure up to 40 MPa, and a temperature of 200 Celsius degrees, which is enough for the hydrothermal pretreatment of microalgae. Another setup was built by Chuayboon et al [72] for the continuous hydrothermal gasification of biomass, in which a parabolic mirror was attached to a solar thermochemical reactor. The temperature in such a setup reached 1300 Celsius degrees using solar power uniquely. Utilizing solar power in hydrothermal liquefaction is accompanied with several challenges; solar energy is not available in all regions in sufficient amounts, in addition, it is not available 24 hours 365 days. Integrating solar power into hydrothermal liquefaction systems can be accomplished based on the requirements of the system. For example, a 24 hours operating system can fully operate on solar energy during day hours, and operate during night hours on other heating modes or stored solar energy.

- Proper balance should be conducted on heat recovery systems; the addition of heat recovery systems reduces the input power needed to the systems, but on the other hand, it increases the building cost and the operating cost to circulate the fluids continuously inside the heat exchangers.

Bibliography

- [1] A. Sertolli, Z. Gabnai, P. Lengyel, and A. Bai, “Biomass Potential and Utilization in Worldwide Research Trends—A Bibliometric Analysis,” *Sustainability*, vol. 14, no. 9, p. 5515, May 2022, doi: 10.3390/su14095515.
- [2] “Is There Enough Biomass to Fuel the World? Part I,” *Mr. Sustainability*. <https://www.mr-sustainability.com/stories/2020/7/26/is-there-enough-biomass-to-fuel-the-world-1> (accessed Oct. 06, 2022).
- [3] Y. Li, L. W. Zhou, and R. Z. Wang, “Urban biomass and methods of estimating municipal biomass resources,” *Renew. Sustain. Energy Rev.*, vol. 80, no. C, pp. 1017–1030, 2017.
- [4] S. Nizamuddin *et al.*, “An overview of effect of process parameters on hydrothermal carbonization of biomass,” *Renew. Sustain. Energy Rev.*, vol. 73, pp. 1289–1299, Jun. 2017, doi: 10.1016/j.rser.2016.12.122.
- [5] “Biomass explained - U.S. Energy Information Administration (EIA).” <https://www.eia.gov/energyexplained/biomass/> (accessed Jun. 28, 2022).
- [6] S. Zafar |, “Biochemical Conversion of Biomass,” *BioEnergy Consult*, Jun. 17, 2019. <https://www.bioenergyconsult.com/biochemical-conversion-technologies/> (accessed Dec. 06, 2019).
- [7] “Sustainable Forestry for Bioenergy & Bio-based Products.” <http://www.forestandrange.org/Biomass/Modules/Module%206/Unit%202/Lesson%202.asp> (accessed Dec. 06, 2019).
- [8] A. R. K. Gollakota, N. Kishore, and S. Gu, “A review on hydrothermal liquefaction of biomass,” *Renew. Sustain. Energy Rev.*, vol. 81, pp. 1378–1392, Jan. 2018, doi: 10.1016/j.rser.2017.05.178.
- [9] M. Déniel, G. Haarlemmer, A. Roubaud, E. Weiss-Hortala, and J. Fages, “Hydrothermal liquefaction of blackcurrant pomace and model molecules: understanding of reaction mechanisms,” *Sustain. Energy Fuels*, vol. 1, no. 3, pp. 555–582, May 2017, doi: 10.1039/C6SE00065G.
- [10] B. Ciuffi, M. Loppi, A. M. Rizzo, D. Chiamonti, and L. Rosi, “Towards a better understanding of the HTL process of lignin-rich feedstock,” *Sci. Rep.*, vol. 11, no. 1, Art. no. 1, Jul. 2021, doi: 10.1038/s41598-021-94977-w.
- [11] Y. H. Chan *et al.*, “Effect of process parameters on hydrothermal liquefaction of oil palm biomass for bio-oil production and its life cycle assessment,” *Energy Convers. Manag.*, vol. 104, pp. 180–188, Nov. 2015, doi: 10.1016/j.enconman.2015.03.075.

- [12] Y. Genel, H. Durak, T. Aysu, and İ. Genel, “Effect of process parameters on supercritical liquefaction of Xanthium strumarium for bio-oil production,” *J. Supercrit. Fluids*, vol. 115, pp. 42–53, Sep. 2016, doi: 10.1016/j.supflu.2016.04.009.
- [13] R. K. Mishra, V. kumar, P. Kumar, and K. Mohanty, “Hydrothermal liquefaction of biomass for bio-crude production: A review on feedstocks, chemical compositions, operating parameters, reaction kinetics, techno-economic study, and life cycle assessment,” *Fuel*, vol. 316, p. 123377, May 2022, doi: 10.1016/j.fuel.2022.123377.
- [14] S. Karagöz, T. Bhaskar, A. Muto, Y. Sakata, and Md. A. Uddin, “Low-Temperature Hydrothermal Treatment of Biomass: Effect of Reaction Parameters on Products and Boiling Point Distributions,” *Energy Fuels*, vol. 18, no. 1, pp. 234–241, Jan. 2004, doi: 10.1021/ef030133g.
- [15] L. Cao, C. Zhang, S. Hao, G. Luo, S. Zhang, and J. Chen, “Effect of glycerol as co-solvent on yields of bio-oil from rice straw through hydrothermal liquefaction,” *Bioresour. Technol.*, vol. 220, pp. 471–478, Nov. 2016, doi: 10.1016/j.biortech.2016.08.110.
- [16] U. Jena, K. C. Das, and J. R. Kastner, “Comparison of the effects of Na_2CO_3 , $\text{Ca}_3(\text{PO}_4)_2$, and NiO catalysts on the thermochemical liquefaction of microalga *Spirulina platensis*,” *Appl. Energy*, vol. 98, pp. 368–375, Oct. 2012, doi: 10.1016/j.apenergy.2012.03.056.
- [17] P. Adams, T. Bridgwater, A. Lea-Langton, A. Ross, and I. Watson, “Chapter 8 - Biomass Conversion Technologies,” in *Greenhouse Gas Balances of Bioenergy Systems*, P. Thornley and P. Adams, Eds. Academic Press, 2018, pp. 107–139. doi: 10.1016/B978-0-08-101036-5.00008-2.
- [18] S. Zafar |, “Biochemical Conversion of Biomass,” *BioEnergy Consult*, Jun. 17, 2019. <https://www.bioenergyconsult.com/biochemical-conversion-technologies/> (accessed Dec. 06, 2019).
- [19] S. Nizamuddin *et al.*, “An overview of effect of process parameters on hydrothermal carbonization of biomass,” *Renew. Sustain. Energy Rev.*, vol. 73, pp. 1289–1299, Jun. 2017, doi: 10.1016/j.rser.2016.12.122.
- [20] M. J. Cocero *et al.*, “Understanding biomass fractionation in subcritical & supercritical water,” *J. Supercrit. Fluids*, vol. 133, pp. 550–565, Mar. 2018, doi: 10.1016/j.supflu.2017.08.012.
- [21] A. R. K. Gollakota, N. Kishore, and S. Gu, “A review on hydrothermal liquefaction of biomass,” *Renew. Sustain. Energy Rev.*, vol. 81, pp. 1378–1392, Jan. 2018, doi: 10.1016/j.rser.2017.05.178.
- [22] A. Kruse, “Hydrothermal biomass gasification,” *J. Supercrit. Fluids*, vol. 47, no. 3, pp. 391–399, Jan. 2009, doi: 10.1016/j.supflu.2008.10.009.
- [23] D. Castello, T. H. Pedersen, and L. A. Rosendahl, “Continuous Hydrothermal Liquefaction of Biomass: A Critical Review,” *Energies*, vol. 11, no. 11, p. 3165, Nov. 2018, doi: 10.3390/en11113165.

- [24] D. Xu, G. Lin, S. Guo, S. Wang, Y. Guo, and Z. Jing, "Catalytic hydrothermal liquefaction of algae and upgrading of biocrude: A critical review," *Renew. Sustain. Energy Rev.*, vol. 97, pp. 103–118, Dec. 2018, doi: 10.1016/j.rser.2018.08.042.
- [25] T. Mathimani and N. Mallick, "A review on the hydrothermal processing of microalgal biomass to bio-oil - Knowledge gaps and recent advances," *J. Clean. Prod.*, vol. 217, pp. 69–84, Apr. 2019, doi: 10.1016/j.jclepro.2019.01.129.
- [26] J. Yang, Q. (Sophia) He, and L. Yang, "A review on hydrothermal co-liquefaction of biomass," *Appl. Energy*, vol. 250, pp. 926–945, Sep. 2019, doi: 10.1016/j.apenergy.2019.05.033.
- [27] X. Gu, J. S. Martinez-Fernandez, N. Pang, X. Fu, and S. Chen, "Recent development of hydrothermal liquefaction for algal biorefinery," *Renew. Sustain. Energy Rev.*, vol. 121, p. 109707, Apr. 2020, doi: 10.1016/j.rser.2020.109707.
- [28] R. F. Beims, Y. Hu, H. Shui, and C. (Charles) Xu, "Hydrothermal liquefaction of biomass to fuels and value-added chemicals: Products applications and challenges to develop large-scale operations," *Biomass Bioenergy*, vol. 135, p. 105510, Apr. 2020, doi: 10.1016/j.biombioe.2020.105510.
- [29] V. K. Ponnusamy *et al.*, "Review on sustainable production of biochar through hydrothermal liquefaction: Physico-chemical properties and applications," *Bioresour. Technol.*, vol. 310, p. 123414, Aug. 2020, doi: 10.1016/j.biortech.2020.123414.
- [30] Y.-H. Xu and M.-F. Li, "Hydrothermal liquefaction of lignocellulose for value-added products: Mechanism, parameter and production application," *Bioresour. Technol.*, vol. 342, p. 126035, Dec. 2021, doi: 10.1016/j.biortech.2021.126035.
- [31] B. E. Morales-Contreras, N. Flórez-Fernández, M. Dolores Torres, H. Domínguez, R. M. Rodríguez-Jasso, and H. A. Ruiz, "Hydrothermal systems to obtain high value-added compounds from macroalgae for bioeconomy and biorefineries," *Bioresour. Technol.*, vol. 343, p. 126017, Jan. 2022, doi: 10.1016/j.biortech.2021.126017.
- [32] A. Biswas, "(book)The Engineering Of Chemical Reactions L. D. Schmidt OXFORD UNIVERSITY PRESS", Accessed: Dec. 06, 2019. [Online]. Available: https://www.academia.edu/36952527/_book_The_Engineering_Of_Chemical_Reactions_L._D._Schmidt_oxford_university_press
- [33] K. Prapaiwatcharapan, S. Sunphorka, P. Kuchonthara, K. Kangvansaichol, and N. Hinchiranan, "Single- and two-step hydrothermal liquefaction of microalgae in a semi-continuous reactor: Effect of the operating parameters," *Bioresour. Technol.*, vol. 191, pp. 426–432, Sep. 2015, doi: 10.1016/j.biortech.2015.04.027.
- [34] T. K. Vo *et al.*, "Kinetics study of the hydrothermal liquefaction of the microalga *Aurantiochytrium* sp. KRS101," *Chem. Eng. J.*, vol. 306, pp. 763–771, Dec. 2016, doi: 10.1016/j.cej.2016.07.104.

- [35] S. Xiu, A. Shahbazi, V. Shirley, and D. Cheng, "Hydrothermal pyrolysis of swine manure to bio-oil: Effects of operating parameters on products yield and characterization of bio-oil," *J. Anal. Appl. Pyrolysis*, vol. 88, no. 1, pp. 73–79, May 2010, doi: 10.1016/j.jaap.2010.02.011.
- [36] Z. Bi *et al.*, "Biocrude from pretreated sorghum bagasse through catalytic hydrothermal liquefaction," *Fuel*, vol. 188, pp. 112–120, Jan. 2017, doi: 10.1016/j.fuel.2016.10.039.
- [37] S. Makishima *et al.*, "Development of continuous flow type hydrothermal reactor for hemicellulose fraction recovery from corncob," *Bioresour. Technol.*, vol. 100, no. 11, pp. 2842–2848, Jun. 2009, doi: 10.1016/j.biortech.2008.12.023.
- [38] M. Wądrzyk, R. Janus, M. P. Vos, and D. W. F. Brilman, "Effect of process conditions on bio-oil obtained through continuous hydrothermal liquefaction of *Scenedesmus* sp. microalgae," *J. Anal. Appl. Pyrolysis*, vol. 134, pp. 415–426, Sep. 2018, doi: 10.1016/j.jaap.2018.07.008.
- [39] C. Jazrawi, P. Biller, A. B. Ross, A. Montoya, T. Maschmeyer, and B. S. Haynes, "Pilot plant testing of continuous hydrothermal liquefaction of microalgae," *Algal Res.*, vol. 2, no. 3, pp. 268–277, Jul. 2013, doi: 10.1016/j.algal.2013.04.006.
- [40] C. Xiao *et al.*, "A solar-driven continuous hydrothermal pretreatment system for biomethane production from microalgae biomass," *Appl. Energy*, vol. 236, pp. 1011–1018, Feb. 2019, doi: 10.1016/j.apenergy.2018.12.014.
- [41] N. Tippayawong, P. Rerkkriangkrai, P. Aggarangsi, and A. Pattiya, "Biochar Production from Cassava Rhizome in a Semi-continuous Carbonization System," *Energy Procedia*, vol. 141, pp. 109–113, Dec. 2017, doi: 10.1016/j.egypro.2017.11.021.
- [42] A. Hammerschmidt *et al.*, "Catalytic conversion of waste biomass by hydrothermal treatment," *Fuel*, vol. 90, no. 2, pp. 555–562, Feb. 2011, doi: 10.1016/j.fuel.2010.10.007.
- [43] M. R. Haverly *et al.*, "Continuous solvent liquefaction of biomass in a hydrocarbon solvent," *Fuel*, vol. 211, pp. 291–300, Jan. 2018, doi: 10.1016/j.fuel.2017.09.072.
- [44] J. L. Wagner, C. D. Le, V. P. Ting, and C. J. Chuck, "Design and operation of an inexpensive, laboratory-scale, continuous hydrothermal liquefaction reactor for the conversion of microalgae produced during wastewater treatment," *Fuel Process. Technol.*, vol. 165, pp. 102–111, Oct. 2017, doi: 10.1016/j.fuproc.2017.05.006.
- [45] "Visual Encyclopedia of Chemical Engineering." <http://encyclopedia.che.engin.umich.edu/> (accessed Dec. 06, 2019).
- [46] "Coefficients of Linear Thermal Expansion." https://www.engineeringtoolbox.com/linear-expansion-coefficients-d_95.html (accessed Dec. 06, 2019).

- [47] P. Kiran Kumar *et al.*, “Bio oil production from microalgae via hydrothermal liquefaction technology under subcritical water conditions,” *J. Microbiol. Methods*, vol. 153, pp. 108–117, Oct. 2018, doi: 10.1016/j.mimet.2018.09.014.
- [48] B. Guo, V. Walter, U. Hornung, and N. Dahmen, “Hydrothermal liquefaction of *Chlorella vulgaris* and *Nannochloropsis gaditana* in a continuous stirred tank reactor and hydrotreating of biocrude by nickel catalysts,” *Fuel Process. Technol.*, vol. 191, pp. 168–180, Aug. 2019, doi: 10.1016/j.fuproc.2019.04.003.
- [49] K. Ocfemia, Y. Zhang, and T. L. Funk, “Hydrothermal processing of swine manure into oil using a continuous reactor system: Development and testing,” *Trans. ASABE*, vol. 49, Mar. 2006, doi: 10.13031/2013.20408.
- [50] D. C. Elliott *et al.*, “Process development for hydrothermal liquefaction of algae feedstocks in a continuous-flow reactor,” *Algal Res.*, vol. 2, no. 4, pp. 445–454, Oct. 2013, doi: 10.1016/j.algal.2013.08.005.
- [51] M. Bidy, R. Davis, and S. Jones, “Whole Algae Hydrothermal Liquefaction Technology Pathway,” PNNL-22314, NREL/TP-5100-58051, 1076659, Mar. 2013. doi: 10.2172/1076659.
- [52] K. O. Albrecht *et al.*, “Impact of heterotrophically stressed algae for biofuel production via hydrothermal liquefaction and catalytic hydrotreating in continuous-flow reactors,” *Algal Res.*, vol. 14, pp. 17–27, Mar. 2016, doi: 10.1016/j.algal.2015.12.008.
- [53] J. R. Collett *et al.*, “Renewable diesel via hydrothermal liquefaction of oleaginous yeast and residual lignin from bioconversion of corn stover,” *Appl. Energy*, vol. 233–234, pp. 840–853, Jan. 2019, doi: 10.1016/j.apenergy.2018.09.115.
- [54] D. C. Elliott, P. Biller, A. B. Ross, A. J. Schmidt, and S. B. Jones, “Hydrothermal liquefaction of biomass: Developments from batch to continuous process,” *Bioresour. Technol.*, vol. 178, pp. 147–156, Feb. 2015, doi: 10.1016/j.biortech.2014.09.132.
- [55] S. S. Toor, L. Rosendahl, M. P. Nielsen, M. Glasius, A. Rudolf, and S. B. Iversen, “Continuous production of bio-oil by catalytic liquefaction from wet distiller’s grain with solubles (WDGS) from bio-ethanol production,” *Biomass Bioenergy*, vol. 36, pp. 327–332, Jan. 2012, doi: 10.1016/j.biombioe.2011.10.044.
- [56] P. R. Christensen, A. J. Mørup, A. Mamakhel, M. Glasius, J. Becker, and B. B. Iversen, “Effects of heterogeneous catalyst in hydrothermal liquefaction of dried distillers grains with solubles,” *Fuel*, vol. 123, pp. 158–166, May 2014, doi: 10.1016/j.fuel.2014.01.037.
- [57] I. V. Gürsel, T. Noël, Q. Wang, and V. Hessel, “Separation/recycling methods for homogeneous transition metal catalysts in continuous flow,” *Green Chem.*, vol. 17, no. 4, pp. 2012–2026, Apr. 2015, doi: 10.1039/C4GC02160F.

- [58] I. M. Dărăban, L. A. Rosendahl, T. H. Pedersen, and S. B. Iversen, “Pretreatment methods to obtain pumpable high solid loading wood–water slurries for continuous hydrothermal liquefaction systems,” *Biomass Bioenergy*, vol. 81, pp. 437–443, Oct. 2015, doi: 10.1016/j.biombioe.2015.07.004.
- [59] K. O. Albrecht *et al.*, “Impact of heterotrophically stressed algae for biofuel production via hydrothermal liquefaction and catalytic hydrotreating in continuous-flow reactors,” *Algal Res.*, vol. 14, pp. 17–27, Mar. 2016, doi: 10.1016/j.algal.2015.12.008.
- [60] S. Y. Lee, J. M. Cho, Y. K. Chang, and Y.-K. Oh, “Cell disruption and lipid extraction for microalgal biorefineries: A review,” *Bioresour. Technol.*, vol. 244, pp. 1317–1328, Nov. 2017, doi: 10.1016/j.biortech.2017.06.038.
- [61] C. R. Engler and C. W. Robinson, “Disruption of *Candida utilis* cells in high pressure flow devices*,” *Biotechnol. Bioeng.*, vol. 23, no. 4, pp. 765–780, 1981, doi: 10.1002/bit.260230408.
- [62] M. Kurokawa, P. M. King, X. Wu, E. M. Joyce, T. J. Mason, and K. Yamamoto, “Effect of sonication frequency on the disruption of algae,” *Ultrason. Sonochem.*, vol. 31, pp. 157–162, Jul. 2016, doi: 10.1016/j.ultsonch.2015.12.011.
- [63] D. L. Miller, “Effects of a High-Amplitude 1-MHz Standing Ultrasonic Field on the Algae *Hydrodictyon*,” *IEEE Trans. Ultrason. Ferroelectr. Freq. Control*, vol. 33, no. 2, pp. 165–170, Mar. 1986, doi: 10.1109/T-UFFC.1986.26810.
- [64] A. K. Lee, D. M. Lewis, and P. J. Ashman, “Disruption of microalgal cells for the extraction of lipids for biofuels: Processes and specific energy requirements,” *Biomass Bioenergy*, vol. 46, pp. 89–101, Nov. 2012, doi: 10.1016/j.biombioe.2012.06.034.
- [65] X. Peng, X. Ma, Y. Lin, X. Wang, X. Zhang, and C. Yang, “Effect of process parameters on solvolysis liquefaction of *Chlorella pyrenoidosa* in ethanol–water system and energy evaluation,” *Energy Convers. Manag.*, vol. 117, pp. 43–53, Jun. 2016, doi: 10.1016/j.enconman.2016.03.029.
- [66] D. Carullo *et al.*, “Effect of pulsed electric fields and high pressure homogenization on the aqueous extraction of intracellular compounds from the microalgae *Chlorella vulgaris*,” *Algal Res.*, vol. 31, pp. 60–69, Apr. 2018, doi: 10.1016/j.algal.2018.01.017.
- [67] P. Kumar, D. M. Barrett, M. J. Delwiche, and P. Stroeve, “Methods for Pretreatment of Lignocellulosic Biomass for Efficient Hydrolysis and Biofuel Production,” *Ind. Eng. Chem. Res.*, vol. 48, no. 8, pp. 3713–3729, Apr. 2009, doi: 10.1021/ie801542g.
- [68] J. R. Collett *et al.*, “Renewable diesel via hydrothermal liquefaction of oleaginous yeast and residual lignin from bioconversion of corn stover,” *Appl. Energy*, vol. 233–234, pp. 840–853, Jan. 2019, doi: 10.1016/j.apenergy.2018.09.115.

- [69] L. Hadhoum, M. Balistrrou, G. Burnens, K. Loubar, and M. Tazerout, "Hydrothermal liquefaction of oil mill wastewater for bio-oil production in subcritical conditions," *Bioresour. Technol.*, vol. 218, pp. 9–17, Oct. 2016, doi: 10.1016/j.biortech.2016.06.054.
- [70] L. Hadhoum, G. Burnens, K. Loubar, M. Balistrrou, and M. Tazerout, "Bio-oil recovery from olive mill wastewater in sub-/supercritical alcohol-water system," *Fuel*, vol. 252, pp. 360–370, Sep. 2019, doi: 10.1016/j.fuel.2019.04.133.
- [71] "Electric Resistance Heating," *Energy.gov*. <https://www.energy.gov/energysaver/home-heating-systems/electric-resistance-heating> (accessed Dec. 06, 2019).
- [72] S. Chuayboon, S. Abanades, and S. Rodat, "Insights into the influence of biomass feedstock type, particle size and feeding rate on thermochemical performances of a continuous solar gasification reactor," *Renew. Energy*, vol. 130, pp. 360–370, Jan. 2019, doi: 10.1016/j.renene.2018.06.065.
- [73] K. F. Tzanetis, J. A. Posada, and A. Ramirez, "Analysis of biomass hydrothermal liquefaction and biocrude-oil upgrading for renewable jet fuel production: The impact of reaction conditions on production costs and GHG emissions performance," *Renew. Energy*, vol. 113, pp. 1388–1398, Dec. 2017, doi: 10.1016/j.renene.2017.06.104.
- [74] "Solex Thermal Sciences | Energy Efficient Heat Exchanger Technology," *Solex Thermal Sciences*. <https://www.solexthermal.com/> (accessed Dec. 06, 2019).
- [75] B. H. Y. Ong, T. G. Walmsley, M. J. Atkins, M. R. W. Walmsley, J. R. Neale, and P. S. Varbanov, "Optimising Energy Recovery in Hydrothermal Liquefaction of Radiata Pine and Kraft Mill Black Liquor," *Chem. Eng. Trans.*, vol. 70, pp. 1009–1014, Aug. 2018, doi: 10.3303/CET1870169.
- [76] K. Anastasakis, P. Biller, R. Madsen, M. Glasius, and I. Johannsen, "Continuous Hydrothermal Liquefaction of Biomass in a Novel Pilot Plant with Heat Recovery and Hydraulic Oscillation," *Energies*, vol. 11, Oct. 2018, doi: 10.3390/en11102695.
- [77] R. Shakya *et al.*, "Influence of biochemical composition during hydrothermal liquefaction of algae on product yields and fuel properties," *Bioresour. Technol.*, vol. 243, pp. 1112–1120, Nov. 2017, doi: 10.1016/j.biortech.2017.07.046.
- [78] M. S. Vlaskin, N. I. Chernova, S. V. Kiseleva, O. S. Popel', and A. Z. Zhuk, "Hydrothermal liquefaction of microalgae to produce biofuels: state of the art and future prospects," *Therm. Eng.*, vol. 64, no. 9, pp. 627–636, Sep. 2017, doi: 10.1134/S0040601517090105.
- [79] B. E. Eboibi, "Effects of separation methods on yield and quality of biocrude after thermochemical liquefaction of marine microalgae," 2018. doi: 10.4314/njt.v37i3.18.
- [80] J. Chen, L. Wang, B. Zhang, R. Li, and A. Shahbazi, "Hydrothermal Liquefaction Enhanced by Various Chemicals as a Means of Sustainable Dairy Manure Treatment," *Sustainability*, vol. 10, no. 1, pp. 1–14, 2018.

- [81] C. Xu and T. Etcheverry, “Hydro-liquefaction of woody biomass in sub- and super-critical ethanol with iron-based catalysts,” *Fuel*, vol. 87, no. 3, pp. 335–345, Mar. 2008, doi: 10.1016/j.fuel.2007.05.013.
- [82] Y. H. Chan, S. Yusup, A. T. Quitain, Y. Uemura, and M. Sasaki, “Bio-oil production from oil palm biomass via subcritical and supercritical hydrothermal liquefaction,” *J. Supercrit. Fluids*, vol. 95, pp. 407–412, Nov. 2014, doi: 10.1016/j.supflu.2014.10.014.
- [83] H. K. Reddy *et al.*, “Temperature effect on hydrothermal liquefaction of *Nannochloropsis gaditana* and *Chlorella sp.*,” *Appl. Energy*, vol. 165, pp. 943–951, Mar. 2016, doi: 10.1016/j.apenergy.2015.11.067.
- [84] T. Muppaneni *et al.*, “Hydrothermal liquefaction of *Cyanidioschyzon merolae* and the influence of catalysts on products,” *Bioresour. Technol.*, vol. 223, pp. 91–97, Jan. 2017, doi: 10.1016/j.biortech.2016.10.022.
- [85] W.-T. Chen *et al.*, “Hydrothermal liquefaction of mixed-culture algal biomass from wastewater treatment system into bio-crude oil,” *Bioresour. Technol.*, vol. 152, pp. 130–139, Jan. 2014, doi: 10.1016/j.biortech.2013.10.111.
- [86] T. H. Pedersen, L. Jasiūnas, L. Casamassima, S. Singh, T. Jensen, and L. A. Rosendahl, “Synergetic hydrothermal co-liquefaction of crude glycerol and aspen wood,” *Energy Convers. Manag.*, vol. 106, pp. 886–891, Dec. 2015, doi: 10.1016/j.enconman.2015.10.017.
- [87] B. Zhang, M. von Keitz, and K. Valentas, “Thermochemical liquefaction of high-diversity grassland perennials,” *J. Anal. Appl. Pyrolysis*, vol. 84, no. 1, pp. 18–24, Jan. 2009, doi: 10.1016/j.jaap.2008.09.005.
- [88] B. Li, T. Yang, R. Li, and X. Kai, “Co-generation of liquid biofuels from lignocellulose by integrated biochemical and hydrothermal liquefaction process,” *Energy*, vol. 200, p. 117524, Jun. 2020, doi: 10.1016/j.energy.2020.117524.
- [89] L. Feng, X. Li, Z. Wang, and B. Liu, “Catalytic hydrothermal liquefaction of lignin for production of aromatic hydrocarbon over metal supported mesoporous catalyst,” *Bioresour. Technol.*, vol. 323, p. 124569, Mar. 2021, doi: 10.1016/j.biortech.2020.124569.
- [90] B. Biswas, A. Kumar, R. Kaur, B. B. Krishna, and T. Bhaskar, “Catalytic hydrothermal liquefaction of alkali lignin over activated bio-char supported bimetallic catalyst,” *Bioresour. Technol.*, vol. 337, p. 125439, Oct. 2021, doi: 10.1016/j.biortech.2021.125439.
- [91] Z.-X. Xu, J.-H. Cheng, Z.-X. He, Q. Wang, Y.-W. Shao, and X. Hu, “Hydrothermal liquefaction of cellulose in ammonia/water,” *Bioresour. Technol.*, vol. 278, pp. 311–317, Apr. 2019, doi: 10.1016/j.biortech.2019.01.061.

- [92] H. Feng, Z. He, B. Zhang, H. Chen, Q. Wang, and S. Kandasamy, "Synergistic bio-oil production from hydrothermal co-liquefaction of *Spirulina platensis* and α -Cellulose," *Energy*, vol. 174, pp. 1283–1291, May 2019, doi: 10.1016/j.energy.2019.02.079.
- [93] N. Phaiboonsilpa, V. Champreda, and N. Laosiripojana, "Comparative study on liquefaction behaviors of xylan hemicellulose as treated by different hydrothermal methods," *Energy Rep.*, vol. 6, pp. 714–718, Feb. 2020, doi: 10.1016/j.egy.2019.11.143.
- [94] J. Akhtar and N. A. S. Amin, "A review on process conditions for optimum bio-oil yield in hydrothermal liquefaction of biomass," *Renew. Sustain. Energy Rev.*, vol. 15, no. 3, pp. 1615–1624, Apr. 2011, doi: 10.1016/j.rser.2010.11.054.
- [95] S. Karagöz, T. Bhaskar, A. Muto, and Y. Sakata, "Hydrothermal upgrading of biomass: Effect of K₂CO₃ concentration and biomass/water ratio on products distribution," *Bioresour. Technol.*, vol. 97, no. 1, pp. 90–98, Jan. 2006, doi: 10.1016/j.biortech.2005.02.051.
- [96] L. Nazari, Z. Yuan, S. Souzanchi, M. B. Ray, and C. (Charles) Xu, "Hydrothermal liquefaction of woody biomass in hot-compressed water: Catalyst screening and comprehensive characterization of bio-crude oils," *Fuel*, vol. 162, pp. 74–83, Dec. 2015, doi: 10.1016/j.fuel.2015.08.055.
- [97] H. Mazaheri, K. T. Lee, and A. R. Mohamed, "Influence of temperature on liquid products yield of oil palm shell via subcritical water liquefaction in the presence of alkali catalyst," *Fuel Process. Technol.*, vol. 110, pp. 197–205, Jun. 2013, doi: 10.1016/j.fuproc.2012.12.015.
- [98] C. Song, H. Hu, S. Zhu, G. Wang, and G. Chen, "Nonisothermal Catalytic Liquefaction of Corn Stalk in Subcritical and Supercritical Water," *Energy Fuels*, vol. 18, no. 1, pp. 90–96, Jan. 2004, doi: 10.1021/ef0300141.
- [99] "energy - Why is double bond stronger than single bond?," *Chemistry Stack Exchange*. <https://chemistry.stackexchange.com/questions/69724/why-is-double-bond-stronger-than-single-bond> (accessed Feb. 26, 2021).
- [100] C. Xiao *et al.*, "A solar-driven continuous hydrothermal pretreatment system for biomethane production from microalgae biomass," *Appl. Energy*, vol. 236, pp. 1011–1018, Feb. 2019, doi: 10.1016/j.apenergy.2018.12.014.
- [101] K. F. Tzanetis, J. A. Posada, and A. Ramirez, "Analysis of biomass hydrothermal liquefaction and biocrude-oil upgrading for renewable jet fuel production: The impact of reaction conditions on production costs and GHG emissions performance," *Renew. Energy*, vol. 113, pp. 1388–1398, Dec. 2017, doi: 10.1016/j.renene.2017.06.104.
- [102] K. Anastasakis, P. Biller, R. Madsen, M. Glasius, and I. Johannsen, "Continuous Hydrothermal Liquefaction of Biomass in a Novel Pilot Plant with Heat Recovery and Hydraulic Oscillation," *Energies*, vol. 11, Oct. 2018, doi: 10.3390/en11102695.

- [103] W.-T. Chen *et al.*, “Hydrothermal liquefaction of mixed-culture algal biomass from wastewater treatment system into bio-crude oil,” *Bioresour. Technol.*, vol. 152, pp. 130–139, Jan. 2014, doi: 10.1016/j.biortech.2013.10.111.
- [104] T. H. Pedersen, L. Jasiūnas, L. Casamassima, S. Singh, T. Jensen, and L. A. Rosendahl, “Synergetic hydrothermal co-liquefaction of crude glycerol and aspen wood,” *Energy Convers. Manag.*, vol. 106, pp. 886–891, Dec. 2015, doi: 10.1016/j.enconman.2015.10.017.
- [105] B. Zhang, M. Keitz, and K. Valentas, “Thermochemical liquefaction of high-diversity grassland perennials,” *J. Anal. Appl. Pyrolysis*, vol. 84, no. 1, pp. 18–24, Jan. 2009, doi: 10.1016/j.jaap.2008.09.005.
- [106] J. Akhtar and N. A. S. Amin, “A review on process conditions for optimum bio-oil yield in hydrothermal liquefaction of biomass,” *Renew. Sustain. Energy Rev.*, vol. 15, no. 3, pp. 1615–1624, Apr. 2011, doi: 10.1016/j.rser.2010.11.054.
- [107] S. Sangon, S. Ratanavaraha, S. Ngamprasertsith, and P. Prasassarakich, “Coal liquefaction using supercritical toluene–tetralin mixture in a semi-continuous reactor,” *Fuel Process. Technol.*, vol. 87, no. 3, pp. 201–207, Feb. 2006, doi: 10.1016/j.fuproc.2005.07.007.
- [108] B. M. Kabyemela, T. Adschiri, R. M. Malaluan, and K. Arai, “Kinetics of Glucose Epimerization and Decomposition in Subcritical and Supercritical Water,” *Ind. Eng. Chem. Res.*, vol. 36, no. 5, pp. 1552–1558, May 1997, doi: 10.1021/ie960250h.
- [109] B. M. Kabyemela, M. Takigawa, T. Adschiri, R. M. Malaluan, and K. Arai, “Mechanism and Kinetics of Cellobiose Decomposition in Sub- and Supercritical Water,” *Ind. Eng. Chem. Res.*, vol. 37, no. 2, pp. 357–361, Feb. 1998, doi: 10.1021/ie9704408.
- [110] I. F. Grigoras, R. E. Stroe, I. M. Sintamarean, and L. A. Rosendahl, “Effect of biomass pretreatment on the product distribution and composition resulting from the hydrothermal liquefaction of short rotation coppice willow,” *Bioresour. Technol.*, vol. 231, pp. 116–123, May 2017, doi: 10.1016/j.biortech.2017.01.056.
- [111] M. K. Jindal and M. K. Jha, “Catalytic Hydrothermal Liquefaction of Waste Furniture Sawdust to Bio-oil,” *Indian Chem. Eng.*, vol. 58, no. 2, pp. 157–171, Apr. 2016, doi: 10.1080/00194506.2015.1006145.
- [112] Y. Genel, H. Durak, T. Aysu, and İ. Genel, “Effect of process parameters on supercritical liquefaction of *Xanthium strumarium* for bio-oil production,” *J. Supercrit. Fluids*, vol. 115, pp. 42–53, Sep. 2016, doi: 10.1016/j.supflu.2016.04.009.
- [113] M. K. Jindal and M. K. Jha, “Catalytic Hydrothermal Liquefaction of Waste Furniture Sawdust to Bio-oil,” *Indian Chem. Eng.*, vol. 58, no. 2, pp. 157–171, Apr. 2016, doi: 10.1080/00194506.2015.1006145.

- [114] C.-C. Chang *et al.*, “Conversion of waste bamboo chopsticks to bio-oil via catalytic hydrothermal liquefaction using K₂CO₃,” *Sustain. Environ. Res.*, vol. 26, no. 6, pp. 262–267, Nov. 2016, doi: 10.1016/j.serj.2016.08.002.
- [115] C. L. Waters, R. R. Janupala, R. G. Mallinson, and L. L. Lobban, “Staged thermal fractionation for segregation of lignin and cellulose pyrolysis products: An experimental study of residence time and temperature effects,” *J. Anal. Appl. Pyrolysis*, vol. 126, pp. 380–389, Jul. 2017, doi: 10.1016/j.jaap.2017.05.008.
- [116] B. Abdullah, S. A. F. A. S. Muhammad, and N. A. N. Mahmood, “Production of Biofuel via Hydrogenation of Lignin from Biomass,” in *New Advances in Hydrogenation Processes - Fundamentals and Applications*, M. T. Ravanchi, Ed. InTech, 2017. doi: 10.5772/66108.
- [117] S. Karagöz, T. Bhaskar, A. Muto, Y. Sakata, and Md. A. Uddin, “Low-Temperature Hydrothermal Treatment of Biomass: Effect of Reaction Parameters on Products and Boiling Point Distributions,” *Energy Fuels*, vol. 18, no. 1, pp. 234–241, Jan. 2004, doi: 10.1021/ef030133g.
- [118] Y. Qu, X. Wei, and C. Zhong, “Experimental study on the direct liquefaction of *Cunninghamia lanceolata* in water,” *Energy*, vol. 28, no. 7, pp. 597–606, Jun. 2003, doi: 10.1016/S0360-5442(02)00178-0.
- [119] H. Huang and X. Yuan, “Recent progress in the direct liquefaction of typical biomass,” *Prog. Energy Combust. Sci.*, vol. 49, pp. 59–80, Aug. 2015, doi: 10.1016/j.pecs.2015.01.003.
- [120] L. Leng *et al.*, “Study on demetalization of sewage sludge by sequential extraction before liquefaction for the production of cleaner bio-oil and bio-char,” *Bioresour. Technol.*, vol. 200, pp. 320–327, Jan. 2016, doi: 10.1016/j.biortech.2015.10.040.
- [121] C. Xu, S. Huasu, and C. Daqiang, “Liquefaction of corn distillers dried grains with solubles (DDGS) in hot-compressed phenol,” *BioResources*, vol. 3, May 2008.
- [122] F. Lai *et al.*, “Liquefaction of sewage sludge in ethanol-water mixed solvents for bio-oil and biochar products,” *Energy*, vol. 148, pp. 629–641, Apr. 2018, doi: 10.1016/j.energy.2018.01.186.
- [123] P. Duan *et al.*, “Thermo-chemical conversion of *Chlorella pyrenoidosa* to liquid biofuels,” *Bioresour. Technol.*, vol. 133, pp. 197–205, Apr. 2013, doi: 10.1016/j.biortech.2013.01.069.
- [124] U. Jena, K. C. Das, and J. R. Kastner, “Effect of operating conditions of thermochemical liquefaction on biocrude production from *Spirulina platensis*,” *Bioresour. Technol.*, vol. 102, no. 10, pp. 6221–6229, May 2011, doi: 10.1016/j.biortech.2011.02.057.
- [125] Y. Guo, T. Yeh, W. Song, D. Xu, and S. Wang, “A review of bio-oil production from hydrothermal liquefaction of algae,” *Renew. Sustain. Energy Rev.*, vol. 48, pp. 776–790, Aug. 2015, doi: 10.1016/j.rser.2015.04.049.

- [126] L. Cao, C. Zhang, S. Hao, G. Luo, S. Zhang, and J. Chen, “Effect of glycerol as co-solvent on yields of bio-oil from rice straw through hydrothermal liquefaction,” *Bioresour. Technol.*, vol. 220, pp. 471–478, Nov. 2016, doi: 10.1016/j.biortech.2016.08.110.
- [127] Y. Wang *et al.*, “Effects of solvents and catalysts in liquefaction of pinewood sawdust for the production of bio-oils,” *Biomass Bioenergy*, vol. 59, pp. 158–167, Dec. 2013, doi: 10.1016/j.biombioe.2013.10.022.
- [128] T. Aysu and H. Durak, “Thermochemical conversion of *Datura stramonium* L. by supercritical liquefaction and pyrolysis processes,” *J. Supercrit. Fluids*, vol. 102, pp. 98–114, Jul. 2015, doi: 10.1016/j.supflu.2015.04.008.
- [129] F. V. Tinaut, A. Melgar, J. F. Pérez, and A. Horrillo, “Effect of biomass particle size and air superficial velocity on the gasification process in a downdraft fixed bed gasifier. An experimental and modelling study,” *Fuel Process. Technol.*, vol. 89, no. 11, pp. 1076–1089, Nov. 2008, doi: 10.1016/j.fuproc.2008.04.010.
- [130] P. Basu, S. Rao, and A. Dhungana, “An investigation into the effect of biomass particle size on its torrefaction,” *Can. J. Chem. Eng.*, vol. 91, Mar. 2013, doi: 10.1002/cjce.21710.
- [131] Y. Yu and H. Wu, “Understanding the Primary Liquid Products of Cellulose Hydrolysis in Hot-Compressed Water at Various Reaction Temperatures,” *Energy Fuels*, vol. 24, no. 3, pp. 1963–1971, Mar. 2010, doi: 10.1021/ef9013746.
- [132] “Flow Chemistry vs. Batch Chemistry,” *Kilolabs*. <https://kilolabs.com/resources/flow-chemistry-vs-batch-chemistry/> (accessed May 23, 2021).
- [133] L. D. Elliott, M. Berry, B. Harji, D. Klauber, J. Leonard, and K. I. Booker-Milburn, “A Small-Footprint, High-Capacity Flow Reactor for UV Photochemical Synthesis on the Kilogram Scale,” *Org. Process Res. Dev.*, vol. 20, no. 10, pp. 1806–1811, Oct. 2016, doi: 10.1021/acs.oprd.6b00277.
- [134] K. Anastasakis, P. Biller, R. Madsen, M. Glasius, and I. Johannsen, “Continuous Hydrothermal Liquefaction of Biomass in a Novel Pilot Plant with Heat Recovery and Hydraulic Oscillation,” *Energies*, vol. 11, Oct. 2018, doi: 10.3390/en11102695.
- [135] R. Li, Y. Xie, T. Yang, B. Li, Y. Zhang, and X. Kai, “Characteristics of the products of hydrothermal liquefaction combined with cellulosic bio-ethanol process,” *Energy*, vol. 114, pp. 862–867, Nov. 2016, doi: 10.1016/j.energy.2016.08.033.
- [136] J.-L. Zheng, M.-Q. Zhu, and H. Wu, “Alkaline hydrothermal liquefaction of swine carcasses to bio-oil,” *Waste Manag.*, vol. 43, pp. 230–238, Sep. 2015, doi: 10.1016/j.wasman.2015.05.010.
- [137] Rizzo Andrea Maria, Dell Orco Stefano, Miliotti Edoardo, and Chiaramonti David, “Design, Commissioning and Start-up of a New Hydrothermal Liquefaction Continuous Pilot Unit,” *Chem. Eng. Trans.*, vol. 80, pp. 367–372, Jun. 2020, doi: 10.3303/CET2080062.

- [138] “Rate of Heating - an overview | ScienceDirect Topics.” <https://www.sciencedirect.com/topics/engineering/rate-of-heating> (accessed May 23, 2021).
- [139] S. Brand, F. Hardi, J. Kim, and D. J. Suh, “Effect of heating rate on biomass liquefaction: Differences between subcritical water and supercritical ethanol,” *Energy*, vol. 68, pp. 420–427, Apr. 2014, doi: 10.1016/j.energy.2014.02.086.
- [140] S. Raikova, C. D. Le, J. L. Wagner, V. P. Ting, and C. J. Chuck, “Chapter 9 - Towards an Aviation Fuel Through the Hydrothermal Liquefaction of Algae,” in *Biofuels for Aviation*, C. J. Chuck, Ed. Academic Press, 2016, pp. 217–239. doi: 10.1016/B978-0-12-804568-8.00009-3.
- [141] K.-Q. Tran, A. J. Klemsdal, W. Zhang, J. Sandquist, L. Wang, and Ø. Skreiberg, “Fast Hydrothermal Liquefaction of Native and Torrefied Wood,” *Energy Procedia*, vol. 105, pp. 218–223, May 2017, doi: 10.1016/j.egypro.2017.03.305.
- [142] Z. Zhang, “COMPUTATIONAL FLUID DYNAMICS MODELING OF A CONTINUOUS TUBULAR HYDROTHERMAL LIQUEFACTION REACTOR,” p. 76.
- [143] A. H. Syed, “CFD modeling for direct liquefaction of biomass in hydrothermal media,” p. 80.
- [144] “Computational Fluid Dynamics simulation of hydrothermal liquefaction of microalgae in a continuous plug-flow reactor - ScienceDirect.” <https://www.sciencedirect.com/science/article/pii/S0960852418302736> (accessed Jan. 30, 2020).
- [145] “CFD analysis of hydrothermal conversion of heavy oil in continuous flow reactor | Elsevier Enhanced Reader.” <https://reader.elsevier.com/reader/sd/pii/S026387621630332X?token=1C8D45DC3A928EE137543D7264437DD15BCCD4467E889D6A4C49F5D06500E4CFDB549C45D068F148581F37CAEB0C85E9> (accessed Jan. 28, 2020).
- [146] S. Mekala, A. Fontanals, and A. Guardo, “CFD study of the supercritical transesterification of triolein: Wall-to-fluid/particle-to fluid transport effects,” *J. Supercrit. Fluids*, vol. 143, pp. 42–54, Jan. 2019, doi: 10.1016/j.supflu.2018.07.024.
- [147] C. A. Coberly and W. R. Marshall, “Temperature gradients in gas streams flowing through fixed granular beds,” *Chem Eng Prog*, vol. 47, no. 3, pp. 141–150, 1951.
- [148] P. V. Danckwerts, “Continuous flow systems: Distribution of residence times,” *Chem. Eng. Sci.*, vol. 2, no. 1, pp. 1–13, Feb. 1953, doi: 10.1016/0009-2509(53)80001-1.
- [149] “orders of reaction and rate equations.” <https://www.chemguide.co.uk/physical/basicrates/orders.html> (accessed May 07, 2020).
- [150] P. J. Valdez, V. J. Tocco, and P. E. Savage, “A general kinetic model for the hydrothermal liquefaction of microalgae,” *Bioresour. Technol.*, vol. 163, pp. 123–127, Jul. 2014, doi: 10.1016/j.biortech.2014.04.013.

- [151] J. D. Sheehan and P. E. Savage, "Modeling the effects of microalga biochemical content on the kinetics and biocrude yields from hydrothermal liquefaction," *Bioresour. Technol.*, vol. 239, pp. 144–150, Sep. 2017, doi: 10.1016/j.biortech.2017.05.013.
- [152] G. Y. Zhu, X. Zhu, Z. B. Xiao, F. P. Yi, Y. H. Ma, and W. Q. Ji, "Kinetics of Glucose Production from Cellulose by Hydrolysis in Sub-Critical Water," *Advanced Materials Research*, 2012. /AMR.347-353.2672 (accessed May 07, 2020).
- [153] T. L.-K. Yong and Y. Matsumura, "Kinetic Analysis of Lignin Hydrothermal Conversion in Sub- and Supercritical Water," *Ind. Eng. Chem. Res.*, vol. 52, no. 16, pp. 5626–5639, Apr. 2013, doi: 10.1021/ie400600x.
- [154] C. Pronyk and G. Mazza, "Kinetic Modeling of Hemicellulose Hydrolysis from Triticale Straw in a Pressurized Low Polarity Water Flow-Through Reactor," *Ind. Eng. Chem. Res.*, vol. 49, no. 14, pp. 6367–6375, Jul. 2010, doi: 10.1021/ie1003625.
- [155] T. M. Brown, P. Duan, and P. E. Savage, "Hydrothermal Liquefaction and Gasification of *Nannochloropsis* sp.," *Energy Fuels*, vol. 24, no. 6, pp. 3639–3646, Jun. 2010, doi: 10.1021/ef100203u.
- [156] B. E. Poling, J. M. Prausnitz, and J. P. O'Connell, *The Properties of Gases and Liquids 5E*. McGraw Hill Professional, 2000.
- [157] H. W. Xiang, A. Laesecke, and M. L. Huber, "A New Reference Correlation for the Viscosity of Methanol," *J. Phys. Chem. Ref. Data*, vol. 35, no. 4, pp. 1597–1620, Nov. 2006, doi: 10.1063/1.2360605.
- [158] R. D. Goodwin, "Methanol Thermodynamic Properties From 176 to 673 K at Pressures to 700 Bar," *J. Phys. Chem. Ref. Data*, vol. 16, no. 4, pp. 799–892, Oct. 1987, doi: 10.1063/1.555786.
- [159] "(PDF) Numerical modeling of continuous flow microwave heating: A critical Comparison of COMSOL and ANSYS," *ResearchGate*. https://www.researchgate.net/publication/51459843_Numerical_modeling_of_continuous_flow_microwave_heating_A_critical_Comparison_of_COMSOL_and_ANSYS (accessed May 07, 2020).
- [160] "Hydrothermal liquefaction of biomass: Developments from batch to continuous process | Elsevier Enhanced Reader." <https://reader.elsevier.com/reader/sd/pii/S0960852414013911?token=782793AB73AEC287AC7674C82F6B54731D2836F196F89D5641382F9417EA59FBB596CFC014C86BA33D7E47BE0FDBA190&originRegion=eu-west-1&originCreation=20211117151624> (accessed Nov. 17, 2021).
- [161] D. Castello, T. H. Pedersen, and L. A. Rosendahl, "Continuous Hydrothermal Liquefaction of Biomass: A Critical Review," *Energies*, vol. 11, no. 11, p. 3165, Nov. 2018, doi: 10.3390/en11113165.

- [162] R. Obeid, "Reaction Kinetics for Hydrothermal Liquefaction of Biomass," Thesis, 2020. Accessed: Oct. 04, 2021. [Online]. Available: <https://digital.library.adelaide.edu.au/dspace/handle/2440/126627>
- [163] R. Obeid, D. Lewis, N. Smith, and P. van Eyk, "The elucidation of reaction kinetics for hydrothermal liquefaction of model macromolecules," *Chem. Eng. J.*, vol. 370, pp. 637–645, Aug. 2019, doi: 10.1016/j.cej.2019.03.240.
- [164] D. Kusdiana and S. Saka, "Kinetics of transesterification in rapeseed oil to biodiesel fuel as treated in supercritical methanol," *Fuel*, vol. 80, no. 5, pp. 693–698, Apr. 2001, doi: 10.1016/S0016-2361(00)00140-X.
- [165] W. R. Gambill, *Chem Eng*, vol. 66, no. 1, p. 127, 1959.
- [166] "Ideal Gases | MIT OpenCourseWare | Free Online Course Materials." <https://ocw.mit.edu/high-school/physics/exam-prep/kinetic-theory-thermodynamics/ideal-gases/> (accessed Nov. 09, 2021).
- [167] "Real Gases | Introductory Chemistry." <https://courses.lumenlearning.com/suny-introductory-chemistry/chapter/real-gases/> (accessed Nov. 09, 2021).
- [168] "Isochoric Process - an overview | ScienceDirect Topics." <https://www.sciencedirect.com/topics/mathematics/isochoric-process> (accessed Nov. 17, 2021).
- [169] P. D. Harvey, *Engineering Properties of Steel*. American Society for Metals, 1982.
- [170] "COMSOL Documentation." https://doc.comsol.com/5.6/docserver/#!TOC:/com.comsol.help.matlib/toc.xml:SOURCE:resource_tocfile_-650047560.html (accessed Nov. 17, 2021).
- [171] "Thermophysical Properties of Fluid Systems." <https://webbook.nist.gov/chemistry/fluid/> (accessed Jul. 03, 2022).
- [172] "Thermal Insulation Characteristic - an overview | ScienceDirect Topics." <https://www.sciencedirect.com/topics/engineering/thermal-insulation-characteristic> (accessed Nov. 10, 2021).
- [173] S. B. Lohner Svenja, "Vanishing Baking Soda," *Scientific American*. <https://www.scientificamerican.com/article/vanishing-baking-soda/> (accessed Dec. 03, 2021).
- [174] M. C. Ball, C. M. Snelling, A. N. Strachan, and R. M. Strachan, "Thermal decomposition of solid sodium bicarbonate," *J. Chem. Soc. Faraday Trans. 1 Phys. Chem. Condens. Phases*, vol. 82, no. 12, p. 3709, 1986, doi: 10.1039/f19868203709.
- [175] Y.-L. Wu and S.-M. Shih, "Intrinsic kinetics of the thermal decomposition of sodium bicarbonate," *Thermochim. Acta*, vol. 223, pp. 177–186, Aug. 1993, doi: 10.1016/0040-6031(93)80132-T.
- [176] W. Hu, J. M. Smith, T. Do??u, and G. Do??u, "Kinetics of sodium bicarbonate decomposition," *AIChE J.*, vol. 32, no. 9, pp. 1483–1490.

- [177] M. Hartman, K. Svoboda, M. Pohořelý, and M. Šyc, “Thermal Decomposition of Sodium Hydrogen Carbonate and Textural Features of Its Calcines,” *Ind. Eng. Chem. Res.*, vol. 52, no. 31, pp. 10619–10626, Aug. 2013, doi: 10.1021/ie400896c.
- [178] Y. Cai *et al.*, “Effective Capture of Carbon Dioxide Using Hydrated Sodium Carbonate Powders,” *Materials*, vol. 11, no. 2, p. 183, Jan. 2018, doi: 10.3390/ma11020183.
- [179] P. Ranganathan and S. Savithri, “Computational Fluid Dynamics simulation of hydrothermal liquefaction of microalgae in a continuous plug-flow reactor,” *Bioresour. Technol.*, vol. 258, pp. 151–157, Jun. 2018, doi: 10.1016/j.biortech.2018.02.076.
- [180] S. Mazloum, S. Awad, Y. abou msallem, N. Allam, K. Loubar, and M. Tazerout, “Modeling of a pyrolysis batch reactor using COMSOL Multiphysics,” *MATEC Web Conf.*, vol. 261, p. 04003, Jan. 2019, doi: 10.1051/mateconf/201926104003.
- [181] X. Chen, Z. F. Tian, P. J. van Eyk, D. Lewis, and G. ‘Gus’ J. Nathan, “Numerical simulation of hydrothermal liquefaction of algae in a lab-scale coil reactor,” *Exp. Comput. Multiph. Flow*, vol. 4, no. 2, pp. 113–120, Jun. 2022, doi: 10.1007/s42757-020-0104-0.
- [182] “Pros and Cons of Continuous Flow versus Batch Processing Systems.” <https://www.labx.com/resources/pros-and-cons-of-continuous-flow-versus-batch-processing-systems/170> (accessed Aug. 02, 2022).
- [183] <https://www.blogger.com/profile/17286156098467576500>, “Types of Reactors,” *Chemical World*. <https://chemico-world.blogspot.com/2021/12/types-of-reactors.html> (accessed Aug. 02, 2022).
- [184] “Advantages of Continuous Flow Production | Vapourtec Ltd,” *Vapourtec*. <https://www.vapourtec.com/flow-chemistry/advantages-of-continuous-flow-production/> (accessed Aug. 02, 2022).
- [185] “Plug Flow Reactors (PFRs).” <http://websites.umich.edu/~elements/asyLearn/bits/pfrfinal/index.htm> (accessed Aug. 02, 2022).
- [186] H. Jahromi, T. Rahman, P. Roy, and S. Adhikari, “Hydrotreatment of solvent-extracted biocrude from hydrothermal liquefaction of municipal sewage sludge,” *Energy Convers. Manag.*, vol. 263, p. 115719, Jul. 2022, doi: 10.1016/j.enconman.2022.115719.
- [187] K. Prapaiwatcharapan, S. Sunphorka, P. Kuchonthara, K. Kangvansaichol, and N. Hinchiranan, “Single- and two-step hydrothermal liquefaction of microalgae in a semi-continuous reactor: Effect of the operating parameters,” *Bioresour. Technol.*, vol. 191, pp. 426–432, Sep. 2015, doi: 10.1016/j.biortech.2015.04.027.
- [188] S. Makishima *et al.*, “Development of continuous flow type hydrothermal reactor for hemicellulose fraction recovery from corncob,” *Bioresour. Technol.*, vol. 100, no. 11, pp. 2842–2848, Jun. 2009, doi: 10.1016/j.biortech.2008.12.023.

- [189] A. Hammerschmidt *et al.*, “Catalytic conversion of waste biomass by hydrothermal treatment,” *Fuel*, vol. 90, no. 2, pp. 555–562, Feb. 2011, doi: 10.1016/j.fuel.2010.10.007.
- [190] M. R. Haverly *et al.*, “Continuous solvent liquefaction of biomass in a hydrocarbon solvent,” *Fuel*, vol. 211, pp. 291–300, Jan. 2018, doi: 10.1016/j.fuel.2017.09.072.
- [191] J. L. Wagner, C. D. Le, V. P. Ting, and C. J. Chuck, “Design and operation of an inexpensive, laboratory-scale, continuous hydrothermal liquefaction reactor for the conversion of microalgae produced during wastewater treatment,” *Fuel Process. Technol.*, vol. 165, pp. 102–111, Oct. 2017, doi: 10.1016/j.fuproc.2017.05.006.
- [192] “ASM Material Data Sheet.” <https://asm.matweb.com/search/SpecificMaterial.asp?bassnum=mq316q> (accessed Aug. 02, 2022).
- [193] “Pacific Northwest National Laboratory | PNNL.” <https://www.pnnl.gov/> (accessed Aug. 02, 2022).
- [194] “CATALYTIC HYDROTHERMAL GASIFICATION OF BIOMASS FOR THE PRODUCTION OF HYDROGEN-CONTAINING FEEDSTOCK (METHANE) | PNNL.” <https://www.pnnl.gov/publications/catalytic-hydrothermal-gasification-biomass-production-hydrogen-containing-feedstock> (accessed Aug. 02, 2022).
- [195] “Stress in Thick-Walled Cylinders or Tubes.” https://www.engineeringtoolbox.com/stress-thick-walled-tube-d_949.html (accessed Aug. 02, 2022).
- [196] “What is von Mises Stress?,” *SDC Verifier*, May 05, 2022. <https://sdcverifier.com/articles/what-is-von-mises-stress/> (accessed Aug. 02, 2022).
- [197] J. Billing *et al.*, “Design, Fabrication, and Testing of the Modular Hydrothermal Liquefaction System (MHTLS),” p. 31.
- [198] B. Patel and K. Hellgardt, “Hydrothermal upgrading of algae paste in a continuous flow reactor,” *Bioresour. Technol.*, vol. 191, pp. 460–468, Sep. 2015, doi: 10.1016/j.biortech.2015.04.012.
- [199] B. Rehm, D. Consultant, A. Haghshenas, A. S. Paknejad, and J. Schubert, “CHAPTER TWO - Situational Problems in MPD,” in *Managed Pressure Drilling*, B. Rehm, J. Schubert, A. Haghshenas, A. S. Paknejad, and J. Hughes, Eds. Gulf Publishing Company, 2008, pp. 39–80. doi: 10.1016/B978-1-933762-24-1.50008-5.
- [200] “Reynolds’ Number - an overview | ScienceDirect Topics.” <https://www.sciencedirect.com/topics/engineering/reynolds-number> (accessed Aug. 08, 2022).
- [201] G. F. FROMENT and K. B. BISCHOFF, “The Plug Flow Reactor,” in *Chemical Reactors Analysis and Design*, 2nd ed.,
- [202] F. P. INCORPERA, D. P. DEWITT, T. L. BERGMAN, and A. S. LAVINE, “Internal Flow,” in *Fundamentals of Heat and Mass Transfer*, 6th ed.,

- [203] G. F. FROMENT and K. B. BISCHOFF, “The Perfectly Mixed Flow Reactor,” in *Chemical Reactor Analysis and Design*,
- [204] F. A. Holland and F. S. Chapman, *Liquid Mixing and Processing in Stirred Tanks*. Reinhold Publishing Corporation, 1966.
- [205] P. Trambouze, *Chemical Reactors, from Design to Operation*. Editions Technip, 2004.
- [206] V. R. and S. M. Kresta*, “Comparison of Continuous Blend Time and Residence Time Distribution Models for a Stirred Tank,” *ACS Publications*, Dec. 15, 2007. <https://pubs.acs.org/doi/pdf/10.1021/ie070955r> (accessed Sep. 07, 2022).
- [207] K. W. Norwood and A. B. Metzner, “Flow patterns and mixing rates in agitated vessels,” *AIChE J.*, vol. 6, no. 3, pp. 432–437, Sep. 1960, doi: 10.1002/aic.690060317.
- [208] “Biodiesel Production Process - What is Esterification,” *Burt Process Equipment*. <https://burtprocess.com/biodiesel-production-process-esterification> (accessed Sep. 13, 2022).
- [209] E. Berglin, C. Enderlin, and A. Schmidt, “Review and Assessment of Commercial Vendors/Options for Feeding and Pumping Biomass Slurries for Hydrothermal Liquefaction,” PNNL, Nov. 2012.
- [210] “Home | MyPutzmeister.” <https://www.putzmeister.com/> (accessed Oct. 05, 2022).
- [211] “feluwa.de - Feluwa Pumpen GmbH.” <https://www.feluwa.com/> (accessed Oct. 05, 2022).
- [212] “ZEILFELDER Gear Pumps and Rotary Lobe Pumps API, CR-TU 10-12,” *Zeifelder Pumps*. <http://www.zeifelder-pumpen.com/> (accessed Oct. 05, 2022).
- [213] “The Basics of Pressure Regulators,” *Beswick Engineering*. <https://www.beswick.com/resources/the-basics-of-pressure-regulators/> (accessed Sep. 14, 2022).
- [214] “Product Detail - Beswick’s PRD4HP,” *Beswick Engineering*. <https://www.beswick.com/catalog/product-detail/PRD4HP> (accessed Sep. 19, 2022).
- [215] Larissa P. Cunico, Roberta Ceriani, and Reginaldo Guirardello, “Estimation of physical properties of vegetable oils and biodiesel, using group contribution methods,” *Chem. Eng. Trans.*, vol. 32, pp. 535–540, May 2013, doi: 10.3303/CET1332090.
- [216] Z. Zhang, “COMPUTATIONAL FLUID DYNAMICS MODELING OF A CONTINUOUS TUBULAR HYDROTHERMAL LIQUEFACTION REACTOR,” p. 76.
- [217] K. Anastasakis and A. B. Ross, “Hydrothermal liquefaction of four brown macro-algae commonly found on the UK coasts: An energetic analysis of the process and comparison with bio-chemical conversion methods,” *Fuel*, vol. 139, pp. 546–553, Jan. 2015, doi: 10.1016/j.fuel.2014.09.006.

Titre : Etudes Numériques et Expérimentales pour la Conception d'un Réacteur de Liquéfaction Hydrothermale

Mots clés : biomasse, réacteur, conception, liquéfaction hydrothermale, simulation.

Résumé : Dans cette thèse, une conception d'un système continu de liquéfaction hydrothermale de biomasse est proposée. Après une étude des différents procédés existants de liquéfaction hydrothermale et des différents mécanismes qui entrent en jeu, des modèles simulant les différents phénomènes thermochimiques entrant en jeu ont été proposés. Ces phénomènes ont été étudiés à l'échelle d'un réacteur batch de 1L et modélisés à l'aide du logiciel COMSOL Multiphysics. Pour ce faire, une campagne expérimentale est menée sur le réacteur, en partant du chauffage du réacteur vide et en terminant par une réaction chimique élémentaire complète; la transestérification supercritique de l'huile de colza. Les courbes expérimentales de température à différents endroits du réacteur et de pression ont aidé à calibrer différents modèles de diffusion de la chaleur, de pressurisation, d'évaporation et transport des espèces.

Finally, the chemical kinetics model of the reaction of the transesterification supercritical des lipides a été validé expérimentalement en se servant du taux de conversion comme paramètre de comparaison. L'erreur relative maximale sur les différents paramètres modélisés est inférieure à 6 %. Le modèle de réacteur batch validé aide à la conception d'un système continu. Un procédé combinant un réacteur agité (CSTR) et d'un réacteur piston (PFR) a été proposé. Après un balayage des différentes plages de températures et de débits, un CSTR de 1 L et un PFR de 2, 44 m et de 1 cm de diamètre ont été choisis pour traiter un débit de 10 L/h de mélange réactif. Après le dimensionnement des différents organes, un système complet et intégré a été proposé.

Title: Numerical and Experimental Studies for the Conception of a Robust Hydrothermal Liquefaction Reactor

Keywords: biomass, reactor, design, hydrothermal liquefaction, simulation.

Abstract: In this thesis, a design of a continuous biomass hydrothermal liquefaction system is proposed. After a study of the different existing hydrothermal liquefaction processes and the different mechanisms involved, models simulating the different underpinning thermochemical phenomena have been proposed. These phenomena were studied at the scale of a 1L batch reactor and modeled using COMSOL Multiphysics software. To do so, an experimental campaign is carried out, starting from the heating of the empty reactor and ending with a complete elementary chemical reaction; supercritical transesterification of rapeseed oil. The experimental curves of temperature at different places in the reactor and of pressure helped to calibrate different models of heat diffusion, pressurization, evaporation and transport of species.

Finally, the chemical kinetics model of the supercritical transesterification of lipids was experimentally validated using the conversion rate as a comparison parameter. The maximum relative error on the different modeled parameters is less than 6%. The validated batch reactor model helps in the design of a continuous system. A process combining a continuous stirred tank reactor (CSTR) and a plug flow reactor (PFR) has been proposed. After scanning the different temperature and flow rate ranges, a 1 L CSTR and a 2.44 m x 1 cm diameter PFR were chosen to handle a flow rate of 10 L/h of reactive mixture. After the dimensioning of the various organs, a complete and integrated system was proposed.